Half-Lap Cross Laminated Timber Pegged Joints

Parker Kraenzlein

Thesis submitted to the faculty of the Virginia Polytechnic Institute and State University in partial fulfillment of the requirements for the degree of

Master of Science

In

Forest Products

Daniel Hindman, Chair

Adam Phillips

Joseph Loferski

April 17, 2025

Blacksburg, VA

Keywords: Cross Laminated Timber, Half-lap CLT, CLT Connections, Pegged Connections, Pegged Joints, Dowel Connections

Half-Lap Cross Laminated Timber Pegged Joints

Parker Kraenzlein

ABSTRACT

Cross laminated timber (CLT) is a panelized structural system consisting of odd layers of dimension sawn lumber stacked perpendicularly to the previous layer. Since the introduction of CLT to North America, man research projects have been conducted on the material properties of CLT panels as well as the three primary methods of joining CLT with metallic fasteners: the butt joint, half-lap joint, and spline joint. Currently, there are efforts to reduce the embodied energy associated with CLT buildings, leading to research exploring alternatives to metallic fasteners.

This research investigates the shear yield load and stiffness of red oak (*Quercus rubra*) hardwood pegs in half-lap 3-ply Austrian spruce (*Picea abies*) and yellow-poplar *(Liriodendron tulipifera)* CLT diaphragm connections. In addition to the use of Austrian spruce and yellow-poplar CLT, both 1 inch and 1.25 inch diameter pegs were tested in the half-lap connections. The influence of both the CLT species and peg diameter were evaluated for their impact on connection yield load and stiffness when subjected to both monotonic and cyclic loading. The replacement of metallic fasteners with hardwood pegs could represent a significant reduction to embodied energy in buildings.

Experimental testing showed that the yellow-poplar connections for both 1 inch and 1.25 inch diameter pegs had a greater 5% offset yield load than the Austrian spruce specimens. Yield Mode II and V were the two identified failure modes, with Mode II occurring primarily in the Austrian spruce specimens and Mode V predominantly occurring in the yellow-poplar specimens. Connection yield loads were predicted using Yield Mode II and V predictive

equations and compared to experimental results, with varying degrees of agreement. Through a two-way ANOVA analysis, it was determined that there was a significant difference in the 5% offset yield loads of the connections due to both CLT species and peg diameter. When evaluating the impact of CLT species and peg diameter on connection stiffness using a two-way ANOVA, a significant difference in stiffness was attributed to CLT species but not peg diameter.

Half-Lap Cross Laminated Timber Pegged Joints

Parker Kraenzlein

GENERAL AUDIENCE ABSTRACT

Cross laminated timber (CLT) is a panelized structural system consisting of odd layers of dimensionally sawn lumber stacked perpendicularly to the previous layer. Since the introduction of CLT to North America, much research has been conducted on the material properties of CLT panels and methods of connecting panels using metallic fasteners. With growing concerns over embodied carbon in buildings, more emphasis is currently being placed on more sustainable connection techniques.

This research is a study into the possibility of replacing metallic fasteners with hardwood pegs in CLT connections. This study used red oak pegs in both Austrian spruce and yellow-poplar half-lap CLT connections. The shear yield load and stiffness of the connections subjected to both monotonic and cyclic loading was evaluated.

Experimental results showed that the yellow-poplar connections had a greater average yield load than the Austrian spruce connections. Two distinct failure modes were observed in the testing of the connections: Yield Mode II (CLT bearing failure), which was most common in the Austrian Spruce, and Mode V (shearing of peg), which was dominant in the yellow-poplar specimens. Yield load predictions based on these failure modes were compared to experimental results, showing varying degrees of accuracy. Statistical analysis confirmed that both CLT species and peg diameter significantly influenced connection yield load, while stiffness was primarily affected by CLT species.

ACKNOWLEDGEMENTS

The author wishes to express sincere gratitude to his committee for their invaluable support throughout the writing of this document. Special thanks are extended to Dr. Daniel Hindman for recruiting the author to Virginia Tech and for his sponsorship of the author's two master's degrees. The author also appreciates Dr. Adam Phillips for his practical guidance in navigating the research process and Dr. Aivars Vilguts for providing a comprehensive introduction to working in a laboratory environment as a graduate student.

The author would also like to thank those who supported him on his journey to Virginia Tech. From his undergraduate studies at Iowa State University, Dr. Jiehua Shen and Dr. In-Ho Cho, for their willingness to discuss structural engineering, careers, and coursework whenever the author stopped by (which was nearly daily). At the time, the author did not fully appreciate how fortunate he was to have such accessibility. The author would also like to recognize his classmate Mira Johnson for her industriousness in checking and discussing homework assignments when the author was treading water in his many 18+ credit semesters.

On a more personal level, the author would like to thank his mother for convincing him not to drop out of college after his freshman year and start a fast-food franchise or flip houses. Finally, the author is deeply grateful to his grandparents for their ongoing support, frequently reminding the author, "Don't be in any hurry to get out of school."

TABLE OF CONTENTS

LIST OF FIGURES

LIST OF TABLES

LIST OF EQUATIONS

1.0 INTRODUCTION

Cross-laminated timber (CLT) is a relatively new construction material that has the ability to be erected faster than other conventional construction materials. Research has focused on evaluating the material properties and performance of CLT panels. Yet, many research questions remain about connections and force transfer between CLT elements. When considering the established methods of joining CLT used in a floor system, there are three common ways of connecting the panels: the butt joint, lap joint, and surface spline (Karacabeyli & Douglas, 2013). All three joints rely on the use of metallic screws for fastening and transferring forces from panel to panel (Mahamid, 2020). The most common connection of the three is the surface spline as it is easy to install and does not require significant machining compared to the lap joint. The butt joint requires no machining; however, obtaining specified gap tolerances required for fire protection can be problematic for field installation. An advantage of the lap joint is the panel-on-panel bearing at the lap which reduces the need for fireproofing along the joints of the panels.

With growing concerns over the carbon emission output and the global warming potential (GWP) of erected structures, it is ever more important to understand the impact material choices have on the structure as a whole. In a traditional GWP analysis, it is common for the fasteners to be ignored as they are viewed as insignificant relative to the whole structure (Lukić et al., 2021). It is only a matter of time before fasteners are included in a GWP analysis and as such it will be imperative that more carbon-efficient fasteners are employed. As engineers search for alternative methods for joining CLT panels, it may be beneficial to examine traditional timber frame construction joinery methods. It is possible that the use of hardwood dowels (pegs) for connecting CLT panels via a half-lap joint is a viable solution that not only meets the

performance needs of a structure but may also be beneficial from a cost and time of installation perspective.

By determining the yield load, ultimate load, and stiffness of the half-lapped CLT pegged connections using 1 inch and 1.25 inch diameter pegs subjected to shear forces, feasibility of using the half-lap pegged connection as an alternative to metallic fasteners can be evaluated.

1.1 OBJECTIVES AND SCOPE OF WORK

The goal of this research is to evaluate the use of hardwood pegs in half-lap CLT panel-to-panel connections. By determining the yield load and stiffness of the connections, pegs can be evaluated as a practical replacement for metallic fasteners.

The objectives of this study are to:

(1) Evaluate the yield load and stiffness of half-lap CLT pegged connections subject to monotonic shear loading according to ISO 6891.

(2) Evaluate the yield load and stiffness of half-lap CLT pegged connections subject to cyclic shear loading according to ASTM E2126.

(3) Compare the experimental yield loads to predicted values.

(4) Determine the impact peg diameter and CLT species have on connection yield load and stiffness.

2.0 LITERATURE REVIEW

2.1 DESIGN OF CONNECTIONS ACCORDING TO THE NDS

The NDS details a series of yield limit equations for fasteners subjected to single and double shear. The equations are based on the bending resistance of a metallic fastener and the crushing resistance of the wood. As the half lap joint geometry only has one shear plane, only the single shear yield modes and capacities will be relevant.

The NDS presents a total of four yield modes I-IV, in which modes I and III include a designation as to which member the yield occurs in, either the main or side. Mode I_m and I_s denote yielding in bearing in the wood of either the main or side member, respectively. Mode II is characteristic of a pivoting of the fastener about the shear plane with wood yielding in bearing near the exterior faces of the wood members. Mode III_m and III_s describe a fastener that has yielded due to the creation of a single plastic hinge in either the main or side member, respectively. Lastly, Mode IV is typical of a formation of two plastic hinges per shear plane with wood bearing failures near the shear plane (AWC, 2018). It shall be noted that the yield modes presented in the NDS were derived for metallic fasteners. Consequently, the equations provided by Miller et al. (2010), which were derived for the use of hardwood dowels can be used instead. Yield limit equations I-IV are presented in Table 1 and the corresponding failure methods are shown in Figure 1.

Table 1: NDS Yield Limit Equations (AWC, 2018)

Yield Limit Equations		
Yield Mode	**Single Shear**	
I_m	$Z = \frac{D\ell_m F_{em}}{R_d}$	$k_1 = \frac{\sqrt{R_e + 2R_e{}^2(1 + R_t + R_t^2) + R_t^2 R_e^3} - R_e(1 + R_t)}{(1 + R_e)}$
I_s	$Z = \frac{D\ell_s F_{es}}{R_d}$	$k_2 = -1 + \sqrt{2(1 + R_e) + \frac{2F_{yb}(1 + 2R_e)D^2}{3F_{em}\ell_m^2}}$
II	$Z = \frac{k_1 D\ell_s F_{es}}{R_d}$	$k_3 = -1 + \sqrt{\frac{2(1 + R_e)}{R_e} + \frac{2F_{yb}(2 + R_e)D^2}{3F_{em}\ell_s^2}}$
III_m	$Z = \frac{k_2 D\ell_m F_{em}}{(1 + 2R_e)R_d}$	
III_s	$Z = \frac{k_3 D\ell_s F_{em}}{(2 + 2R_e)R_d}$	
IV	$Z = \frac{D^2}{R_d}\sqrt{\frac{2F_{em}F_{yb}}{3(1 + R_e)}}$	

Where,

D = diameter, in.

F_{yb} = dowel bending yield strength, psi

R_d = reduction term

$R_e = F_{em}/F_{es}$

$R_t = \ell_m/\ell_s$

ℓ_m = main member dowel bearing length, in.

ℓ_s = side member dowel bearing length, in.

F_{em} = main member dowel bearing strength, psi

F_{es} = side member dowel bearing strength, psi

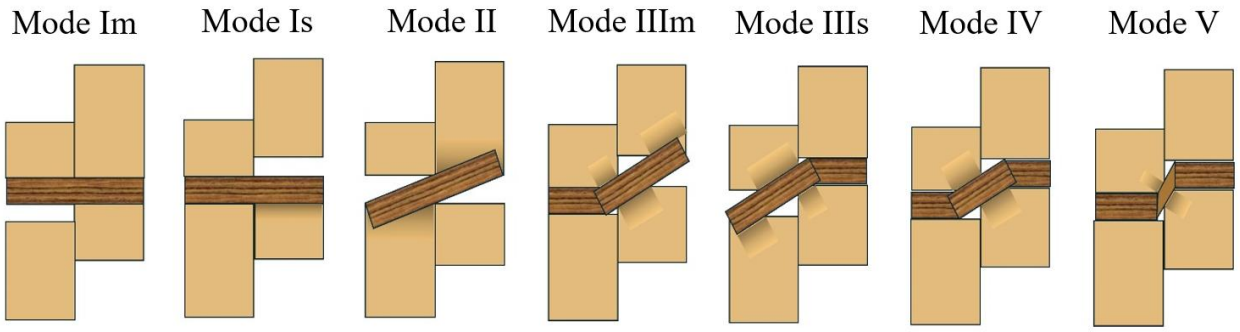

Figure 1: Yield Modes I-V (AWC, 2018; Miller et al, 2010)

In addition to presenting yield modes for metallic fasteners, the NDS also provides recommendations for connection geometry and the spacing of fasteners in relation to each other and the edges and end of the members. The spacings the NDS provides guidance on include: the edge distance, end distance, as well as the spacing between rows of fasteners and fasteners in a row (AWC, 2018).

When considering the end distances and the spacing of fasteners in a row, the engineer must consider the geometry factor, C_Δ, which can reduce the reference lateral design value, Z, depending on the specified spacing. For end distances, the NDS provides minimum end spacing requirements to achieve a geometry factor equal to 0.5 and 1.0. Different spacing requirements are provided depending on whether the loading is perpendicular to grain, parallel to grain subject to compression, parallel to grain subject to tension and in a softwood, or parallel to grain subject to tension in a hardwood (AWC, 2018). If the end distance specified is not that specified by the NDS to achieve a geometry factor of one, but greater than the minimum specified to obtain a geometry factor of a half, the NDS specifies a way for the engineer to calculate the geometry factor. The non-prescribed geometry factor is equal to the actual end distance spacing divided by

the minimum end distance spacing to achieve a geometry factor of one (AWC, 2018). End distance requirements are presented in Table 2.

Table 2: NDS End Distance Requirements (AWC, 2018)

End Distance Requirements

Direction of Loading	End Distances: Minimum end distances for CΔ = 0.5	End Distances: Minimum end distances for CΔ = 1.0
Perpendicular to Grain	2D	4D
Parallel to Grain, Compression	2D	4D
Parallel to Grain, Tension		
softwoods	3.5D	7D
hardwoods	2.5D	5D

When considering the spacing of fasteners in a row, the NDS (AWC, 2018) provides both minimum spacings and minimum spacings to achieve a geometry factor of 1.0. The recommended spacings are then further broken into subcategories depending on the direction of loading, either parallel or perpendicular to grain. Spacing requirements for fasteners in a row are presented in Table 3.

Table 3: NDS Spacing Requirements for Fasteners in a Row (AWC, 2018)

Spacing Requirements for Fasteners in a Row

Direction of Loading	Spacing: Minimum spacing	Spacing: Minimum spacing for CΔ = 1.0
Parallel to Grain	3D	4D
Perpendicular to Grain	3D	Required spacing for attached members

Edge distance requirements are provided for both parallel and perpendicular to grain loadings and are not subject to a geometry factor. The NDS subdivides the parallel to grain

loading by comparing ℓ /D to 6. Depending on whether ℓ /D is less than or equal to 6 or greater than 6 determines the required edge distance spacing. Where ℓ /D is taken as the lesser of the length of the fastener in the wood main member divided by the diameter of the fastener or the total length of the fastener in the wood side member divided by the diameter of the fastener (AWC, 2018). When loading is perpendicular to grain, spacing requirements are specified based on whether the edge is loaded or unloaded (AWC, 2018). Table 4 summarizes the edge distance requirements per the NDS.

Table 4: NDS Edge Distance Requirements (AWC, 2018)

Edge Distance Requirements	
Direction of Loading	**Minimum Edge Distance**
Parallel to Grain:	
where ℓ /D ≤ 6	1.5D
where ℓ /D > 6	greater of 1.5D or 1/2 the spacing between rows
Perpendicular to Grain:	
loaded edge	4D
unloaded edge	1.5D

2.2 PEGGED CONNECTIONS IN TRADIONAL TIMBER FRAMES

The most traditional form of wood structures is a timber frame, consisting of large timbers cut from large-diameter trees and milled by hand. Connections in timber frames consist of interlocking wood-to-wood connections held in place by hardwood pegs (TFEC 1, 2019). The most common connection type in traditional timber framing is the mortise and tenon joint which is secured using wood pegs (Figure 2). As timber frame construction predates the mass production of nails from the Industrial Revolution, as traditional timber framing does not use metallic fasteners. However, modern timber frames often use metal fasteners as more advanced fasteners have recently been developed and can assist in meeting requirements prescribed by modern codes (TFEC 1, 2019).

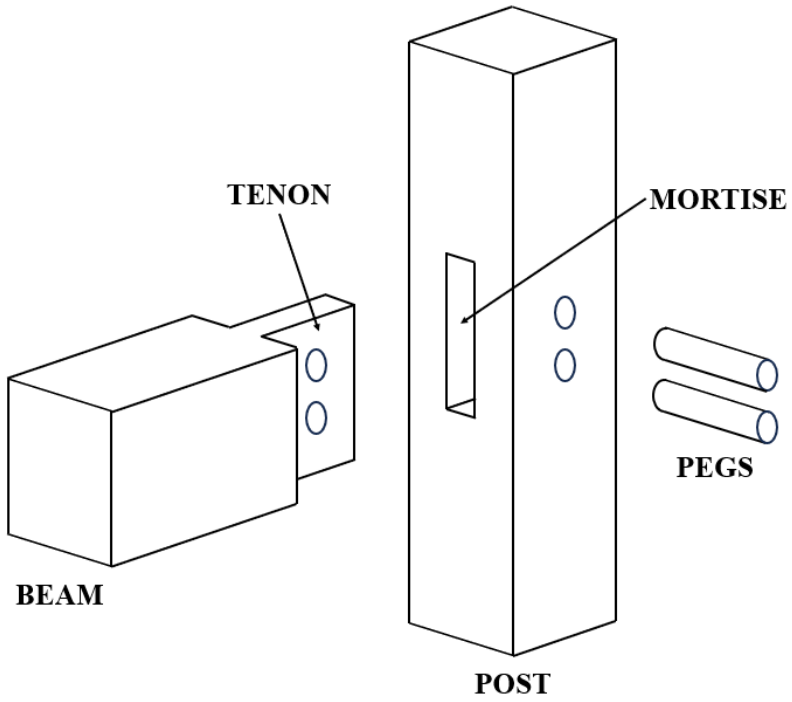

Figure 2: Mortise and Tenon Joint Adapted from Miller (2004)

Brungraber (1985) investigated the performance of timber frame bents and mortise and tenon connections validated by finite element modeling. Bulleit et al. (1999) examined the behavior of four types of mortise and tenon joints and provided commentary on the proper modeling of timber frames in structural analysis software. The four types of connections studied were the mortise and tenon, mortise and tenon with a shoulder, mortise and tenon with a shoulder and knee brace, and fork and tongue. Bulleit et al. (1999) determined the tightness of the joint significantly impacted the damage caused to the peg by loading. Further, when modeling timber frames without knee braces, connections can be modeled as pins. The same is true for when knee braces are included; however, a reduction in axial stiffness in the knee brace must be applied to account for the peg capacity (Bulleit et al.,1999).

Sandberg et al. (2000) modeled the stiffness of oak pegs in mortise and tenon joints to estimate the stiffness of pegged knee brace joints. Both maple and pine joints were examined

with tenons oriented both parallel and perpendicular to the grain and two different mortise thicknesses were tested. Additionally, the experimental capacity of the pegged connections, Z, was compared to the European Yield Model (EYM) equations provided by the NDS, which are based on steel fasteners in wood joints (Sandberg et al., 2000).

Miller (2004) conducted research to determine peg shear strength using full-sized mortise and tenon joints and yellow-poplar pegs. Finite element models were used to validate experimental results. A design method for tension-loaded mortise and tenon joints was developed based on the allowable shear stress and specific gravities of the peg, mortise, and tenon. The research also established yellow-poplar as a viable hardwood for timber framing.

Shanks and Walker (2009) investigated green oak mortise and tenon connections common to the United Kingdom. The pegged connection strength and stiffness were modeled using an energy approach and a four-point beam bending analogy. The research suggested that the stiffness of the connection is inversely proportional to the length of the shear span of the peg and that the connection stiffness can be increased by ensuring a stiff bearing and tight fit between the mortise and tenon (Shanks and Walker, 2009).

Miller et al. (2010) proposed a new failure mode for wood pegs, Mode V, which quantifies the cross-grain yielding of the peg. Yield Mode V is a conglomerate peg shearing, peg bending, and peg dowel-bearing yield mode (Miller et al., 2010). A new yield limit equation was developed for Mode V which can be used in conjunction with those provided in the NDS, shown in Equation 1 and Equation 2, for single shear and double shear, respectively. The Mode V failure mode is currently included in Timber Frame Engineering Council (TFEC) literature (TFEC-1, 2019), which can be used as a compliment to the NDS for specific timber frame projects. Miller et al. (2010) also produced two regression equations to predict dowel-bearing

strength based on the orientation of the grain relative to the loading direction. The dowel-bearing strength is shown in Equation 3 and Equation 4 for perpendicular to grain and parallel to grain, respectively.

$$Z_V = \frac{\pi D^2 F_{vy}}{4} \text{(single shear)} \quad (1)$$

$$Z_V = \frac{\pi D^2 F_{vy}}{2R_d} \text{(double shear)} \quad (2)$$

Where,

D = dowel diameter

F_{vy} = average Mode V yield stress in kPa (psi)

$F_{vy} = 33{,}440\ G_{PEG}\ G_{BASE}^{3/4}$ ($F_{vy} = 4{,}850\ G_{PEG}\ G_{BASE}^{3/4}$)

G_{PEG} = specific gravity of the peg material

G_{BASE} = specific gravity of the base material

R_d = 3.5 (reduction term)

(3)

$$F_{e\perp} = 33{,}780\ G_{PEG}\sqrt{G_{BASE}}\ \left(F_{e\perp} = 4{,}850\ G_{PEG}G_{BASE}^{\frac{3}{4}}\right)$$

(4)

$$Fe_{||} = 32{,}890\ G_{PEG}^{1.32}\ (Fe_{||} = 4{,}770\ G_{PEG}^{1.32})$$

Where,

$F_{e\perp}$ = dowel-bearing strength in kPa (psi) at yield of the base timber when loaded perpendicular to the grain

$Fe_{||}$ = dowel-bearing strength in kPa (psi) at yield of the base timber when loaded parallel to the grain

Hindman (2019) performed bending tests on 360 pegs of four different species and various diameters. The 5% offset yield load was used to determine the yield strength of all pegs. From the 5% offset yield equations Hindman developed linear, 1-factor power, and 2-factor power regression equations to predict the yield strength of the pegs. Ultimately, the linear regression model was chosen as the best model to predict the yield strength of the pegs due to its simplicity and similar R^2 value to the more complex 1-factor power and 2-factor power regression models (Hindman, 2019).

Xu et al. (2024) investigated the use of densified wood dowels and the impact the number of dowels in a connection had on the load capacity, stiffness, and ductility of double-shear joints loaded parallel to grain. Additionally, Xu et al. (2024) also examined connection geometries by testing both the NDS prescribed spacing between fasteners, and end and edge distances to obtain

a C_Δ = 1.0 with those required to obtain a C_Δ = 0.5. The impact of relative humidity on the performance of the connections was examined by Xu et al. (2024) by storing specimens at either 65% or 85% relative humidity. All densified wood dowels used were 12mm in diameter and were compared to the results of 12mm dowels. Ultimately, the research determined that the use of reduced fastener spacings, end and edge distances had no statistical impact on the connection capacity, stiffness, or ductility (Xu et al., 2024). Further, Xu et al. (2024) determined that the load carrying capacity of a group of densified dowels could be predicted from the performance of just one dowel by simply multiplying the capacity of one dowel by the number of dowels in the connection. The research proved that with a greater moisture content of the wood, the performance of the connection when fastened with steel dowel decreased. Conversely, when using densified wood dowels at two different moisture contents, no statistically significant difference was observed in the connection capacity, stiffness, or ductility (Xu et al., 2024).

2.3 CROSS-LAMINATED TIMBER

CLT is defined as, "a prefabricated engineered wood product made of at least three orthogonal layers of graded sawn lumber or structural composite lumber (SCL) that are laminated by gluing with structural adhesives" (ANSI/APA, 2019). Many have cited the CLT as originating in Austria in the 1990s through a joint venture between academia and industry (Karacabeyli & Douglas, 2013). However, through a deep search into the United States Patent and Trademark Office's Public Patent Search it was determined that two men from Tacoma, Washington filed and obtained a patent for what they called composite lumber in the early 1920's (Walsh & Watts, 1923). Although Walsh and Watts did not coin the term cross-laminated timber, a simple inspection of the figures in the patent undoubtedly illustrates what is now called cross-laminated timber. Despite CLT being patented over 100 years ago and further developed in the

1990s, CLT did not gain much traction until the early 2000s in Europe and until the early 2010s in North America (Karacabeyli & Douglas, 2013).

Prior to code adoption, CLT was promoted as the building material of the future in the *CLT Handbook* which was originally published in Canada (Gagnon & Pirvu, 2011) and later adopted for the United States (Karacabeyli & Douglas, 2013). The technical insight presented in the handbooks was a catalyst for the addition of CLT to the *Canadian Standard for Engineering Design in Wood* (CSA, 2016), the *National Design Specification for Wood Construction* (NDS) (AWC, 2018), and *Special Design Provisions for Wind and Seismic* (SDPWS) (AWC, 2021) in the United States. By adding CLT to the NDS, CLT was now included in the International Building Code (IBC) (ICC, 2021). With this addition came three new types of construction including Type IV-A, IV-B, and IV-C which allow for the construction of mass timber buildings up to 18 stories (ICC, 2021).

Since the permittance of mass timber buildings to be constructed up to 18 stories, the research time devoted to finding more efficient and sustainable methods for erecting mass timber structures has grown significantly. There are many advantages to using CLT as a building material including shorter construction times, high strength-to-weight ratio, seismic and acoustic performance, fire protection, and a reduced carbon footprint (Brandner et al., 2016).

Guidance for the design of structures using CLT in the United States is presented in the NDS and SDPWS, however, the specifications for the production of CLT are governed by ANSI/APA PRG-320 - *Standard for Performance-rated Cross-Laminated Timber* (ANSI/APA, 2019). The standard currently provides requirements and test methods solely for softwood species. After the promising work of several researchers on hardwoods species in CLT (Aicher et al., 2016; Hematabadi et al., 2020; Kramer et al., 2014; Mohamadzadeh & Hindman, 2015; Satir et al.,

2024), revisions are in place for the next publishing of PRG-320 in 2025 to include guidance on the use of hardwood species in CLT.

2.4 CROSS-LAMINATED TIMBER CONSTRUCTION METHODS

Due to its mechanical properties and inherent size, there are only certain elements in a building which benefit from the advantages of using CLT. Initially, CLT was primarily considered as a bending element for its ability to resist gravity forces in a building system. However, in smaller buildings and homes, CLT was used as a shear wall. With time the idea of using CLT as a lateral force-resisting system (LRFS) grew out of its inherent in-plane strength and stiffness (Barber et al., 2022; Breneman et al., 2023). After CLT's initial adoption into the NDS in 2018, CLT was adopted into SDPWS in 2021, which provides design guidance for the use of CLT as a LFRS (AWC, 2018; AWC, 2021).

There are two distinct typers of LFRS: vertical and horizontal. A horizontal LRFS is known as a diaphragm. There are several different types of vertical LFRS with the most common being the shear wall. Lateral forces from wind and seismic loads travel from their point of origin through the diaphragm into the vertical LFRS and then into the foundation (Breneman et al., 2023).

A diaphragm consists of two main elements. First, is the shear resisting element. In a CLT diaphragm this would be considered the CLT panel. The second element is a boundary member which consists of chords and collectors. In a CLT diaphragm, the connections and fasteners are the chords and collectors. Chords are responsible for resisting moment forces in the diaphragm and are perpendicular to the applied force (Breyer et al., 2020; AWC, 2021). Collectors, also known as struts, are members that are parallel to the applied force and transmit the forces to the shear walls or braced frame (Breyer et al., 2020; AWC, 2021). Figure 3 is a diagram of the shear

and moment transfer in a diaphragm. A diaphragm must be designed for loading in both the transverse and longitudinal directions. The purpose of an element depends on the direction of the loading. As illustrated in Figure 4, when the loading shifts from transverse to longitudinal, chords become collectors and vice versa. CLT diaphragms are designed based on engineering mechanics principles with diaphragm connections following guidance in the NDS (Barber et al., 2022; AWC, 2021). The design loads, allowable deformations, and deflections for CLT diaphragms can be determined from ASCE 7 (ASCE, 2022). The primary advantage of a CLT diaphragm compared to other materials is the ability to eliminate structural sheathing or a concrete topping from the assembly (Barber et al., 2022).

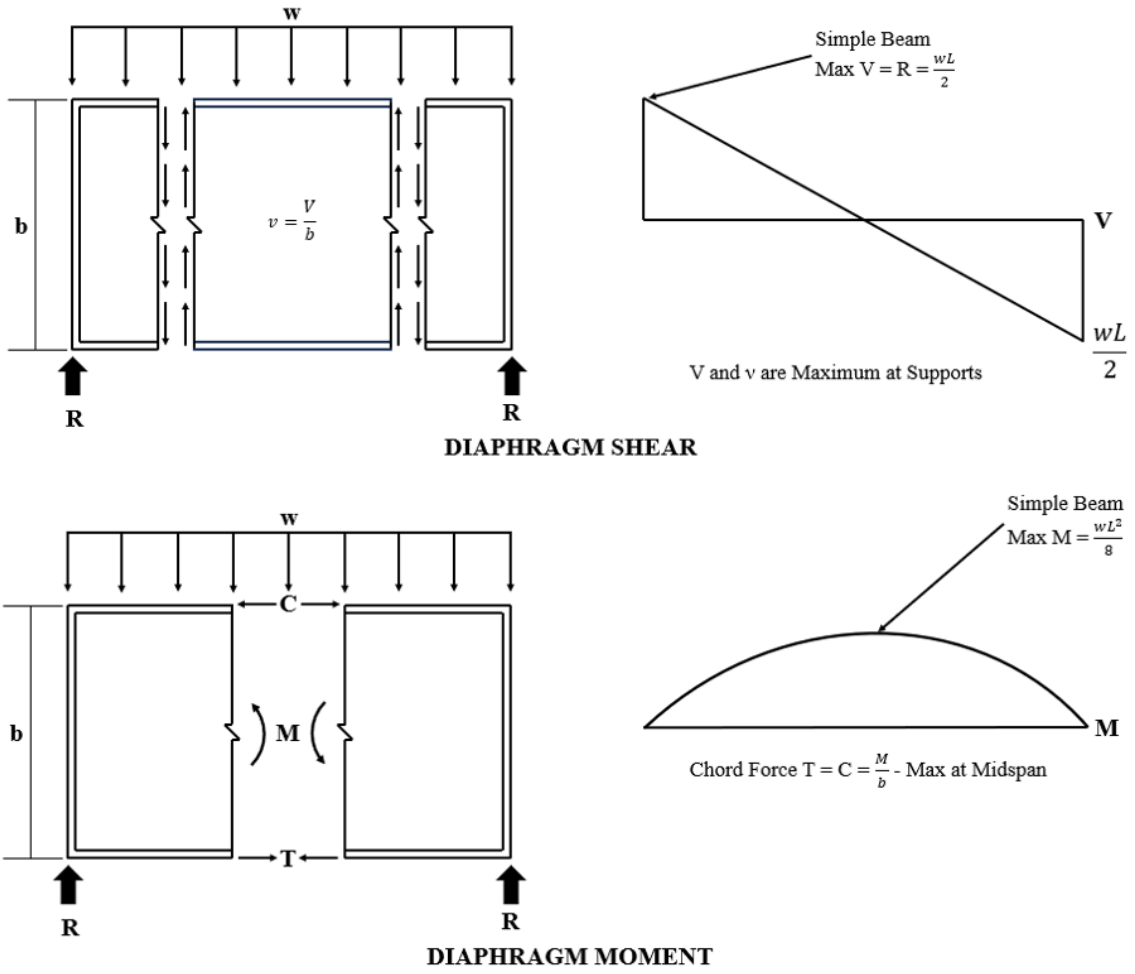

Figure 3: Diaphragm Forces Adapted from Design of Wood Structures (Breyer et al., 2020)

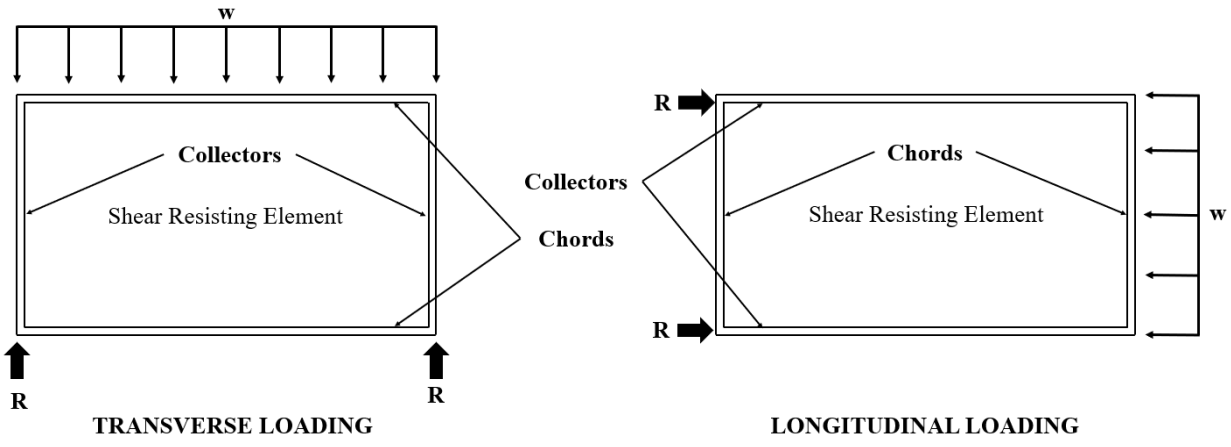

Figure 4: Diaphragm Boundary Members Adapted from Design of Wood Structures (Breyer et al., 2020)

Another important aspect of diaphragms is their flexibility. The flexibility of a diaphragm is important in determining how forces are distributed into the diaphragm. Typically, diaphragms fall into one of two categories: flexible or rigid. In a flexible diaphragm the loads are distributed by area (AWC, 2021). Conversely, in a rigid diaphragm, the loads are distributed by stiffness of the supporting elements (AWC, 2021). If a diaphragm cannot obviously be designated as rigid or flexible, it is known as semi-rigid (TFEC, 2020). In a semi-rigid diaphragm, the loads are distributed based on the stiffness of the diaphragm and the vertical elements (AWC, 2021). Alternatively, a semi-rigid diaphragm can be designed based on the worst loading case resulting from a flexible and rigid diaphragm analysis (AWC, 2021).

CLT diaphragms are commonly assumed to be rigid, however, there are some exceptions (TFEC, 2020). The aspect ratio (length: width) of a CLT diaphragm should not be greater than 3:1 if a non-composite concrete topping is present, or 2:1 if no concrete topping is present (TFEC, 2020). If the aspect ratio is greater than the limits listed previously, but less than 4:1, a semi-rigid model may be used for the diaphragm (TFEC, 2020). It should be noted that the CLT diaphragm should be considered flexible if the in-plane deflection is more than twice the average drift of the vertical LFRS as determined by ASCE 7 (TFEC, 2020; ASCE 2022). Lastly, in no case should the diaphragm aspect ratio exceed 4:1 (TFEC, 2020).

It is typical for the fasteners in CLT diaphragms to be uniformly spaced along the panel edges. The uniformly spaced fasteners are designed to resist shear forces in the diaphragm and prevent CLT panels from sliding past each other. Given that the fasteners are uniformly spaced, a unit shear capacity, v_n, of the fasteners can be calculated using Equation 5 (AWC, 2021). The unit shear may only be applied in the design of fasteners used in the transferring of shear forces between CLT panels and between CLT panels and their connecting boundary elements (AWC,

2021). It shall be noted that the strength of the CLT diaphragm is usually limited by the strength of the connections, as such, the importance of properly specifying fasteners cannot be overstated (TFEC, 2020; Barber et al., 2022).

(5)

$$v_n = 4.5Z^* \frac{12\frac{in.}{ft}}{s}$$

Where,

Z^* = NDS ASD reference lateral design value for a single fastener connection, Z, multiplied by all applicable NDS adjustment factors except C_d, K_F , φ, and λ.

4.5 = constant to adjust an NDS reference lateral design value, Z, from a normal duration ASD basis to a short duration ASD basis duration SDPWS nominal shear capacity.

s = diaphragm shear fastener spacing, in.

2.5 CROSS-LAMINATED TIMBER DIAPHRAGM CONNECTION TYPES

There are three primary joints used in panel-to-panel CLT diaphragm connections. The three joint types are known as the butt, half-lap, and spline as illustrated in Figure 5. The butt joint is the simplest joint which does not require any machining. There are two primary methods for connecting CLT panels in a butt joint. The first method is joined by butting the adjacent panels together and then fastening the joint with fully threaded shear screws driven at 45˚ to the surface. The screws in the butt joint can add significant ductility to the connection. One of the challenges with installing 45˚ fully threaded screws into a butt joint is making sure the panels are pulled tightly together so that the screws do not lock in any unwanted gaps in the joint

(Mahamid, 2020). The second method for fastening the butt joint is with steel straps or plates fastened to both the top and bottom of the joint. The plates and straps are manufactured with predrilled holes for the fasteners. Nails or screws may be used with straps and plates depending on the forces and desired performance of the connection.

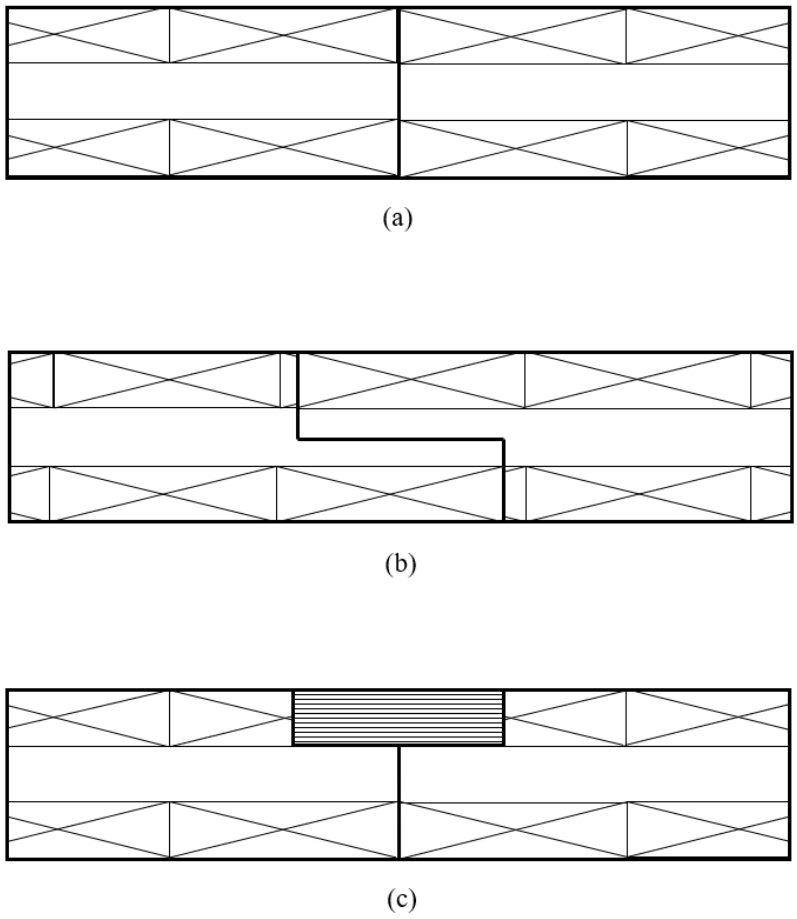

Figure 5: CLT Panel-to-Panel Connections (a) Butt Joint (b) Half-Lap Joint (c) Spline Joint

The lap joint requires significant machining compared to the butt and spline joints. To fabricate a lap joint, half of the depth of the CLT panel is removed over the width of the joint on each adjoining panel edge. When assembled, the panels are oriented so that one half-lap sits on the half-lap of the adjacent panel. Once in place, both partially threaded, or fully threaded screws can be employed to fasten the joint. Partially threaded screws are often used in half-lap joints to

eliminate gaps and transfer in-plane shear forces, but fully threaded screws can also be employed for the transferring of shear forces between panels (Mahamid, 2020). In addition to resisting shear forces along the joint, half-lap connections can also be used to resist tension forces pulling the joint apart (Mahamid, 2020). Figure 6(a) shows shear in the major panel direction (parallel to the joint), and tensile forces in the minor panel direction are shown in Figure 6(b). Lastly, the half-lap provides equal potential for dowel bearing on either side of the joint which ultimately provides greater strength and stiffness to the joint (Mahamid, 2020).

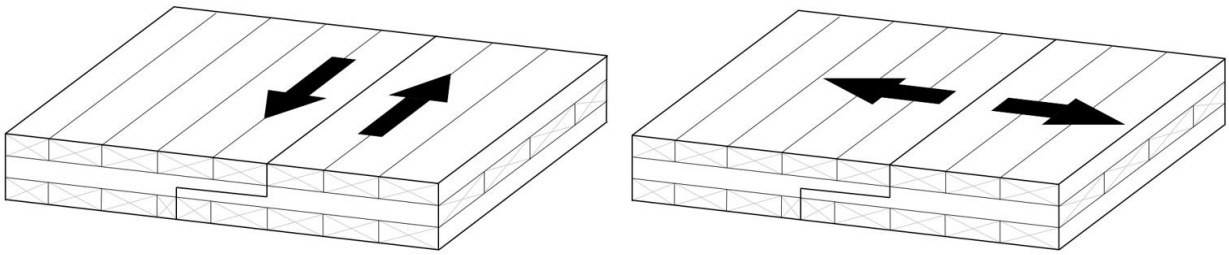

Figure 6: CLT Half-Lap Joint Subject to (a) Shear Forces Parallel to the Joint and (b) Tensile Forces Perpendicular to the Joint

Spline joints require less machining than the half-lap joint but more than the butt joint. The spline joint is similar to a butt joint, except a small portion on the top face of each adjoining panel is machined to the depth of the spline material. The spline is typically a strip of plywood, LVL, or another SCL fastened to each side of the joint with screws or nails. The advantage of the spline joint lies in its ease and speed of installation due to the ability to use slender fasteners (Mahamid, 2020).

2.6 CROSS-LAMINATED TIMBER CONNECTION RESEARCH

Several different authors have researched different methods of joining CLT in panel-to-panel connections. Gavric et al. (2012) performed one of the earliest and most comprehensive test regimes for CLT-to-CLT connections in which the mechanical properties of the fasteners and failure mechanisms of the connections were evaluated. Surface spline and half-lap joints fastened by screws were tested in both shear and tension in wall-to-wall, wall-to-floor, and floor-to-floor connections. The primary failure mechanism for the half-lap joint and the surface spline joints was the formation of a single plastic hinge in the screws. In wall-to-wall connections subject to shear, the half-lap joint was determined to be much stiffer than the surface spline joint. However, the ultimate displacement of the surface spline was greater than that of the half-lap. As such, the half-lap joint failed in a much more brittle manner than the surface spline joint. In the future, it was suggested that sufficient spacings, end distances, and edge distances be employed to prevent the creation of brittle failures (Gavric et al., 2012).

Sullivan et al. (2018) evaluated the performance of surface spline and half-lap joints in combination with vertical and angled fasteners under monotonic and cyclic loading. Ultimately the experimental results were compared to the calculated design capacities presented in the NDS and Eurocode. Sullivan et al. (2018) determined that surface splines had a lower initial stiffness, but higher ductility than the half-lap connections. Through the comparison of experimental to predicted values, an estimation index was calculated. Estimation index values greater than one indicated a conservative design approach. All the tests yielded an estimation index of at least two meaning that the actual safety factor was greater than the target safety factor (Sullivan et al., 2018).

Hossain et al. (2019) developed group-effect reduction factors for strength, stiffness, and ductility for self-tapping screws (STS) in CLT panel-to-panel connections loaded in shear under monotonic and cyclic loading. Five different STS joints were evaluated, the spline with STS in shear, half-lap with STS in shear, half-lap with STS in withdrawal, butt joint with STS in shear, and butt joint with STS in withdrawal. Hossain et al. (2019) determined that the capacity and stiffness of the joints were 9% lower when subjected to reversed cyclic loading compared to monotonic loading (Hossain et al., 2019). Lastly, the study built on and confirmed the results of Hossain et al. (2016) and Hossain et al. (2018), showing that when loaded in withdrawal the STS exhibit low ductility compared to when loaded in shear.

Jalilifar et al. (2021) explored the use of nails and screws in both half-lap and surface spline joints when subjected to monotonic and cyclic loading. Fastener orientation, type, length, and spacing were varied in the connections to determine their impact on the performance of the joints. The results of the half-lap joint subjected to shear were then validated against a finite element model. Jalilifar et al. (2021) concluded that the screwed connections have up to five times the load carrying capacity of the nailed connections when subject to monotonic loading and 1.75 times the load carrying capacity when subjected to cyclic loading (Jalilifar et al., 2021). Further, the fasteners driven at 90° carried a peak load 50% greater than that of fasteners driven at 45°. Lastly, the surface spline was determined to be a much more ductile connection than the half-lap due to there being twice the number of fasteners in the connection as compared to the half-lap connection (Jalilifar et al., 2021).

Hindman et al. (2022) examined the dowel-bearing capacity of southern pine CLT. Along with determining the dowel-bearing strength of the CLT, Hindman et al. (2022) proposed an alternative to the NDS method of determining dowel-bearing strength in CLT. Rather than

modifying the effective length of a fastener as the NDS suggests, Hindman et al. (2022) proposed an equation that considers the dowel bearing strength, thickness, and orientation of each layer of the CLT as shown in Equation 6. ASTM D5764, the 5% yield offset method was employed to determine the bearing capacity of the CLT. Ultimately, Hindman et al. (2022) found that the bearing strength was greater when more layers were oriented parallel to grain as opposed to perpendicular to grain. Hindman et al. (2022) also determined that the proposed method of calculating dowel bearing strength produced similar or slightly less conservative values than the NDS method.

(6)

$$f_{proposed} = \frac{\sum_{i=1}^{n=1} f_{NDS(i)} t_i}{l}$$

Where,

$f_{NDS(i)}$ = dowel bearing strength corresponding to load-grain angle for layer i (psi)

t_i = thickness of layer i (in)

n = total number of layers of layers of fastener penetration

l = total thickness of panel (in)

Hayes et al. (2023) investigated the seismic performance of CLT half-lap and surface spline joints used in the walls of balloon-framed structures. The experiments showed that the half-lap joints were much stiffer than the surface spline joints, however, the surface spline joints were much more ductile than the half-lap joints (Hayes et al., 2023). Hayes et al. (2023) also noted that the connections can be designed for both stiffness and ductility through the use of

fasteners oriented at 45° and 90° through the loading of the screws in shear and withdrawal. From a constructability perspective, it was noted that the half-lap joint may be more practical due to the reduction in fasteners employed and consequently the shorter assembly time (Hayes et al., 2023).

Vilguts et al. (2024) determined the single-shear capacity of hardwood dowels in CLT joints. Red oak and birch hardwood dowels were used and four species of CLT (Douglas-fir, grand-fir, western hemlock, and spruce-pine-fir) were employed to determine the impact of the specific gravity of the CLT on the shear strength of the connection. The research builds on the findings of Miller et al. (2010), primarily with the inclusion of yield Mode V, which is not included in the NDS. Through an ANOVA analysis, the CLT specific gravity was proven to have no statistical significance on the yield force of the joint. The specific gravity, dowel diameter, and CLT specific gravity did however statistically impact the serviceability stiffness (Vilguts et al., 2024). Further, a new equation was proposed for the yielding strength of the joint based solely on the specific gravity of the dowel as shown in Equation 7. Additionally, equations to predict the serviceability (Equation 8) and yield stiffness (Equation 9) of the joint were developed based on the specific gravity and diameter of the dowel and the specific gravity of the CLT. It was determined that the stiffness and strength of large diameter hardwood dowels are comparable to those of typical steel screws employed in CLT-to-CLT single shear connections. Most notable, 25.4 mm dowels had a greater yield strength than 7 mm, 10 mm, and 13 mm screws by a factor of 1.5 - 2 (Vilguts et al., 2024).

(7)

$$F_{vy} = 0.031\ G_{PEG}^{1.1}$$

(8)

$$K_{SER} = 0.7\ G_{PEG}^{2.7}\ G_{CLT}^{0.25}\ D$$

(9)

$$K_y = \frac{7}{10} K_{SER}$$

Where,

K_{SER} = serviceability stiffness, kPa

G_{CLT} = specific gravity of CLT

$K_y = \frac{7}{10} K_{SER}$

K_y = yielding stiffness, kPa

2.7 CROSS-LAMINATED TIMBER PEGGED CONNECTIONS

Hardwood dowels (pegs) have long been used as a method of joining timbers for both structural and furniture uses. Despite the long history of the use of pegs in structural timber applications, not until recently were pegs considered for use in CLT and other mass timber applications. Not only do pegs provide another method for connecting structural elements, but they may also prove useful in the construction industry's effort to be more sustainable. Wooden fasteners such as hardwood dowels, have a smaller carbon footprint than traditional steel fasteners (Sotayo et al., 2020; Lukić et al., 2021). Another advantage pegs have is the ability to join elements without the use of adhesives. In many instances the use of adhesives not only reduces recyclability but also raises concerns about the release of toxic gases and volatile organic

compounds, especially with formaldehyde and isocyanate-based adhesives (Sotayo et al., 2020; Pereira et al., 2021). Several authors have noted similar performance from connections using hardwood dowels instead of steel fasteners (Lukić et al., 2021; Morris et al., 2021; Sandoli et al., 2023; Vilguts et al., 2024). Based on the similar strengths of screws and pegs, it could be suggested that pegs may be a cost-effective alternative to screws, noting however that prices fluctuate and vary by manufacturer. Lastly, the use of pegs can be beneficial when considering deconstruction and reuse of CLT panels due to their ability to be to make connections componentized and ability to be machined without being removed (Marmo, R, 2010).

2.8 LITERATURE REVIEW SUMMARY

The NDS provides a solid foundation of reference material for this research when considering the specified spacing and failure modes of the pegs in the research. Research conducted on timber frames and pegged connections provides insight into the expected performance of joints and the addition of Yield Mode V which is not included in the NDS. Experiments conducted on various CLT connections prove that the butt, half-lap, and spline joint are effective methods for joining CLT in a panel-to-panel connection and it can be joined using modern fasteners like nails and screws.

This research plans to fill a gap in knowledge about the use of pegs in half-lap CLT panel-to-panel connections. By building upon the methods of joining members from the timber frame industry and applying them to a modern material like CLT, it is the hope that this research establishes new, more efficient methods for joining CLT. The use of pegs in half-lap joints may allow for faster construction, deconstruction, and the ability to reuse CLT panels without removing the pegs unlike metallic fasteners. Lastly, it is the hope that this research inspires further research into traditional methods for joining mass timber structures.

3.0 MATERIALS AND METHODS

3.1 MATERIALS

To reduce the number of testing variables, one species of hardwood peg was used. The species was chosen to be red oak (*Quercus rubra*) as it is readily available and relatively inexpensive. The pegs were manufactured by Northcott Wood Turning in Walpole, New Hampshire. The pegs used to join the half-laps were 1 inch and 1.25 inch in diameter. 1 inch diameter pegs were chosen as they are a common diameter employed in traditional timber framing and have comparable stiffness to 10 mm and 13mm diameter screws (Vilguts et al., 2024). The 1.25 inch diameter pegs were chosen with the goal of increasing peg spacing in the joint due to the larger diameter peg increasing the strength of the joint. An increase in the required peg spacing would be beneficial as fewer pegs would be needed per joint and installation times would decrease as fewer pegs would need to be installed. Additionally, most of the research on pegged connections was conducted using 1 inch diameter and smaller pegs, without much information on the performance pegs greater than 1 inch in diameter.

Upon arrival of the red oak pegs to the Thomas M. Brooks Forest Products Center at Virginia Tech (Brooks Center), the pegs were placed into an environmental chamber at 20˚C and 65% relative humidity, which roughly brought the pegs to an equilibrium moisture content of 13%. The moisture content of the pegs in the environmental chamber was verified by the use of a Delmhorst J-2000 Wood Moisture Meter. Prior to installation of the pegs into the half-lap joints, the dowels were placed into a Blue M Stabil-Therm Oven at 100˚C for 24 hours. After 24 hours the moisture content of the pegs was taken with the Delmhorst Moisture Meter. If an individual peg had an average moisture content at or below 8.5%, the pegs were considered dry enough for installation.

Based on the findings of Vilguts et al. (2024) the specific gravity of the CLT had no statistical influence on the yield capacity of pegged connections. To confirm the findings of Vilguts et al., (2024) both 3-ply yellow-poplar *(Liriodendron tulipifera)* and 3-ply Austrian spruce (*Picea abies*) CLT was used. The yellow-poplar CLT panels were manufactured by SmartLam North America in Dothan, Alabama. A one-part polyurethane (PUR) adhesive was used to face glue No.2 lumber selected for no knots using a cold-air bag press at a pressure of 965 kilopascals (140 psi).

The Austrian spruce CLT panels were produced by KLH Massivholz GmbH in Austria. A one-part, formaldehyde-free PUR adhesive was applied to both the face and edge joint of the three-ply Austrian spruce panels which were pressed at a pressure of 600 kilopascals (87 psi). The yellow-poplar and Austrian spruce CLT was stored in the Wood Engineering Laboratory at the Brooks Center at Virginia Tech. A comparable CLT species to Austrian spruce that is readily available in the United States is spruce-pine-fir, which has an NDS (AWC, 2018) tabulated specific gravity of 0.42.

Originally the yellow-poplar CLT panels were pressed as 7-ply panels and cut into 12 inch wide beams with respect to the minor axis. To increase the number of test specimens and obtain a thickness of CLT commonly used, the 7-ply panels were cut in half and milled into 3-ply panels. Figure 7 is a photograph of planed 3-ply yellow-poplar CLT prior to planning. Figure 8 is a photograph of a 1.25 inch diameter yellow-poplar joint post machining of the half-lap.

Figure 7: Planed 3-Ply Yellow-Poplar Prior to Half-Lap Cut

Figure 8: 1.25 Inch Diameter Yellow-Poplar Half-lap Post Machining

Prior to testing, the Austrian spruce CLT was used in full-scale shear wall tests at the Thomas M. Murray Structures and Materials Laboratory in which all failures in the panel were located near the top and bottom of the panel. Undamaged sections of the Austrian spruce panels were cut into smaller sizes for ease of transport to the Brooks Center. Figures 9 and 10 are

photographs of a machined center and side member, respectively for a 1 inch diameter Austrian spruce test specimen. The half-lap notches were cut using a table saw. After every stage of cutting the specimens, the specimens were measured to ensure accuracy of the cuts.

Figure 9: 1 Inch Diameter Austrian Spruce Machined Center Member

Figure 10: 1 Inch Diameter Austrian Spruce Machined Side Member

The location of holes for the half lap joints were measured and marked on the side members of the specimens as shown in Figure 11. Once the hole locations were identified, a pilot hole of 0.125 inch was drilled into all of the hole locations on the side members. With a pilot hole drilled, a spade bit was used to create the proper size hole for the peg. Once about halfway

through the side member, the member was flipped and drilled from the other direction in an attempt to prevent a blowout from occurring on the back of the member.

Figure 11: 1 Inch Diameter Yellow-Poplar Side Member with Hole Locations Identified Prior to Drilling

It shall be noted that the spade bit used to drill the holes was 0.0625 inch smaller than the nominal diameter of the peg used in the connection. For the 1 inch pegs a 0.9375 inch diameter spade bit was used and for the 1.25 inch pegs a 1.1875 inch diameter spade bit was used. Through trial and error, it was determined that a spade bit of the nominal dimension of the peg was large and led to the peg falling out of the hole. Conversely, a spade bit sized 0.125 inch smaller than the nominal peg diameter was too snug and, in all cases, led to the splitting of the

face lamination of the specimen. In other cases, the repeated hitting of the peg into the snug hole led to splitting of the dowel. As such, it was determined that the appropriate sized spade bit was 0.0625 inch smaller than the nominal peg diameter. An example of the splitting of a face lamination and peg due to using a 1.125 inch diameter spade bit on a 1.25 inch nominal diameter peg is shown in Figure 12.

Figure 12: Splitting of Face Lamination and Peg Due to Undersized Holes

Once the holes were drilled into the two side members, the center member was placed between the two side members and clamped in place. By clamping the three members together the goal was to reduce the gaps in the joints that may have resulted from the machining of the panels. Four clamps were placed on the faces of the members to reduce the gaps between the surfaces perpendicular to the dowel and two claps were placed on each end of the entire

specimen to eliminate gaps between the three members constituting a specimen as shown in Figure 13.

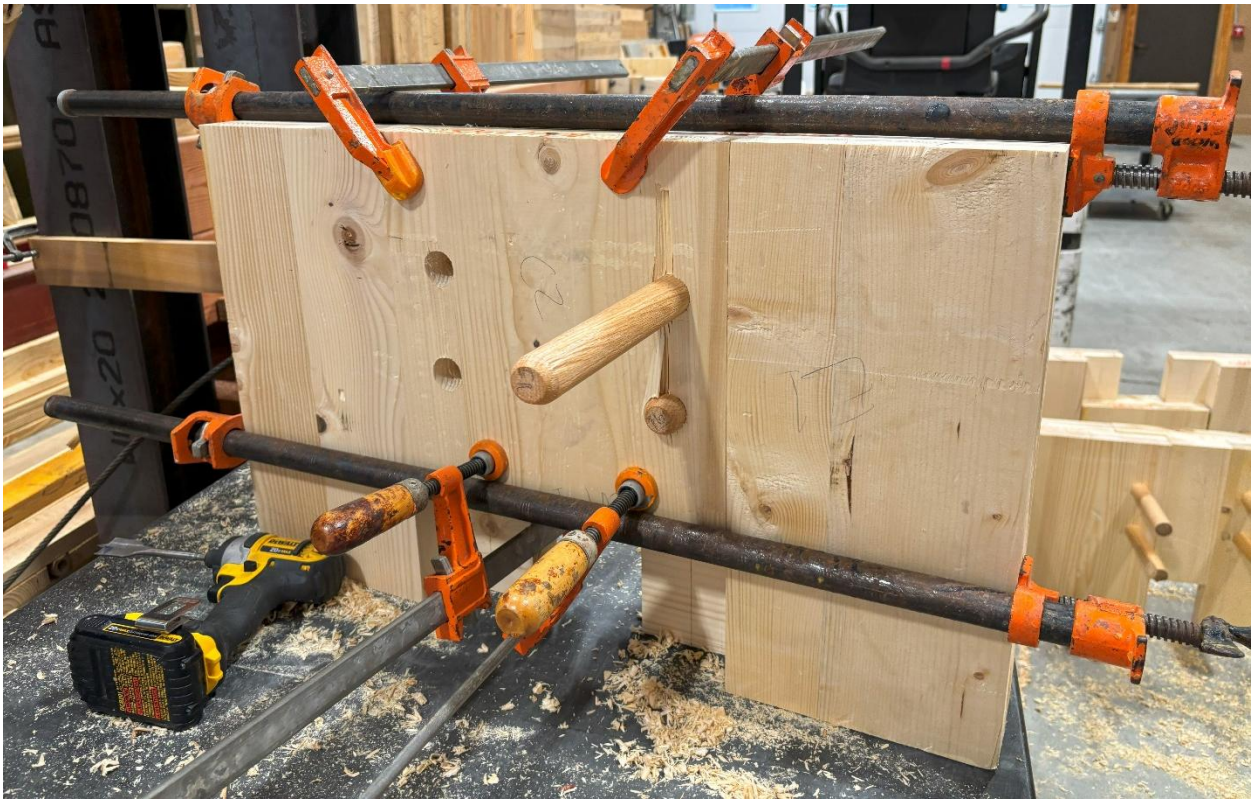

Figure 13: 1.25 Inch Austrian Spruce Specimen Showing Typical Clamp Orientation

Once the three members were clamped together, the spade bit was used to continue to drill the hole into the middle member from the existing holes in the side members. When the hole was drilled about halfway through the center member, a 0.125 inch drill bit was used to make a pilot hole through the rest of the center member. The pilot hole was then used to guide the drilling of the spade bit from the other face of the center member to prevent blowout.

The reason that the holes in the center members were not drilled based on the prescribed dimensions and then assembled is due to concerns of the hole misalignment. Further, by

clamping the members prior to drilling the holes in the center member, a tighter joint was created. Predrilling would have likely created gaps in the half-lap joints. From a constructability perspective, the method employed in the fabrication of the specimens is similar to what would occur in actual construction. If the pegged half-lap joint to be used in actual construction, it is likely that the top panel of the half-lap joint would arrive the site with the holes predrilled by a computer numerical control (CNC) machine. Once both panels constituting the half-lap joint were placed, the joint would be pulled tight with a series of panel pullers and then the holes would be completely drilled, using the predrilled holes as a guide. After drilling the holes all the way through the joint, the pegs would be driven. The assembly process previously described is beneficial in that it allows for construction tolerance errors, which fully predrilled joints would not allow for.

With the holes drilled all the way through both joints in the specimen, the clamps remained on the specimen and the pegs are driven into the specimen using a dead blow mallet. Once the pegs were fully installed, the clamps were removed, and the specimen was ready for testing.

3.1.1 Shear Test Specimens

Due to the constraints of the material availability at the time of testing, when designing the specimen connections according to the NDS, a C_Δ of 0.5 was employed. Although greater yield and ultimate loads may have been obtained by following the NDS recommended edge and end spacings for C_Δ = 1, the yellow-poplar CLT available to produce the test specimens was only 12 inch wide in its minor direction. Consequently, it was not possible to manufacture specimens with a C_Δ = 1 that would have appropriately simulated field conditions (AWC, 2018). Figure 14

is a dimensioned diagram of the shear test specimens for each species and Figure 15 is a diagram of the assembled test specimen section view.

A total of 36 shear tests were performed. Eighteen tests were performed with 1 inch diameter pegs and 18 tests were performed with 1.25 inch diameter holes. 3 monotonic tests and 6 cyclic tests were performed on joints with both peg diameters and both CLT species. A complete test schedule is shown in Table 5.

Table 5: Full Test Schedule

Test Schedule			
Peg Diameter (in)	CLT Species	Loading Type	No. Specimens
1	AS	Monotonic Shear	3
1	YP	Monotonic Shear	3
1.25	AS	Monotonic Shear	3
1.25	YP	Monotonic Shear	3
1	AS	Cyclic Shear	6
1	YP	Cyclic Shear	6
1.25	AS	Cyclic Shear	6
1.25	YP	Cyclic Shear	6
Total			**36**

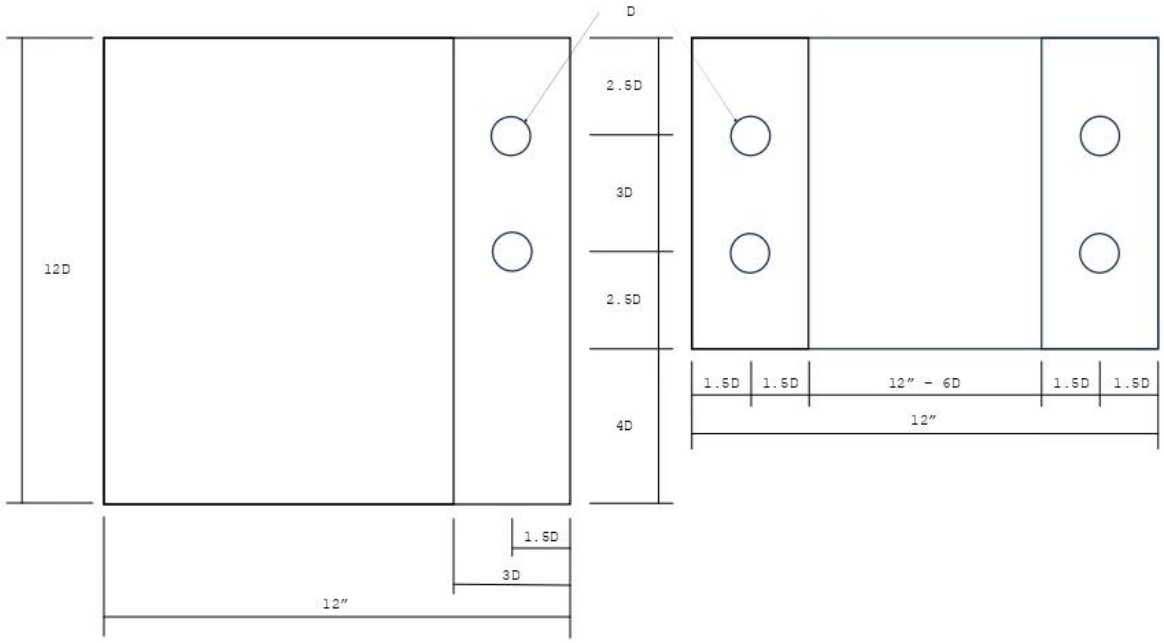

(a)

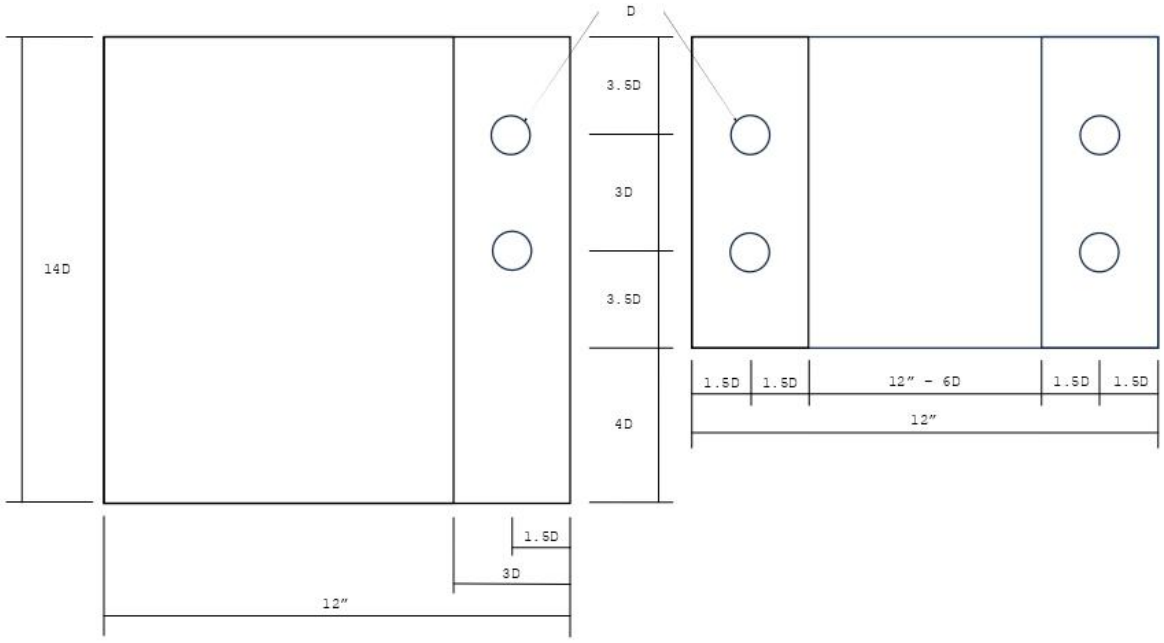

(b)

Figure 14: Shear Test Specimens Elevation View (a) Yellow-Poplar (b) Austrian Spruce

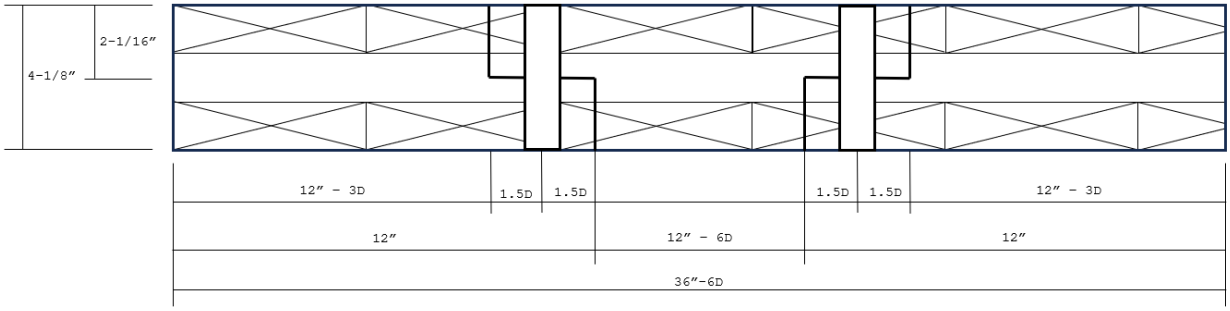

Figure 15: Shear Test Specimens Section View

3.2 METHODS

The primary objectives of the shear testing of the half-lap CLT pegged joint are to determine the yield load, ultimate load, stiffness of the connection, and determine the impact peg diameter and CLT species have on the performance of the connection.

3.2.1 Moisture Content and Specific Gravity

Following each test, the moisture content and specific gravity of each component of the assembly was determined using ASTM D4442 and ASTM D2395, respectively. Method A – Primary Oven-Drying Method of ASTM D4442 was followed. After cutting samples from the test specimens, the specimens were promptly weighed; this mass was considered the original mass of the sample. Method A requires a consistent oven temperature of 103 ± 2˚C throughout the duration of the test. The samples were considered dry when after a 3-hour interval in the oven the mass loss was equal to or less than twice the balance sensitivity. The balance sensitivity was determined to be 0.01 g. The weight of the specimen that met the balance sensitivity requirements was considered the oven-dry mass. The moisture content was calculated using Equation 10.

(10)

$$MC, \% = \frac{A - B}{B} \times 100$$

Where,

MC = moisture content

A = original mass of sample, g

B = oven-dry mass, g

The specific gravity of the specimens was determined following ASTM D2395 (ASTM, 2017). Test Method A – Volume by Measurement was employed due to the specimens being of a cuboid shape which made it easy to make linear measurements of the specimen's dimensions. After preparation of the sample the specimen was weighed and then placed in the oven and removed from the oven following the guidelines in ASTM D4442 (ASTM, 2020). The oven-dry mass of the specimen was taken as the final mass of the specimen once it had been completely oven dried. Moisture content samples were taken from each of the three components of each test specimen – one from each of the fixed side pieces, and one from the center piece. The method for determining the moisture content is presented in Equation 11. The equation used to calculate the density of the specimen during testing is presented in Equation 12. The specific gravity of the specimens is calculated using the Equation 13.

(11)

$$M = \frac{m_M - m_O}{m_O} \times 100$$

Where,

M = moisture content of specimen at the time of test, %

m_M = initial mass, g

m_O = oven-dry mass, g

(12)

$$\rho_M = \frac{m_M}{V_M}$$

Where,

ρ_M = density at testing moisture content

V_M = volume of specimen at testing moisture content

(13)

$$S_M = \frac{K \times m_O}{V_M}$$

K = constant depending on units used in measurement of mass and volume

3.2.2 5% Offset Method

To determine the yield load of the connection subjected to shear the 5% offset yield method was followed as recommended by ASTM D5652 (2021) and ASTM D5764 (2024), which is the procedure for the testing of bolted wood connections. In this procedure, a straight

line is fit to the initial linear portion of the load-displacement curve and that line is then offset by 5% of the fastener diameter. The load at which the load-displacement curve intersects with the 5% offset line is taken as the yield load as shown in Figure 16.

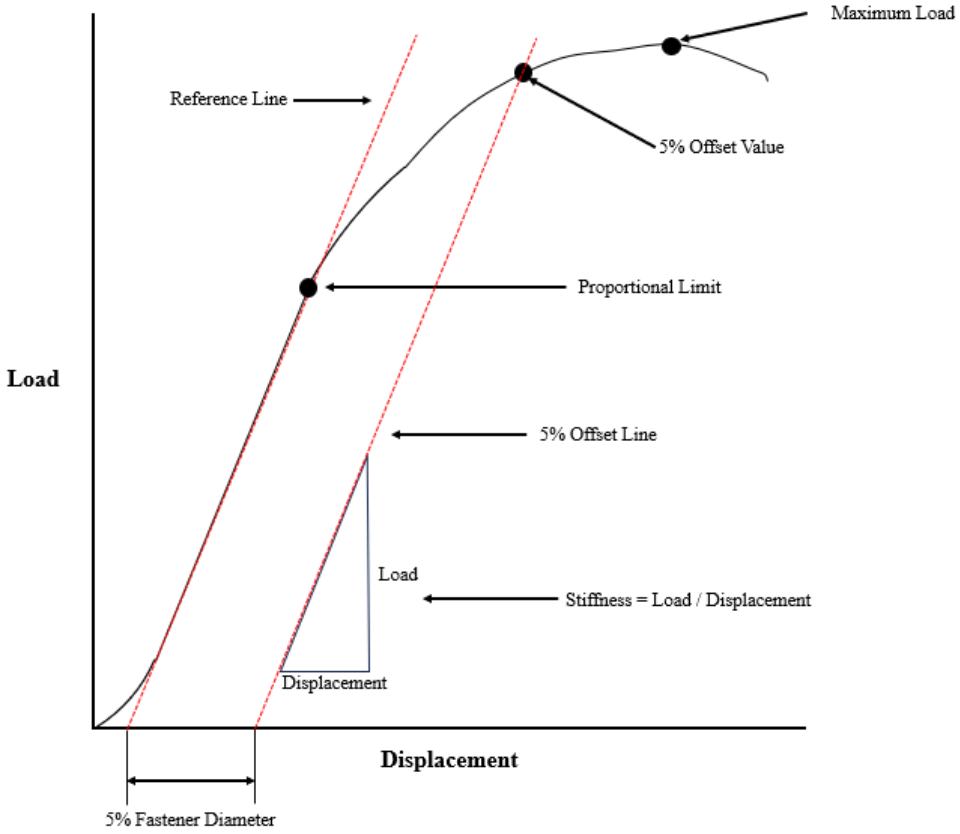

Figure 16: 5% Offset Method per ASTM D5652 (2021) and ASTM D5764 (2024)

The ultimate load is taken as the maximum load from the load-displacement curve as shown in Figure 16. Additionally, the stiffness of the connection is taken as the slope of the initial linear portion of the load-displacement curve per ASTM D5652 and ASTM D5764. The 5% offset method is somewhat arbitrary in the choosing of the initial stiffness line, however in most cases, stiffness was taken as a line of best fit between 10% and 50% of maximum load.

In the case of the shear test, it is assumed that the load is distributed equally among the four red oak pegs, as shown in Figure 17. Consequently, it is possible to determine the yield load,

maximum load, and stiffness of one peg in the connection following this assumption. Using the values obtained via the 5% offset method it is possible to compare experimental values to predicted values using the yield limit equations provided in the NDS.

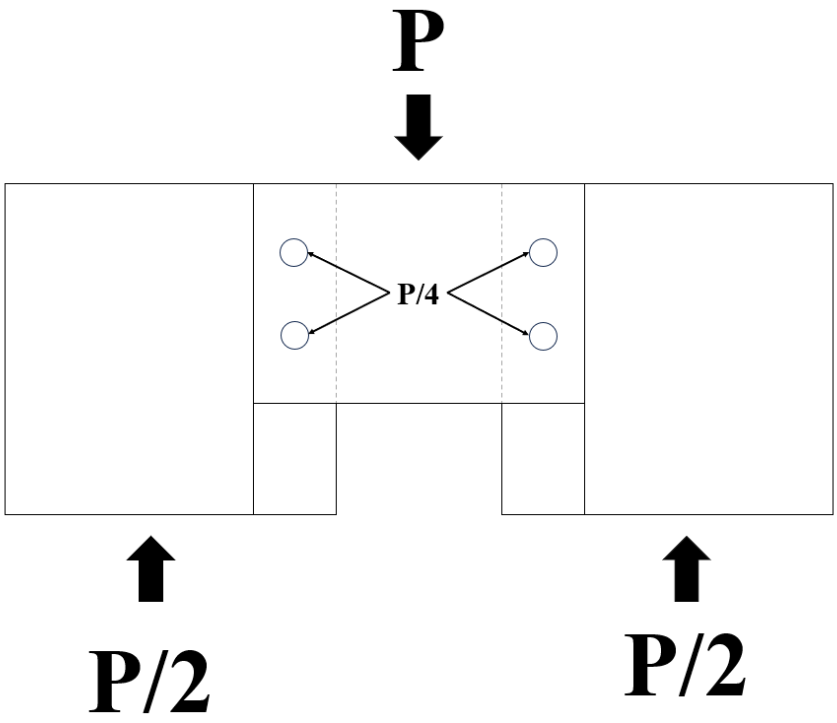

Figure 17: Assumed Loading Distribution Diagram for Shear Test

3.2.3 Shear Test Procedure

Shear testing of the half-lapped connections was conducted using an MTS Servo-Hydraulic Test Machine with a 50-kip load cell. A linear variable differential transducer (LVDT) was attached to each of the two joints to measure vertical displacement. Data pertaining to the load and deformation was acquired by the load cell and LVDTs. This data was then processed by the MTS FlexTest 40 data acquisition software to generate load-deformation curves.

For monotonic loading, ISO 6891 (ISO, 1983) was followed, which calls for one force-controlled cycle prior to the monotonic loading of the connection. The initial cyclic loading is

used to simulate as if the connection had been stressed prior to extreme loading as would be expected in field application. The ISO 6891 cyclic loading prior to monotonic loading peaks at 40% of the predicted yield load of the connection which is representative of service loads on a connection. For monotonic loading, the displacement rate was 0.787 in/min (2 mm/min). Testing continued until failure, defined as when the load dropped more than 20% of the peak load. The results from the monotonic testing were then used in the determination of the amplitudes of the cycles per the CUREE loading protocol. Photographs of the monotonic and cyclic test setup prior to testing are shown in Figure 18 and Figure 19, respectively.

Figure 18: Monotonic Test Setup

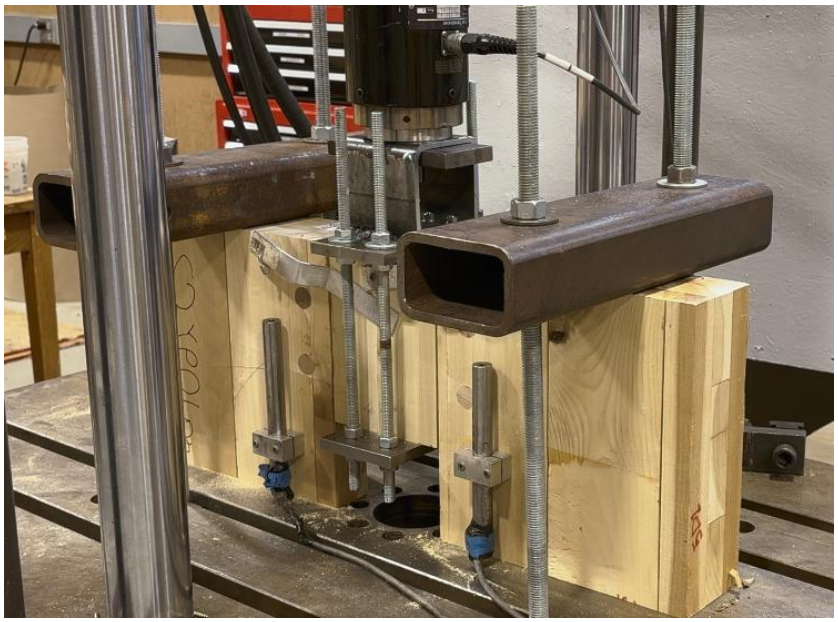

Figure 19: Cyclic Test Setup

Per ASTM E2126 (2019), at least one monotonic test is required to initially define the cyclic test displacement and a minimum of two cyclic tests are required if there is less than a 10% difference in the peak shear load of the connection. If the less than 10% difference in shear yield loads of the connections is not met, then a third cyclic test must be performed. A total of 3 monotonic and 6 cyclic shear tests were performed for each species and peg diameter satisfying the base requirements of ASTM E2126 (2019).

The cyclic shear testing protocol followed the CUREE testing recommendation as specified in the *Development of a Testing Protocol for Woodframe Structures* (Krawlinker et al., 2001) and ASTM E2126 (2019). The procedures relating to the loading and analysis from ASTM E2126 were followed. However, as the standard is written for vertical elements, modifications needed to be made to the Test Setup section as the specimen is intended as a horizontal (diaphragm) element.

3.2.4 Monotonic Loading Procedure

The monotonic loading for both the shear and tension tests followed the ISO 6891 standard titled: *Timber structures – Joints made with mechanical fasteners – General principles for the determination of strength and deformation characteristics*. Prior to the monotonic loading of the connection, the connection is loaded to $0.4F_{est}$ and held for 30 seconds (ISO, 1983), where F_{est} is the estimated maximum load. Then the load is reduced to $0.1F_{est}$ and held for 30 seconds. After being held at $0.1F_{est}$ for 30 seconds, the monotonic loading begins (ISO, 1983). Below $0.7F_{est}$, the applied displacement rate was $0.2F_{est}$ per minute. Above $0.7F_{est}$, the displacement rate is applied is constant so that the ultimate load is reached in 3 to 5 minutes beyond the $0.7F_{est}$ threshold (ISO, 1983). Figure 20 is a diagram of the loading procedure.

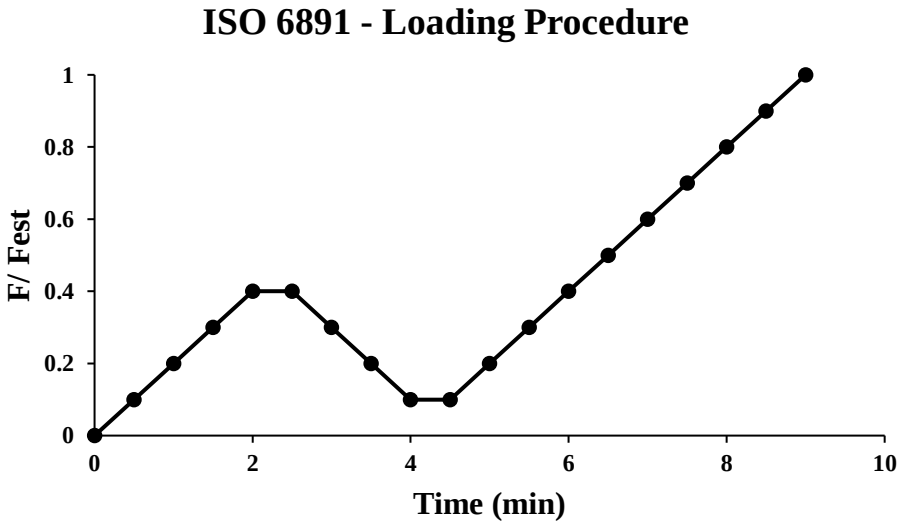

Figure 20: Loading Procedure per ISO 6891 (ISO, 1983)

3.2.5 Cyclic Loading Procedure

The cyclic loading procedure followed ASTM E2126-19 Method C which employs the use of the Consortium of Universities for Research in Earthquake Engineering (CUREE) Basic Loading Protocol (ASTM, 2019). The loading procedure prescribes incrementally increasing displacement cycles after six initiation cycles. The primary loading cycles are expressed as a percentage of the of a reference deformation, Δ, from the monotonic loading (ASTM, 2019). Following the primary loading cycle, the remaining cycles in the step are specified as 75% of the displacement of the primary loading cycle, known as trailing cycles. A table of the prescribed amplitudes and the corresponding minimum number of cycles are provided in Table 6. As is specified by Krawlinker et al. (2001), the monotonic deformation capacity, Δ_m , is taken as the first deformation point from monotonic loading that the load falls below 80% of peak load. From the monotonic deformation, the reference deformation is obtained by multiplying by a factor, γ, which is typically 0.6. The γ factor was taken as 0.6 in for the determination of the reference deformation in this study. The reference deformation, Δ, is equal to the monotonic deformation capacity multiplied by γ. In all steps 9 and beyond, α was taken as 0.5. Figure 21 is a diagram of the loading procedure for the CUREE Basic Loading Protocol.

Table 6: Amplitude of Primary Cycles per ASTM E2126 (ASTM, 2019)

Pattern	Step	Minimum Number of Cycles	Amplitude of Primary Cycle, %Δ
1	1	6	5
2	2	7	7.5
	3	7	10
3	4	4	20
	5	4	30
4	6	3	40
	7	3	70
	8	3	100
	9	3	100 + 100α*
	10	3	Additional increments of 100α until failure

* α = 0.5.

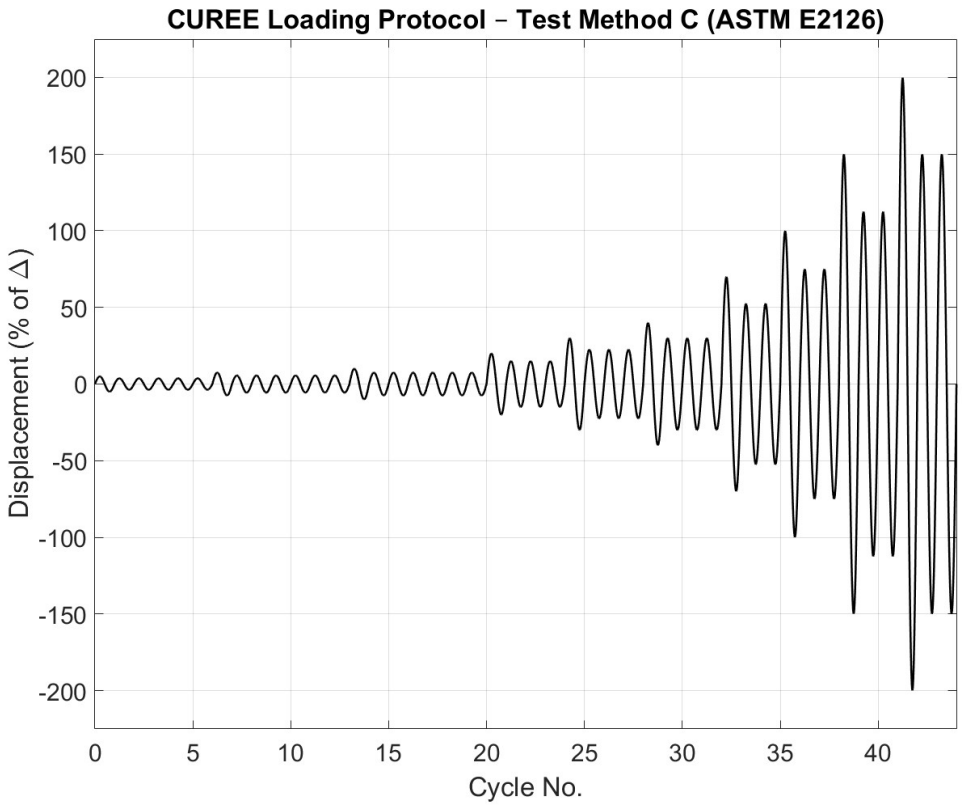

Figure 21: CUREE Loading Protocol per ASTM E2126 (ASTM, 2019)

3.2.6 Two-way ANOVA

To determine if the increase of peg diameter from 1 inch to 1.25 inch or the use of yellow-poplar versus Austrian spruce CLT had any effect on the yield load and stiffness of the connection, a two-way analysis of variance (ANOVA) was used. A two-way ANOVA is used to determine if there is an interaction between two independent variables on the dependent variable (Laerd, 2025). In this research, the peg diameter and CLT species are independent variables, and the yield load and stiffness of the connection are the dependent variables. The use of the two-way ANOVA will allow for confirmation of whether the findings of Vilguts et al. (2024) hold true in that the CLT species did not significantly affect the yield load of the connection. Further, from the two-way ANOVA it will also be possible to determine if there is a significant difference in yield load or stiffness from increasing the peg diameter from 1 inch to 1.25 inch. The null hypothesis, H_o, for an ANOVA analysis is presented below in equation 14, showing that the means are all equal, whereas Equation 15 presents the alternate hypothesis, H_a, in which at least one of the means is not equal to the others.

$$H_o: \mu_i = \mu_j \tag{14}$$

Where,

μ_i, μ_j = means from sample i and j

$$H_a: \mu_i \neq \mu_j \tag{15}$$

For the ANOVA analysis, a $\alpha = 0.05$ was used. In the event the p-value from the ANOVA analysis is less than α, the null hypothesis is rejected, signifying that the averages from the tests including different species and diameter pegs are different. If the p-value is greater than α, then the null hypothesis fails to be rejected.

4.0 RESULTS AND DICUSSION

4.1 MOISTURE CONTENT AND SPECIFIC GRAVITY

The average moisture content and specific gravity of the CLT of each half-lap connections from both monotonic and cyclic testing are shown in Table 7. The average moisture contents for all the tests were less than 6%. The 1 inch diameter Austrian spruce specimens had the greatest average moisture content of 5.43%, while the yellow-poplar 1.25 inch diameter specimens had the lowest moisture content of 5.15%. The 1 inch diameter yellow-poplar specimens had the lowest COV for moisture content of 4.40%. The greatest COV of moisture content was found in the 1.25 inch diameter Austrian spruce specimens, which had a COV of 15.3%.

Table 7: Average Moisture Content and Specific Gravity of CLT in Half-lap Connection

Average Combined Monotonic and Cyclic Moisture Content and Specific Gravity					
Peg Diameter	CLT Species	Moisture Content (%)	Moisture Content COV (%)	Specific Gravity	Specific Gravity COV (%)
1"	AS	5.43	5.89	0.402	7.44
1"	YP	5.16	4.40	0.488	13.0
1.25"	AS	5.15	15.3	0.426	12.0
1.25"	YP	5.18	9.86	0.490	12.8

From Table 7, the greatest average specific gravity was found for the 1.25 inch diameter yellow-poplar specimens (0.490). The lowest specific gravity of 0.402 was found in the 1 inch diameter Austrian spruce specimens. The specific gravity for the Austrian spruce specimens was less than that of the yellow-poplar specimens regardless of diameter. The specific gravity COVs ranged from 12.0% to 13.0% for all specimen groups except for the 1 inch diameter Austrian spruce specimens which had a COV of 7.44%.

The NDS (AWC, 2018) tabulated specific gravity for Austrian spruce is 0.43. For the 1 inch and 1.25 inch diameter Austrian spruce specimens the average specific gravities were found to be 0.402 and 0.426, respectively. The actual specific gravities in both of the Austrian spruce test groups were less than expected. Both specific gravities of the yellow-poplar were greater than the specific gravity value provided by the NDS (AWC, 2018) of 0.43. The average specific gravities of the 1 inch and 1.25 inch yellow-poplar specimens were 0.488 and 0.490, respectively.

The difference in expected and actual specific gravities for both the Austrian spruce and yellow-poplar specimens could lead to differences in the expected versus actual yield loads of the connections. In the case of the Austrian spruce, which had a lower specific gravity than provided in the NDS, the yield load would be less than predicted. For the yellow-poplar, a greater yield load would be expected from the experimental results than predicted yield load due to the greater experimental specific gravity values compared to the tabulated value in the NDS. It shall be noted that the experimental specific gravities of the Austrian spruce, yellow-poplar, and red oak were used in the calculation of the predicted values in Section 4.4.

The moisture content and specific gravity of the pegs are presented in Table 8. Rather than finding the moisture content and specific gravity of all tested pegs, a random sampling of five 1 inch diameter and five 1.25 inch diameter pegs was chosen. From Table 8 it can be seen that the moisture content of the pegs was 5.67% and 5.09% for 1 inch and 1.25 inch diameter pegs, respectively. The specific gravity of the red oak pegs was 0.796 and 0.742 for the 1 inch diameter and 1.25 inch diameter pegs, respectively. The NDS tabulated value for the specific gravity of the pegs is 0.67 (AWC, 2018). When comparing the experimental red oak specific gravities to the NDS provided value, the pegs used in testing had a greater average specific

gravity. For the 1 inch diameter pegs, the moisture content had a COV of 0.041% and the specific gravity had a COV of 3.82%. The 1.25 inch diameter pegs had COV of 0.037% and 4.75% for the moisture content and specific gravity, respectively.

Table 8: Red Oak Peg Moisture Content and Specific Gravity

Red Oak Peg Moisture Content and Specific Gravity				
Peg Diameter	Moisture Content (%)	Moisture Content COV (%)	Specific Gravity	Specific Gravity COV (%)
1"	5.67	0.041	0.796	3.82
1.25"	5.09	0.037	0.742	4.75

4.2 YIELD LOAD, MAXIMUM LOAD, AND STIFFNESS OF CONNECTION SUBJECT TO MONOTONIC LOADING

As noted in Section 3.2, the yield load and stiffness of each individual peg was assumed to be one fourth of the total yield load and stiffness of the connection, respectively. Presented below are the results of the total connection yield load and stiffness of the connection and then the assumed stiffness per peg following the previously stated assumption when subjected to monotonic loading following the ISO 6891 procedure.

The average 5% offset yield load and coefficient of variation (COV) values of the different CLT species and peg diameters are shown in Figure 9. The greatest 5% offset yield loads were found for the yellow-poplar specimens. For 1 inch and 1.25 inch diameter yellow-poplar specimens, the average yield loads were 7,160 lb and 8,910 lb, respectively. The average Austrian spruce yield loads were roughly 1,300 lb less than the average yellow-poplar specimens with yield loads of 5,820 lb and 7,540 lb for the 1 inch and 1.25 inch diameter specimens, respectively. The COV of the yield loads ranged from a minimum of 4.64% for the 1.25 inch diameter Austrian spruce specimens, to a maximum of 20.0% for the 1.25 inch yellow-poplar specimens. The percent difference calculations in Table 9, and all following tables were taken

with respect to the 1 inch Austrian spruce specimens. As can be seen from the right column, the percent difference was 23.0%, 29.5% and 53.1% for the 1 inch yellow-poplar, 1.25 inch Austrian spruce, and 1.25 inch yellow-poplar specimens, respectively.

Table 9: Half-lap Connection Yield Load of Yellow-Poplar and Austrian Spruce Subjected to Monotonic Loading

Average Connection Monotonic Yield Load				
Peg Diameter (in)	CLT Species	5% Offset Yield Load (lb)	5% Offset Yield Load COV (%)	Difference (%)
1	AS	5820	9.86	-
1	YP	7160	13.7	23.0
1.25	AS	7540	4.64	29.5
1.25	YP	8910	20.0	53.1

The average stiffnesses and corresponding COVs of the connections are shown in Table 10. Stiffnesses were determined as the slope of the 5% offset line as specified in ASTM D5652 (ASTM, 2021) and ASTM D5764 (ASTM, 2024). The lowest average stiffness was found for the 1 inch diameter Austrian spruce specimens (28,300 lb/in). The 1 inch yellow-poplar, 1.25 inch Austrian spruce, and 1.25 inch yellow-poplar specimens had similar average stiffness values of 43,700 lb/in, 41,700 lb/in, and 48,200 lb/in, respectively. The COVs were greatest for the 1 inch diameter yellow-poplar and 1.25 inch diamter Austrian spruce specimens which had COVs of 18.1% and 19.5%, respectively. The 1 inch diameter Austrian spruce specimens had a COV of 5.68% and the 1.25 inch diameter yellow-poplar had a COV of 9.51%. Compared to the 1 inch diameter Austrian spruce specimens, the 1 inch diameter yellow-poplar specimens were 54.8% stiffer. The 1.25 inch diameter Austrian spruce and yellow-poplar specimens were 47.4% and 70.5% stiffer respectively than the 1 inch diameter Austrian spruce specimens. When looking at

the general trends from the stiffnesses of the connections, it can be generalized that the yellow-poplar connections were stiffer than the Austrian spruce specimens.

Table 10: Half-lap Connection Stiffness of Yellow-Poplar and Austrian Spruce Subjected to Monotonic Loading

Average Connection Monotonic Stiffness				
Peg Diameter (in)	CLT Species	Connection Stiffness (lb/in)	Connection Stiffness COV (%)	Difference (%)
1	AS	28300	5.68	-
1	YP	43700	18.1	54.8
1.25	AS	41700	19.6	47.4
1.25	YP	48200	9.51	70.5

Shown in Table 11 is the average maximum loads of all the test groups subjected to monotonic loading. For 1 inch both 1.25 inch diameter pegs, there was an increase in maximum load from the Austrian spruce connections to the yellow-poplar specimens. The maximum load of the 1 inch diameter specimens were 7,790 lb and 8,790 lb for Austrian spruce and yellow-poplar specimens, respectively. For the 1.25 inch diameter specimens, the maximum load increased from 9,850 lb for the Austrian spruce specimens to 12,200 lb for the yellow-poplar specimens. The maximum load COVs were lowest for the Austriuan spruce specimens with COVs of 3.17% and 3.74% for the 1 inch and 1.25 inch diameter specimens, respectively. The yellow-poplar specimen COVs were 8.15% and 9.20% for the 1 inch and 1.25 inch diameter specimens, respectively. Evaluating the percent difference in maximum load compared to the 1 inch diameter Austrian spruce specimens, there was a 12.8% increase compared to the 1 inch diameter yellow-poplar specimens, a 26.5% increase compared to the 1.25 inch diameter Austrian spruce specimens, and a 56.6% increase compared to the 1.25 inch diameter yellow-poplar specimens.

Table 11: Half-lap Connection Maximum Load of Yellow-Poplar and Austrian Spruce Subjected to Monotonic Loading

Average Connection Monotonic Maximum Load				
Peg Diameter (in)	CLT Species	Maximum Load (lb)	Maximum Load COV (%)	Difference (%)
1	AS	7790	3.17	-
1	YP	8790	8.15	12.8
1.25	AS	9850	3.74	26.5
1.25	YP	12200	9.20	56.6

Figure 22 is a graph of the load versus displacement for a representative monotonic test of the 1 inch peg diameter Austrian spruce test group. The maximum load and displacement point is denoted by the red circle on the plot. The maximum displacement and load for specimen M2ASD1.00 (monotonic test 2, Austrian spruce CLT, 1 inch diameter pegs) was 0.589 inches and 7.82 kips, respectively. The yield point was determined using the 5% offset method as stated previously. Although, the determination of the initial linear portion of the plot is somewhat arbitrary, the determination of the linear region was generally taken between 10% and 50% of max displacement which occurred after the 40% preload of the connection. The yield load was determined to be 6.31 kips. The stiffness of 26.5 kip/in was determined as the slope of the 5% offset line. The same process was used in the creation of Figure 23, which shows the load deflection plot of M1YPD1.00. Figure 23 shows a yield and maximum load of 8.02 kips and 9.39 kips, respectively. The stiffness was determined by the slope of the 5% offset line to be 43.3 kip/in.

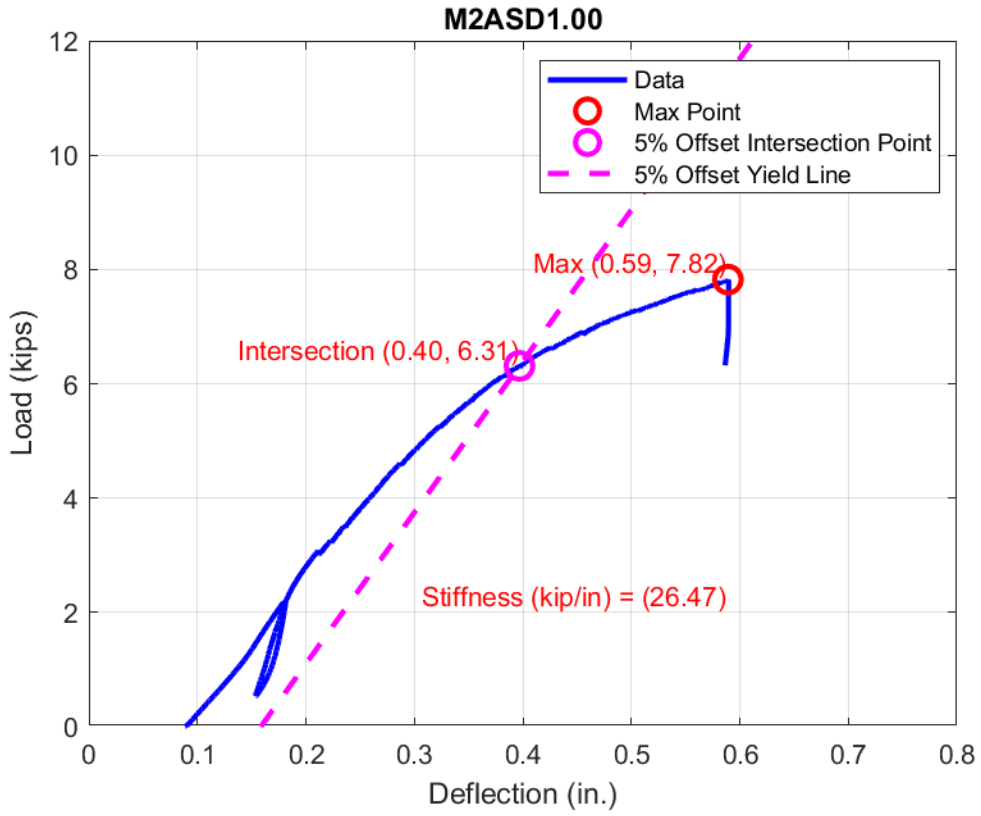

Figure 22: Monotonic Load Versus Displacement Plot for Specimen M2ASD1.00

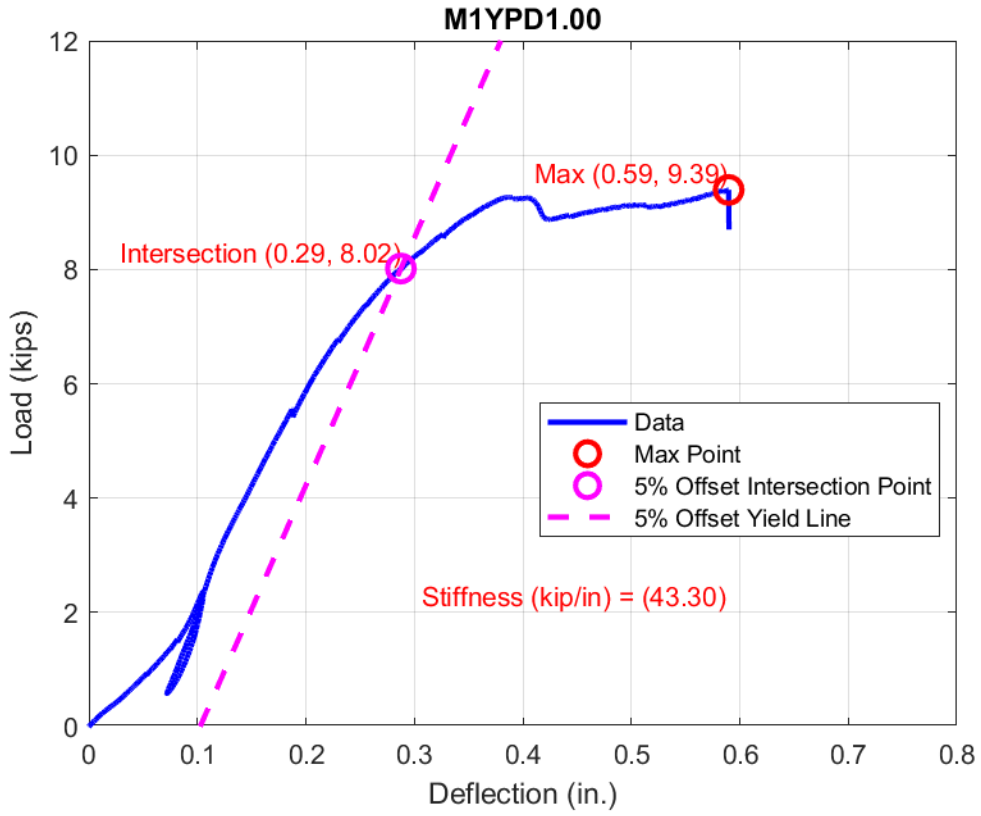

Figure 23: Monotonic Load Versus Displacement Plot for Specimen M1YPD1.00

The two types of failure observed from monotonic testing were best described as fastener Yield Mode II and Mode V. In general, Yield Mode II occurred most often in the Austrian spruce and Yield Mode V occurred most often in the yellow-poplar specimens. Regardless of species, often more than one failure mode was present in a connection. A connection had either solely Yield Mode II or Yield Mode V, or a mix of the two yield modes between the four pegs in the connection. Figure 24 is a photograph of the pegs from test M1YPD1.00 in which all four pegs experienced Yield Mode V. Figure 25 is a photograph of the side view of specimen M2ASD1.25 after testing. The pegs in specimen M2ASD1.25 were left uncut on the backside to help illustrate the Yield Mode II in the Austrian spruce specimens. Note the pegs in Figure 25 are not horizontal

in the specimen and have rotated clockwise within the Austrian spruce CLT signifying a Yield Mode II failure.

Figure 24: Red Oak Pegs from Specimen M1YPD1.00 Exemplifying Yield Mode V

Figure 25: Rotation of Red Oak Pegs in Specimen M2ASD1.25 Exemplifying Yield Mode II

4.3 YIELD LOAD, MAXIMUM LOAD, AND STIFFNESS OF CONNECTION SUBJECT TO CYCLIC LOADING

The cyclic testing was conducted following ASTM E2126 Method C (ASTM, 2019) which is known as the CUREE loading protocol. The average and the COVs of the cyclic yield load values for each test group are shown in Table 12. The 1 inch diameter Austrian spruce and yellow-poplar specimens had 5% offset yield load values of 6,690 lb and 8,550 lb, respectively. The 1.25 inch diameter yellow-poplar specimens had the greatest average yield load of 11,800 lb. The 1.25 inch diameter Austrian spruce specimens had an average 5% offset yield load almost 4,000lb less than the 1.25 inch diameter yellow-poplar specimens, (7,790 lb). When comparing the average cyclic 5% offset yield loads of the test groups, there was a 11.9% increase in load from the 1 inch diameter Austrian spruce specimens to the 1.25 inch diameter Austrian spruce specimens. Both diameter yellow-poplar test groups had a greater average 5% offset yield load than the 1 inch diameter Austrian spruce specimens, with a 22.9% increase for 1 inch diameter specimens and a 69.2% increase for the 1.25 inch diameter specimens. The COV of the average yield loads between all specimen groups was relatively similar, ranging from 10.7% for the 1.25 inch diameter Austrian spruce specimens to 14.2% for the 1 inch diameter Austrian spruce specimens.

Table 12: Half-lap Connection Yield Load of Yellow-Poplar and Austrian Spruce Subjected to Cyclic Loading

Average Connection Cyclic Yield Load				
Peg Diameter (in)	CLT Species	5% Offset Yield Load (lb)	5% Offset Yield Load COV (%)	Difference (%)
1	AS	6960	14.2	-
1	YP	8550	13.3	22.9
1.25	AS	7790	9.72	11.9
1.25	YP	11800	10.7	69.2

The average connection stiffness values are shown in Table 13. For both 1 inch and 1.25 inch diameter pegs, the yellow-poplar specimens had greater average stiffness values than the Austrian spruce values. The stiffness values were the smallest for the Austrian spruce specimens with stiffnesses of 21,900 lb/in and 28,300 lb/in for the 1 inch and 1.25 inch diameter specimens, respectively. The yellow-poplar specimens had stiffness values of 35,700 lb/in and 32,900 lb/in for the 1 inch and 1.25 inch diameter specimens, respectively. The range of COV was similar to the connection yield load, ranging from 11.4% for the 1 inch diameter Austrian spruce specimens to 17.4% for both the 1 inch diameter yellow-poplar and 1.25 inch diameter Austrian spruce specimens. As was found in the monotonic testing, there was little change in stiffnesses between peg diameters and species from the cyclic tests.

Table 13: Half-lap Connection Stiffness of Yellow-Poplar and Austrian Spruce Subjected to Cyclic Loading

Average Connection Cyclic Stiffness				
Peg Diameter (in)	CLT Species	Connection Stiffness (lb/in)	Connection Stiffness COV (%)	Difference (%)
1	AS	21900	11.4	-
1	YP	35700	17.4	62.9
1.25	AS	28300	17.4	29.5
1.25	YP	32900	13.1	50.4

The average maximum load of each test group subjected to cyclic loading is shown in Table 14. The average maximum load of the all yellow-poplar specimens was greater than all of the Austrian spruce specimens at each respective peg diameter. The 1 inch diameter specimens had average maximum loads of 7,580 lb and 8,840 lb for Austrian spruce and yellow-poplar specimens, respectively. For the 1.25 inch diameter specimens, the average maximum load was 9,190 lb and 12,300 lb for the Austrian spruce and yellow-poplar specimens, respectively. For the percent difference in maximum loads between test groups, the greatest difference was 62.6%

with 1.25 inch diameter yellow-poplar. Compared to the 1 inch diameter Austrian spruce specimens, the 1.25 inch diameter Austrian spruce was only 21.2% stronger and the 1 inch yellow-poplar specimens were 16.5% stronger. The COVs were relatively close between test groups for cyclic loading ranging from 9.47% for 1.25 inch diameter yellow-poplar to 12.2% for 1 inch diameter Austrian spruce specimens.

Table 14: Half-lap Connection Maximum Load of Yellow-Poplar and Austrian Spruce Subjected to Cyclic Loading

Average Connection Cyclic Maximum Load				
Peg Diameter (in)	CLT Species	Maximum Load (lb)	Maximum Load COV (%)	Difference (%)
1	AS	7580	12.2	-
1	YP	8840	11.6	16.5
1.25	AS	9190	10.0	21.2
1.25	YP	12300	9.47	62.6

The load-displacement graph of representative Austrian spruce and yellow-poplar 1.25 inch diameter specimens are shown in Figure 26 and 27, respectively. The backbone plot was created by connecting the maximum force values from the primary cycles with a line. The 5% offset method was used in the plotting of the 5% offset yield values. The slope of the 5% offset line was taken as the stiffness of the connection. The intersection point of the positive (compression) offset line and the backbone curve was taken as the yield point.

From Figure 26 and 27, the compression (positive force) cycles are of greater force magnitude than the tension cycles. This is due to the nature of the cyclic loading, with the compression cycle coming before the tension cycle. Due to the order of cycles, the compression magnitudes were larger in magnitude than the tension cycles. This is because in the primary compression cycle the connection undergoes initial inelastic deformation, typically shearing of the peg or local bearing failures. Then when the specimen is subject to the primary tension cycle,

there is less stiffness in the connection due to the inelastic deformation that occurred in the compression cycle.

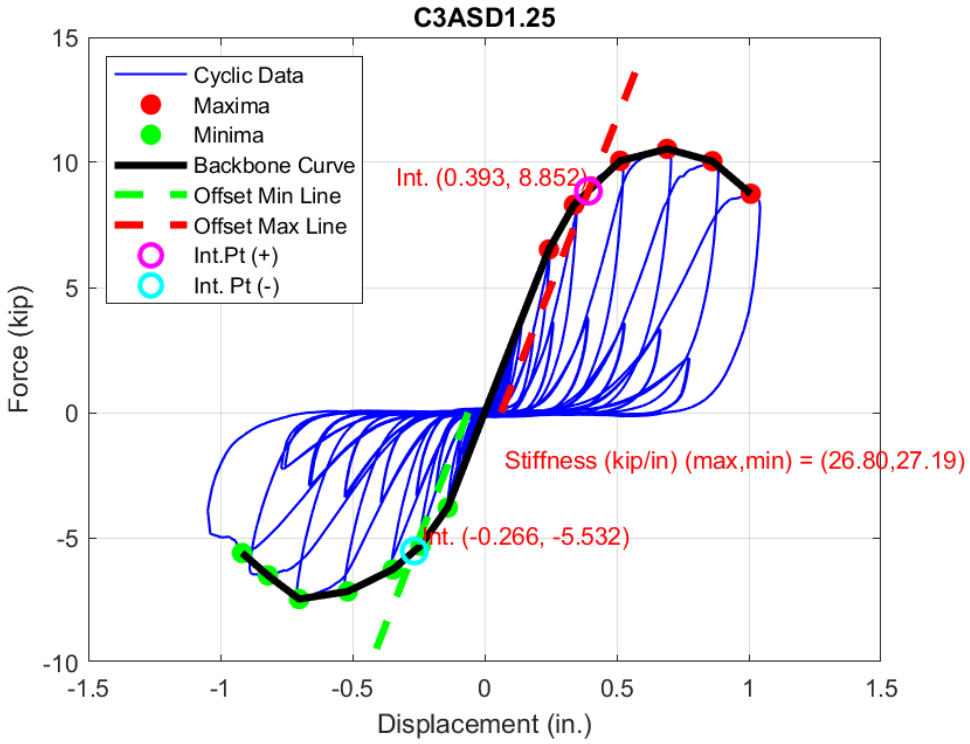

Figure 26 Cyclic Load Versus Displacement Plot for Specimen C3ASD1.25

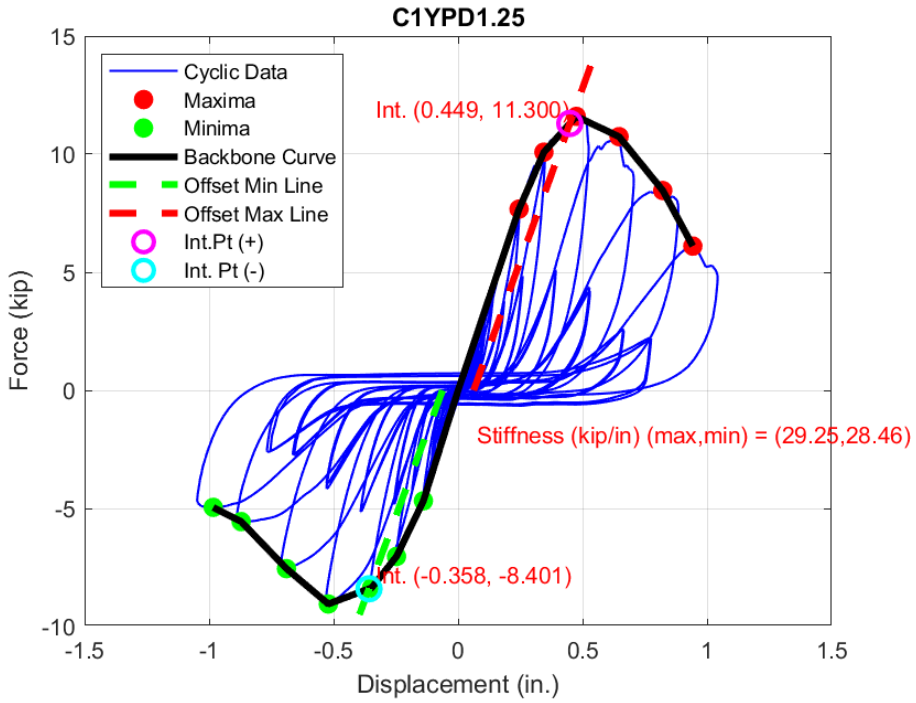

Figure 27 Cyclic Load Versus Displacement Plot for Specimen C1YPD1.25

As noted in the monotonic loading, the cyclic specimens failed in either Yield Mode II or V. Yield Mode II was predominately found in the less dense, Austrian spruce. In the cyclic loading of the Austrian Spruce specimens, the pegs could be seen rotating about the shear plane like rigid bodies in the peg holes. Yield Mode V was primarily found in the yellow-poplar specimens. The pegs that failed in Yield Mode V would not rotate as they did in Yield Mode II but would suddenly crack and the subsequent cycles would effectively turn the peg to chips. It shall also be noted that in a few of the Austrian spruce specimens, there was a mix of Yield Mode II and Yield Mode V. This is thought to have occurred due to localized defects in the wood such as knots or other localized regions of dense material causing the specimens not to fail in Yield Mode II.

Figure 28: Red Oak Pegs from Specimen C3ASD1.25

Figure 28 is a photograph of the pegs from test C3ASD1.25 in which Yield Mode II was observed. The pegs in figure in Figure 28 show almost no damage as the failure mode was in the CLT. Figure 29 is a photograph of the holes in one of the side members from test C3ASD1.25, which held two of the pegs from Figure 28. The elongation of the peg holes is evident Figure 29 signifying Yield Mode II. The elongation of the peg holes also caused tension perpendicular to grain and subsequent splitting of the middle lamination in the half-lap. Figure 30 is a photograph of the pegs from test C1YPD1.25 in which Yield Mode V is evident in two of the pegs due to a shear failure.

Figure 29: Elongation of Peg Holes in Specimen C3ASD1.25 Signifying Yield Mode II

Figure 30: Red Oak Pegs from Specimen C1YPD1.25

4.4 EXPERIMENTAL CONNECTION 5% OFFSET YIELD LOAD COMPARED TO PREDICTED YIELD LOAD

4.4.1 Discussion of Failures, Moisture Content, and Specific Gravity

Considering that wood is an organic material with variable properties depending upon specific growth conditions, the presence of localized defects including knots can have a significant impact on the yield load and predicted failure mode of a connection. From both the monotonic and cyclic testing, two distinct yield modes were present in the testing of the connections.

The first yield mode was Yield Mode II which is best described as bearing failure of both the main and side member as shown in Figure 1. Yield Mode II was primarily found in the Austrian spruce specimens which had the smallest specific gravity of the two CLT species of 0.402 and 0.426 for 1 inch and 1.25 inch diameter specimens, respectively. It shall be noted that there were a few instances of Yield Mode II in the yellow-poplar specimens, however it was not very common.

The second yield mode determined through testing is Yield Mode V, or pure shear of the peg as is shown in Figure 1. Yield Mode V was predominately found in the yellow-poplar specimens which had a higher specific gravity than the Austrian spruce specimens of 0.488 and 0.490 for the 1 inch and 1.25 inch diameter specimens, respectively. Although Yield Mode V was especially present in the yellow-poplar specimens, it was also present in the Austrian spruce specimens which did not fail in Yield Mode II.

Although only two yield modes were identified through testing, in several instances, all the pegs in a connection did not fail in the same failure mode. The lack of a uniform failure mode was primarily found in the Austrian spruce specimens. In some cases, one or two of the pegs would show a Yield Mode V failure and the remaining pegs would show a Yield Mode II failure.

The difference in failure modes within the specimens is believed to be caused by localized increases in specific gravity, differences in slope of grain, and knots near the peg holes. During testing, the failure modes were able to be visually identified. For the Yield Mode II failures, the pegs simply acted as rigid bodies and rotated about the shear plane inside the peg holes. For the Yield Mode V failures, the pegs would not rotate and would gradually fail in shear with increasing load.

The specific gravity of the wood is the best predictor of the yield load of a connection based on its necessity in calculating the main and side member bearing strength. However, in some cases the moisture content of the specimens may contribute to unexpected variations in yield load. Considering that the average moisture contents of specimens from all test groups were between 5.15% and 5.43%, variance in the moisture content can be ruled out as a contributor to connection yield load and the specific gravities of the specimens can be primarily relied upon.

4.4.2 Comparison of Calculated and Experimental Yield Load Values

The predicted yield loads for each connection using their measured specific gravities for Yield Modes II and V are presented in Table 15 using the NDS Yield Mode II equation from Table 1 and the Mode V yield equation from Equation 1. The yield mode equations produced the yield load, or Z value, for one peg in the connection. The predicted connection yield load of the entire connection was calculated by multiplying the Z value for each respective yield mode by four. In Table 15, a load duration factor (C_D) of 1.0 was applied. Yield Mode II should theoretically govern the capacity of the connection, yet Yield Mode II was not the governing failure mode in all specimens. As such, both Yield Modes II and V are presented in Table 15.

Table 15: Predicted Yield Loads for Yield Modes II and V

Predicted Yield Load for Yield Modes II and V					
Peg Diameter (in)	CLT Species	Yield Load Mode II (lb)	**Connection Yield Load Mode II (lb)**	Yield Load Mode V (lb)	**Connection Yield Load Mode V (lb)**
1	AS	1189	**4760**	763	**3050**
1	YP	1638	**6550**	883	**3530**
1.25	AS	5133	**5130**	1160	**4640**
1.25	YP	6680	**6680**	1290	**5170**

All comparisons in Tables 16 through 17 were made using the entire connection yield load, rather than individual peg yield load following the equal distribution of load assumption. As such, the predicted yield loads are the predicted yield load of one peg multiplied by four to account for the four pegs in the connection. It shall also be noted that in comparisons of predicted versus experimental connection 5% offset yield loads, a load duration factor of 1.6 and a geometry factor of 0.5 were used.

The predicted versus experimental yield loads subjected to monotonic loading are shown in Table 16. A load duration factor of 1.6 is most appropriate for the testing procedures as the ISO 6891 loading protocol caused a specimen failure close to ten minutes, varying slightly with each test. The NDS (2018) specifies in Table 2.3.2 that for a load duration of ten minutes a load duration factor of 1.6 should be used. Overall, when applying a load factor of 1.6 to the predicted yield loads for Mode II are more conservative than the Mode V predicted yield loads. For Mode II, the tested to calculated ratios were all less than 1, ranging from 0.683 for the 1 inch diameter yellow-poplar specimens to 0.918 for the 1.25 inch diameter Austrian spruce specimens. For Mode V, the tested to calculated ratios ranged from 1.01 for the 1.25 inch diameter Austrian spruce specimens to 1.27 for the 1 inch diameter yellow-poplar specimens.

Table 16: Predicted Versus Experimental Monotonic Yield Load of Connection, C_D = 1.6

Predicted Versus Experimental Monotonic Yield Load of Connection								
Peg Diameter (in)	CLT Species	5% Offset Yield Load (lb)	Predicted Mode II Yield Load (lb)	Mode II Error (%)	**Mode II Tested to Calculated**	Predicted Mode V Yield Load (lb)	Mode V Error (%)	**Mode V Tested to Calculated**
1	AS	5820	7610	24%	**0.765**	4890	-19.1%	**1.19**
1	YP	7160	10500	32%	**0.683**	5650	-26.7%	**1.27**
1.25	AS	7540	8210	8%	**0.918**	7450	-1.19%	**1.01**
1.25	YP	8910	10700	17%	**0.834**	8280	-7.67%	**1.08**

The predicted versus experimental yield loads from cyclic loading using a load duration factor of 1.6 are in Table 17. The load duration factor of 1.6 is appropriate for the CUREE loading protocol as the failures occurred near a time of ten minutes. The tested to calculated ratios for Yield Mode II ranged from 0.816 for the 1 inch diameter yellow-poplar specimens to 1.10 for the 1.25 inch diameter yellow-poplar specimens. The Mode V tested to calculated ratios were all greater than 1, ranging from 1.05 for 1.25 inch diameter Austrian spruce specimens to 1.51 for 1 inch diameter yellow-poplar specimens.

Table 17: Predicted Versus Experimental Cyclic Yield Load of Connection, C_D = 1.6

Predicted Versus Experimental Cyclic Yield Load of Connection								
Peg Diameter (in)	CLT Species	5% Offset Yield Load (lb)	Predicted Mode II Yield Load (lb)	Mode II Error (%)	**Mode II Tested to Calculated**	Predicted Mode V Yield Load (lb)	Mode V Error (%)	**Mode V Tested to Calculated**
1	AS	5820	7610	9%	**0.915**	4890	-42.5%	**1.42**
1	YP	7160	10500	18%	**0.816**	5650	-51.4%	**1.51**
1.25	AS	7540	8210	5%	**0.949**	7450	-4.54%	**1.05**
1.25	YP	8910	10700	-10%	**1.10**	8280	-42.3%	**1.42**

Overall, for both monotonic and cyclic loading the Yield Mode II predicted equations were unconservative, having tested to calculated ratios all less than 1, with the exception of the

1.25 inch diameter yellow-poplar test group subjected to cyclic loading. For both monotonic and cyclic loading the tested to calculated ratios for Yield Mode V were greater than 1 for all test groups. In general, the tested to calculated ratios for the cyclic loading were greater than those for monotonic loading as the 5% offset yield loads were greater for cyclic loading than

One potential reason for the difference in predicted and experimental yield loads is that the assumption of even load distribution between all four pegs was not true. Due to unpredictability in local stiffness of the CLT due to grain orientation and presence of knots, it is possible that more of the load may have been directed to one of the joints in the connection than the other leading to the difference in expected versus actual yield modes in the connection.

Another potential cause for the difference between experimental and theoretical yield loads is the predictive equations themselves. Foremost, the NDS yield mode equations were all developed for metallic fasteners. Second, both the Yield Mode II and V equations must be adjusted to account for the grain orientation of the CLT. Through the process of predicting peg yield loads in CLT, one must gloss over several fundamental assumptions upon which the original equations were based. Some of the fundamental assumptions that must be glossed over are the material of the fastener and the main and side member material. The result of the compounding assumptions leads to increasing amounts of error and a lack of confidence in the designed connection's actual yield load compared to the predicted yield loads.

4.4.3 Comparison of Monotonic and Cyclic Yield Load and Stiffness

To understand connection performance, the yield loads and stiffnesses of the red oak pegs when subjected to monotonic and cyclic loading should be compared. It shall be noted that the NDS yield mode predictive equations were developed based on monotonic loading. By comparing the 5% offset yield loads and stiffnesses of the pegs subjected to monotonic and

cyclic loading, it is possible to conclude if monotonic and cyclic loading yield similar results despite the difference in loading regimes.

The average 5% offset yield loads of the individual pegs from both the monotonic and cyclic connections are shown in Table 18. The 5% offset yield loads of the pegs were calculated by dividing the connection 5% offset yield load by four which follows the assumption that the load was evenly distributed to all four pegs in the connection. Overall, there is an increase in the average 5% offset yield load of the pegs from monotonic to cyclic loading. For the 1 inch diameter specimens there is an increase of 17.9% and 17.8% from monotonic to cyclic loading for the Austrian spruce and yellow-poplar specimens, respectively. For the 1.25 inch diameter specimens, there is an increase of 3.25% and 27.7% from monotonic to cyclic loading for the Austrian spruce and yellow-poplar specimens respectively. Overall, the percent differences show an increase in 5% offset yield loads for cyclic loading compared to monotonic loading.

Table 18: Monotonic Versus Cyclic 5% Offset Yield Load of Individual Red Oak Pegs

Monotonic Versus Cyclic 5% Offset Yield Load of Red Oak Pegs				
Peg Diameter (in)	CLT Species	Monotonic 5% Offset Yield Load (lb)	Cyclic 5% Offset Yield Load (lb)	Difference (%)
1	AS	1460	1740	17.9
1	YP	1790	2140	17.8
1.25	AS	1890	1950	3.25
1.25	YP	2230	2940	27.7

The stiffnesses of the pegs were calculated by dividing the connection stiffness by four which follows the assumption that the load distributed evenly among all four pegs in the connection. The stiffnesses of the red oak pegs subjected to monotonic and cyclic loading and the corresponding percent differences are shown in Table 19. For 1 inch diameter Austrian spruce

specimens there was a decrease in the peg stiffness from monotonic loading to cyclic loading of 10,900 lb/ in to 5,470 lb/in, resulting in a -66.6% difference in the stiffnesses. The 1 inch diameter yellow-poplar peg stiffness increased from 7,070 lb/in for monotonic to 8,910 lb/in for cyclic loading resulting in a 23.1% difference in stiffness. For the 1.25 inch diameter Austrian spruce specimens, there was a decrease in stiffness from the monotonic to cyclic loading of 3310 lb/in yielding a -38.0% difference. The 1.25 inch diameter yellow-poplar specimens had stiffnesses of 12,000 lb/in and 8,230 lb/in for monotonic and cyclic loading, respectively. From Table 21 it can be concluded that there are no generalized trends in the peg stiffness and that stiffness is an extremely variable property in the laboratory setting and is challenging to get consistent, repeatable results in a laboratory setting with limited sample sizes.

Table 19: Monotonic Versus Cyclic Stiffness of Individual Red Oak Pegs

Monotonic Versus Cyclic Stiffness of Red Oak Pegs				
Peg Diameter (in)	CLT Species	Monotonic Peg Stiffness (lb/in)	Cyclic Peg Stiffness (lb/in)	Difference (%)
1	AS	10900	5470	-66.6
1	YP	7070	8910	23.1
1.25	AS	10400	7090	-38.0
1.25	YP	12000	8230	-37.6

4.5 STATISTICAL COMPARISONS OF CLT SPECIES AND PEG DIAMETER ON CONNECTION YIELD LOAD

Due to the limited sample size of monotonic tests, the statistical analysis of 5% offset yield load was solely performed on cyclic test specimens. A two-way ANOVA was performed using JMP statistical software comparing the CLT species and peg diameter ($\alpha = 0.05$). A p-value less than 0.0001 was calculated for the CLT species factor, which was less than the defined α of 0.05, and the null hypothesis was rejected.

The fact that the CLT species studied and the associated difference in specific gravity do cause a significant difference in the 5% offset yield load contradicts the findings of Vilguts et al. (2024). Vilguts et al. (2024) concluded that the CLT specific gravity of the CLT had no statistical significance on the yield force of the connection. It shall be noted that the connections tested by Vilguts et al. (2024) were typical single shear joints without a half-lap. Other than the connection geometry, a potential cause for the difference in conclusions is that all the species tested by Vilguts et al. (2024) were softwood. In the half-lap connections tests performed in this research, one CLT species was a softwood (Austrian spruce), and one was a hardwood (yellow-poplar). The range of specific gravities tested by Vilguts et al. (2024) was 0.398 to 0.503 which is fairly consistent with the range between the Austrian spruce and yellow-poplar in this study of 0.402 to 0.490.

The p-value of the peg diameter factor was 0.0005 was obtained ($\alpha = 0.05$). Again, the p-value was less than the defined α, as such, the null hypothesis was rejected. The peg diameter causing a significant difference in the 5% offset yield load of the joint is not a significant surprise as with a larger diameter peg, there is more cross-sectional area to resist shear. However, it was a worthwhile experiment because with an increase in peg diameter comes an increase in the likelihood of having a defect in the cross-section. As such, there will be a limit where an increase in peg diameter no longer returns a worthwhile increase in yield load, resulting in the use of more fasteners. Based on the results of this two-way ANOVA test, increasing the peg diameter from 1 inch to 1.25 inch to reduce the number of fasteners in a row is worthwhile.

4.6 STATISTICAL COMPARISONS OF CLT SPECIES AND PEG DIAMETER ON CONNECTION STIFFNESS

Similar to the 5% offset yield load statistical analysis, the statistical analysis for stiffness was only performed on the specimens subjected to cyclic loading due to the small sample size of specimens subjected to monotonic loading. A two-way ANOVA was performed to evaluate the impact of CLT species and peg diameter on connection stiffness ($\alpha = 0.05$). JMP calculated a p-value of 0.0003 for CLT species, which was less than the defined α value, and the null hypothesis was rejected. The significant difference of stiffnesses between the CLT species can be attributed to difference in specific gravities. For both 1 inch and 1.25 inch diameter specimen groups, the yellow-poplar specimens had greater stiffness than the Austrian spruce which mirrors the findings of specific gravity, which were also greater for yellow-poplar than Austrian spruce.

The p-value of the peg diameter factor was 0.3891 ($\alpha = 0.05$). As 0.3891 is greater than the defined α, the null hypothesis was failed to be rejected. The lack of significant difference in stiffnesses caused by the peg diameters can be attributed to the methods used for fabricating the joint. All peg holes were drilled using a spade bit 1/16 inch less than the nominal diameter of the peg. This created a tight, but not tight enough to cause splitting, hole that allowed for the transfer of forces across joints. As the methods of fabrication were the same for the different peg diameters in all CLT species, similar stiffnesses of the connection should be expected.

5.0 CONCLUSIONS

5.1 SUMMARY

The primary goals of this research were to evaluate the shear yield load and stiffness of half-lap CLT pegged connections subjected to monotonic and cyclic loading and to determine the impact of peg diameter and CLT species on the connection yield load and stiffness. The yield load and stiffness of the connections were determined through both monotonic and cyclic loading following the ISO 6891 and CUREE protocols. The yield loads of the connections were determined using the 5% offset method and compared to the predicted yield loads from NDS Yield Mode II and Yield Mode V presented by Miller et al. (2010). Lastly, the impact of CLT species and peg diameter on the yield load and stiffness of the connection was evaluated through a two-way ANOVA.

5.2 CONCLUSIONS

5.2.1 Moisture Content and Specific Gravity

The moisture content was similar between all specimen groups ranging from a minimum of 5.15% to 5.43% for 1.25 inch diameter Austrian spruce specimens and 1 inch Austrian spruce specimens, respectively. The similar moisture content between all specimen groups eliminates the potential to attribute variance in testing results to differences in moisture content. The 1 inch and 1.25 inch diameter Austrian spruce specimens had an average specific gravity of 0.402 and 0.426, respectively. The average specific gravity of the 1 inch and 1.25 inch diameter yellow-poplar specimen groups were 0.488 and 0.490, respectively.

5.2.2 Yield Load, Maximum Load, and Stiffness of Connection Subjected to Monotonic Loading

On average, the yield load of both the 1 inch and 1.25 inch diameter yellow-poplar connections was greater than that of the Austrian spruce connections. The greater yield load in

the yellow-poplar specimens can be attributed to the higher specific gravity of the yellow-poplar CLT compared to the Austrian spruce CLT.

When subjected to monotonic loading, the two failure modes identified were Yield Mode II and Yield Mode V. Yield Mode II was predominantly found in the less dense Austrian spruce specimens. Yield Mode V was primarily found in the yellow-poplar specimens. In some specimens a combination of Yield Mode II and V was found, with some pegs shearing in half and others having local bearing failures. In the specimens in which a combination of the two yield modes was found, the lack of uniformity in yield mode was attributed to localized defects such as knots or localized increases in density of the CLT near the peg holes.

5.2.3 Yield Load, Maximum Load, and Stiffness of Connection Subjected to Cyclic Loading

The yield loads of all specimen test groups were greater when subjected to the CUREE cyclic loading protocol than the monotonic ISO 6891 protocol. Similarly to the monotonic loading, the greater specific gravity yellow-poplar specimens had a greater average yield load. The greater yield load of the yellow-poplar specimens can be attributed to the difference in the failure modes experienced through testing. In the lower specific gravity Austrian spruce specimens, the red oak pegs behaved like rigid bodies in the holes, simply rotating and creating local bearing failures in the inside of the hole. Conversely, in the yellow-poplar specimens the red oak pegs more predominantly experienced Yield Mode V and would gradually develop a shear failure. At the end of the Austrian spruce cyclic tests, a small pile of red oak wood chips would be found below each joint, a result of the shear failure in the red oak pegs.

5.2.4 Experimental Connection Yield Load Compared to Predicted Yield Load

The NDS Yield Mode II predicted strength equations overpredicted the monotonic 5% offset yield load, having tested to calculated ratios ranging from 0.683 to 0.918. When considering Yield Mode V, the monotonic connection strength was underpredicted for all

specimens, having tested to predicted ratios of at least 1.01. These findings suggest that Yield Mode II was unconservative in its predictions of the yield loads of the connections. Conversely, Yield Mode V predictive equations were slightly conservative and predicted closer the actual yield loads.

When considering cyclic tests, Yield Mode II tested to calculated ratios ranged from 0.816 for 1 inch diameter yellow-poplar to 1.10 for 1.25 inch diameter yellow-poplar specimens. Tested to calculated yield load ratios for Yield Mode V ranged from 1.05 to 1.51 for 1.25 inch diameter Austrian spruce and 1 inch yellow-poplar specimens, respectively. Overall, the tested to calculated ratios for cyclic loading were greater than the monotonic tested to calculated ratios due to the increase in 5% offset yield load from monotonic to cyclic loading. The increase in cyclic yield load brought the Yield Mode II tested to predicted ratios closer to unity and increased the Yield Mode V tested to calculated ratios further beyond 1.

5.2.5 Impact of CLT Species and Peg Diameter on 5% Offset Yield Load

From a two-way ANOVA analysis of the 5% offset yield load, the CLT species and peg diameter were significantly different. The result of the ANOVA analysis of the species could be expected as the specific gravity of the yellow-poplar was greater than the Austrian spruce. Considering that the specific gravity of the main and side members are key parameters of the equations for predicting connection yield load the difference in specific gravities for the two species is important. Similarly, for the diameter of pegs, the larger diameter, the more material there is to transfer the force between the main and side members. There may be concern in peg diameters larger than 1.25 inch as with an increase in diameter also comes an increase in the likelihood of defects in the material.

5.2.6 Impact of CLT Species and Peg Diameter on Connection Stiffness

Performing a two-way ANOVA for both the connection stiffness with factors of CLT species and peg diameter, there was a significant difference for CLT species, but not for peg diameter. From the ANOVA, it can be concluded that the CLT specific gravity impacts the stiffness of the joint and the peg diameter does not as long as the same procedure is used for peg installation of all diameters.

5.3 LIMITATIONS OF WORK

It shall be noted that the findings of this research are limited to the use of 3-ply yellow-poplar and Austrian spruce CLT in half-lap joints connected by red oak pegs 1 inch and 1.25 inch in diameter using a C_{Δ} = 0.5. Full scale testing was not performed, as such, the application of the findings of this research may not translate to full scale tests or construction. Lastly, throughout the analysis of the connections, it was assumed that the load applied to the connection was distributed evenly among the four pegs in the connection.

5.4 RECOMMENDATIONS FOR FUTURE WORK

To more completely understand the performance of pegged CLT half-lap connections in actual structures, full-scale testing including tension straps to resist tensile forces perpendicular to the length of the joint could be performed. Additionally, studies into the actual implementation of pegged CLT half-lap connections in buildings should be investigated as there are a number of challenges that are present. Some of the challenges with the pegged CLT half-lap connections include but are not limited to: limitations to peg moisture content prior to installation, drilling of peg holes by CNC machine versus field drilling, joint fabrication time compared to metallic fasteners, and consideration of construction tolerances when fitting panels together during construction. Although it would be very challenging to get pre-machined holes to align in field

conditions, if tolerances are able to be met, it may be possible to use the slightly misaligned holes to drawbore the pegs and create a stiffer, tighter joint.

The performance of pegged CLT half-lap joints with greater than 3-plies could also be investigated. Regarding connection geometry, further research exploring the limits and accuracy of NDS provided C_Δ guidance in pegged connections should be explored. For exploring the impact of the C_Δ factor on pegged connections, it would be beneficial to first replicate the results of this research and compare them to specimens with C_Δ = 1.0. Due to the reduced thickness of the middle lamination in the half-lap joint, it may be beneficial to explore a CLT layup with a middle lamination twice as thick as the other layers so that the joint is less likely to experience a failure in the middle lamination due to its reduced thickness or a bond failure between the half-lap lamination and the next full thickness lamination.

As connections are one of the most challenging parts of structural design due to the high degree of indeterminacy of the forces in the connection, a further study into the design guidance for all connection types specified in the NDS is recommended. More specifically, a revision of the specifications to focus more on the tracking of governing limit states as opposed to following prescribed guidelines for detailing, as is currently done. By tracking limit states in the connection, designers will be able to more accurately predict the failure mode and capacity of the connection as a whole. As mass timber becomes more widely used and used in more complex structures, generating more detailed connection design specifications would be beneficial so that engineers do not primarily have to rely on advanced finite element software.

From a sustainability perspective there is plenty of potential for further research on the use of pegged half-lap CLT connections. A study into the GWP of a pegged half-lap CLT joint versus a surface spline joint joined with metallic fasteners of the same capacity would be of

value. The potential reuse of CLT diaphragm panels fastened with both pegs and metallic fasteners should be investigated particularly with regard to the disassembly time, ability to machine (CNC) after removed from the structure, and the performance the panels once reinstalled in a new structure.

As a general note, further research into the application and modification of traditional timber framing joinery techniques to mass timber building materials is encouraged as it may provide more efficient erection and construction of structures.

6.0 REFERENCES

Aicher, S., Hirsch, M., & Christian, Z. (2016). Hybrid cross-laminated timber plates with beech wood cross-layers. Construction and Building Materials, 124, 1007-1018.

American Society of Civil Engineers (ASCE). *Minimum Design Loads and Associated Criteria for Buildings and Other Structures*. American Society of Civil Engineers, 2022.

ANSI/APA. (2019). Standard for performance-rated cross-laminated timber. In ANSI/APA PRG320. Tacoma, WA: American National Standards Institute/APA—The Engineered Wood Association.

ASTM. (2017). Standard test method for density and specific gravity (relative density) of wood and wood-based materials. In ASTM D2395-17. West Conshohocken, PA: American Society for Testing and Materials.

ASTM. (2019). Standard test methods for cyclic (reversed) load test for shear resistance of vertical elements of the lateral force resisting systems for buildings. In ASTM E2126-19. West Conshohocken, PA: American Society for Testing and Materials.

ASTM. (2020). Standard test methods for direct moisture content measurement of wood and wood based materials. In ASTM D4442-20. West Conshohocken, PA: American Society for Testing and Materials.

ASTM. (2021). Standard test methods for single-bolt connections in wood and wood-based products. In ASTM D5652-21. West Conshohocken, PA: American Society for Testing and Materials.

ASTM. (2024). Standard test method for evaluating dowel-bearing strength of wood and wood-based products. In ASTM D5764-24. West Conshohocken, PA: American Society for Testing and Materials.

AWC. (2018). National design specification for wood construction. In. USA: American Wood Council.

AWC. (2021). Special design provisions for wind and seismic. In. USA: American Wood Council.

Barber, D., Blount, D., Hand, J. J., Roelofs, M., Wingo, L., Woodson, J., & Yang, F. (2022). *Design Guide 37 - Hybrid Steel Frames with Wood Floors*. American Institute of Steel Construction.

Brandner, R., Flatscher, G., Ringhofer, A., Schickhofer, G., & Thiel, A. (2016). Cross Laminated Timber (CLT): Overview and development. *European Journal of Wood and Wood Products*, *74*(3), 331–351. https://doi.org/10.1007/s00107-015-0999-5

Breneman, S., McDonnell, E., Tremayne, B., Llanes, D., Houston, J., Gu, M. ' "Eric," Zimmerman, R., & Montgomery, G. (2023). *CLT Diaphragm Design Guide*. WoodWorks - Wood Products Council.

Breyer, D. E., Cobeen, K., & Martin, Z. (2020). *Design of wood structures- ASD*. McGraw-Hill Education.

Brungraber, R. L. 1985. "Traditional Timber Joinery: A Modern Analysis." Ph.D. diss., Stanford University.

Bulleit, W. M., Sandberg, L. B., Drewek, M. W., & O'Bryant, T. L. (1999). Behavior and modeling of wood-pegged timber frames. *Journal of Structural Engineering*, *125*(1), 3–9. https://doi.org/10.1061/(asce)0733-9445(1999)125:1(3)

CSA. (2016). Engineering design in wood. In CSA O86 Update 1. Ontario, CA: The National Research Council of Canada.

Gagnon, S., & Pirvu, C. (2011). CLT Handbook: Cross-Laminated Timber (Canada Edition). FP Innovations.

Gavric, I., M. Fragiacomo, and A. Ceccotti. 2012. "Strength and deformation characteristics of typical X-lam connections." In Proc., 2012 World Conf. on Timber Engineering, 146–155. Red Hook, NY: Curran Associates.

Hayes, B. N., Koliou, M., & van de Lindt, J. W. (2023). Seismic behavior of balloon frame cross-laminated timber connections. *Journal of Structural Engineering*, *149*(9). https://doi.org/10.1061/jsendh.steng-11984

Hematabadi, H., Madhoushi, M., Khazaeyan, A., Ebrahimi, G., Hindman, D. P., & Loferski, J. (2020). Bending and shear properties of cross-laminated timber panels made of poplar (Populus alba). Construction and Building Materials, 265, 120326.

Hindman, D. P. (2019). Predicting the bending yield strength of timber frame pegs. *Journal of Materials in Civil Engineering*, *31*(3). https://doi.org/10.1061/(asce)mt.1943-5533.0002585

Hindman, D. P., Richardson, B., & Vaanjilnorov, A. (2022). Dowel-bearing strength of southern pine cross-laminated timber. *Journal of Materials in Civil Engineering*, *34*(2). https://doi.org/10.1061/(asce)mt.1943-5533.0004077

Hossain, A., Danzig, I., & Tannert, T. (2016). Cross-laminated timber shear connections with double-angled self-tapping screw assemblies. *Journal of Structural Engineering*, *142*(11). https://doi.org/10.1061/(asce)st.1943-541x.0001572

Hossain, A., Popovski, M., & Tannert, T. (2018). Cross-laminated timber connections assembled with a combination of screws in withdrawal and screws in shear. *Engineering Structures*, *168*, 1–11. https://doi.org/10.1016/j.engstruct.2018.04.052

Hossain, A., Popovski, M., & Tannert, T. (2019). Group effects for shear connections with self-tapping screws in CLT. *Journal of Structural Engineering*, *145*(8). https://doi.org/10.1061/(asce)st.1943-541x.0002357

ICC. (2021). International Building Code. In Types of Construction: International Code Council.

International Organization for Standardization. (1983). *ISO 6891:1983 Timber structures—Joints made with mechanical fasteners—General principles for the determination of strength and deformation characteristics*.

Jalilifar, E., Koliou, M., & Pang, W. (2021). Experimental and numerical characterization of monotonic and cyclic performance of cross-laminated timber dowel-type connections. *Journal of Structural Engineering*, *147*(7). https://doi.org/10.1061/(asce)st.1943-541x.0003059

Karacabeyli, E., & Douglas, B. (2013). CLT Handbook: Cross-Laminated Timber (US Edition). FP Innovations.

Kramer, A., Barbosa, A. R., & Sinha, A. (2014). Viability of hybrid poplar in ANSI approved cross-laminated timber applications. Journal of Materials in Civil Engineering, 26(7), 06014009.

Krawinkler, H., F. Parisi, L. Ibarra, A. Ayoub, and R. Medina. 2001. Development of a testing protocol for woodframe structures. Richmond, CA: Consortium of Universities for Research in Earthquake Engineering.

Laerd Statistics. (2025). *Two-way ANOVA in SPSS statistics*. Two-way ANOVA in SPSS Statistics - Step-by-step procedure including testing of assumptions | Laerd Statistics. https://statistics.laerd.com/spss-tutorials/two-way-anova-using-spss-statistics.php#:~:text=The%20two%2Dway%20ANOVA%20compares,educational%20level%20(undergraduate/postgraduate)?

Lukić, I., Premrov, M., Passer, A., & Žegarac Leskovar, V. (2021). Embodied Energy and GHG emissions of residential multi-storey timber buildings by height – a case with structural connectors and mechanical fasteners. *Energy and Buildings*, *252*, 111387. https://doi.org/10.1016/j.enbuild.2021.111387

Mahamid, Mustafa. *Cross-Laminated Timber Design: Structural Properties, Standards, and Safety*. McGraw-Hill Education, 2020.

Marmo, R. “The use of timber tenon joints with pegs: a sustainable solution for improvising deconstruction.” *Proceedings from the International Symposium on Sustainable*

Construction - A Life Cycle Approach in Engineering at the University of Malta, July 23-25, 2010, pp. 185-191.

Miller, J. F. 2004. "Capacity of Pegged Mortise and Tenon Joints." Master's Thesis., University of Wyoming, Laramie, Wyoming.

Miller, J. F., Schmidt, R. J., & Bulleit, W. M. (2010). New yield model for wood dowel connections. *Journal of Structural Engineering*, *136*(10), 1255–1261. https://doi.org/10.1061/(asce)st.1943-541x.0000224

Mohamadzadeh, M., and Hindman, D. (2015). Mechanical Performance of Yellow-Poplar Cross Laminated Timber (Report No. CE/VPI-ST-15-13), Virginia Tech Structural Engineering and Materials Report Series, Blacksburg, VA, USA.

Morris, F., Allen, S., & Hawkins, W. (2021). On the embodied carbon of structural timber versus steel, and the influence of LCA methodology. *Building and Environment*, *206*, 108285. https://doi.org/10.1016/j.buildenv.2021.108285

Pereira, M. C., Pascal Sohier, L. A., Descamps, T., & Junior, C. C. (2021). Doweled Cross laminated timber: Experimental and analytical study. *Construction and Building Materials*, *273*, 121820. https://doi.org/10.1016/j.conbuildmat.2020.121820

Sandberg, L. B., Bulleit, W. M., & Reid, E. H. (2000). Strength and stiffness of oak pegs in traditional timber-frame joints. *Journal of Structural Engineering*, *126*(6), 717–723. https://doi.org/10.1061/(asce)0733-9445(2000)126:6(717)

Sandoli, A., Ceraldi, C., & Prota, A. (2023). Feasibility of timber pegged joints for seismic design of structures. *Journal of Structural Engineering*, *149*(5). https://doi.org/10.1061/jsendh.steng-11579

Satir, E., Adhikari, S., & Hindman, D. P. (2024). Evaluation of bending and shear properties of mixed softwood & Hardwood cross-laminated timbers. *Journal of Building Engineering*, *96*, 110646. https://doi.org/10.1016/j.jobe.2024.110646

Shanks, J., & Walker, P. (2009). Strength and stiffness of all-timber pegged connections. *Journal of Materials in Civil Engineering*, *21*(1), 10–18. https://doi.org/10.1061/(asce)0899-1561(2009)21:1(10)

Sotayo, A., Bradley, D., Bather, M., Sareh, P., Oudjene, M., El-Houjeyri, I., Harte, A. M., Mehra, S., O'Ceallaigh, C., Haller, P., Namari, S., Makradi, A., Belouettar, S., Bouhala, L., Deneufbourg, F., & Guan, Z. (2020). Review of State of the art of dowel laminated timber members and densified wood materials as sustainable engineered wood products for construction and building applications. *Developments in the Built Environment*, *1*, 100004. https://doi.org/10.1016/j.dibe.2019.100004

Sullivan, K., Miller, T. H., & Gupta, R. (2018). Behavior of cross-laminated timber diaphragm connections with self-tapping screws. *Engineering Structures*, *168*, 505–524. https://doi.org/10.1016/j.engstruct.2018.04.094

Timber Frame Engineering Council (TFEC). 2019. Standard for Design of Timber Frame Structures and Commentary, TFEC 1-2019. Timber Frame Engineering Council, Alstead, NH.

Timber Frame Engineering Council (TFEC). 2020. Cross-Laminated Timber (CLT) Diaphragms, TFEC 19-2020. Timber Frame Engineering Council, Alstead, NH.

Vilguts, A., Phillips, A. R., Jerves, R., Antonopoulos, C., & Griechen, D. (2024). Monotonic testing of single shear-plane CLT-to-CLT joint with hardwood dowels. *Journal of Building Engineering*, *88*, 109252. https://doi.org/10.1016/j.jobe.2024.109252

Walsh, Frank J., and Robert L. Watts. *Composite Lumber*. 21 Aug. 1923.

Xu, B.-H., Jiao, S.-Y., Liu, X., Bouchaïr, A., & Zhang, B. (2024). Mechanical behavior of timber joints with laterally loaded multiple densified wood dowels under the loading parallel to the grain. *Journal of Structural Engineering*, *150*(10). https://doi.org/10.1061/jsendh.steng-13693

7.0 APPENDICES

7.1 APPENDIX A – MONOTONIC AUSTRIAN SPRUCE 1 INCH DIAMETER 5% OFFSET YIELD PLOTS

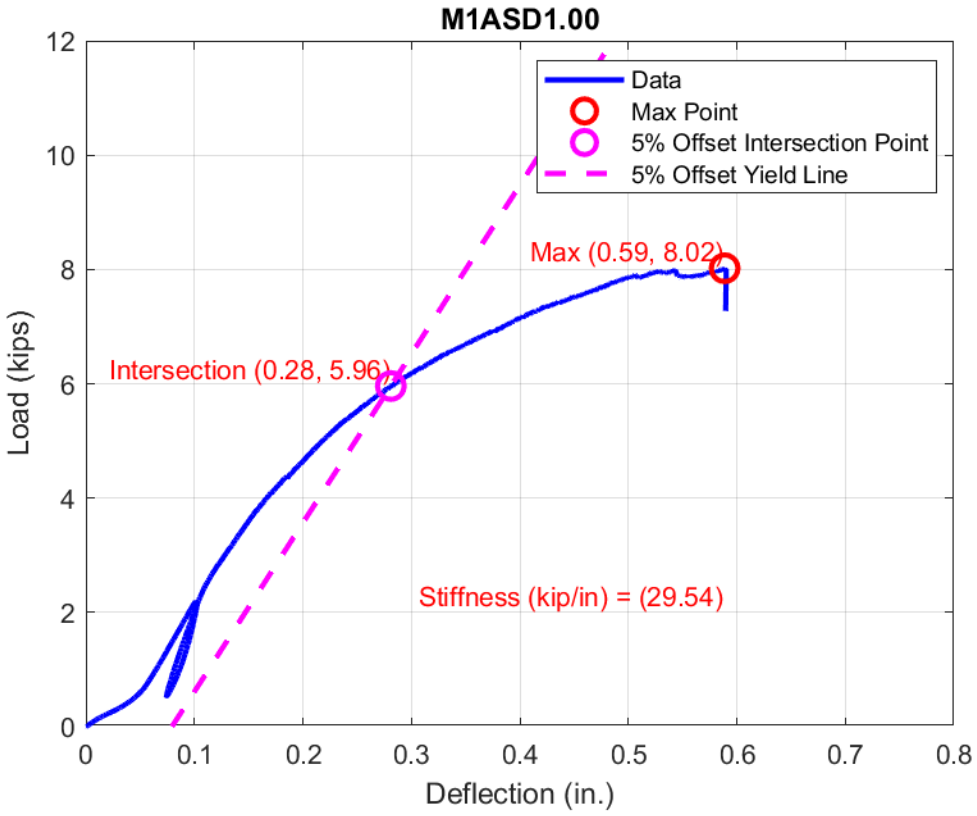

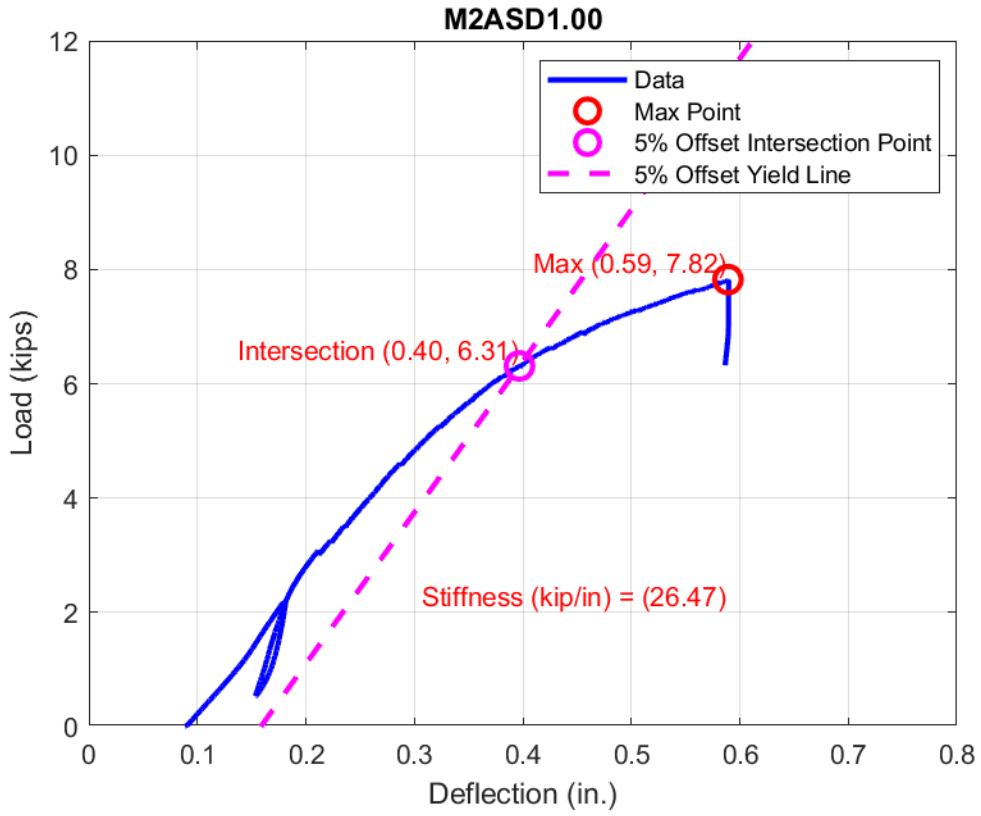
M2ASD1.00
Data
Max Point
5% Offset Intersection Point
5% Offset Yield Line
Max (0.59, 7.82)
Intersection (0.40, 6.31)
Stiffness (kip/in) = (26.47)
Load (kips)
Deflection (in.)
0
2
4
6
8
10
12
0
0.1
0.2
0.3
0.4
0.5
0.6
0.7
0.8

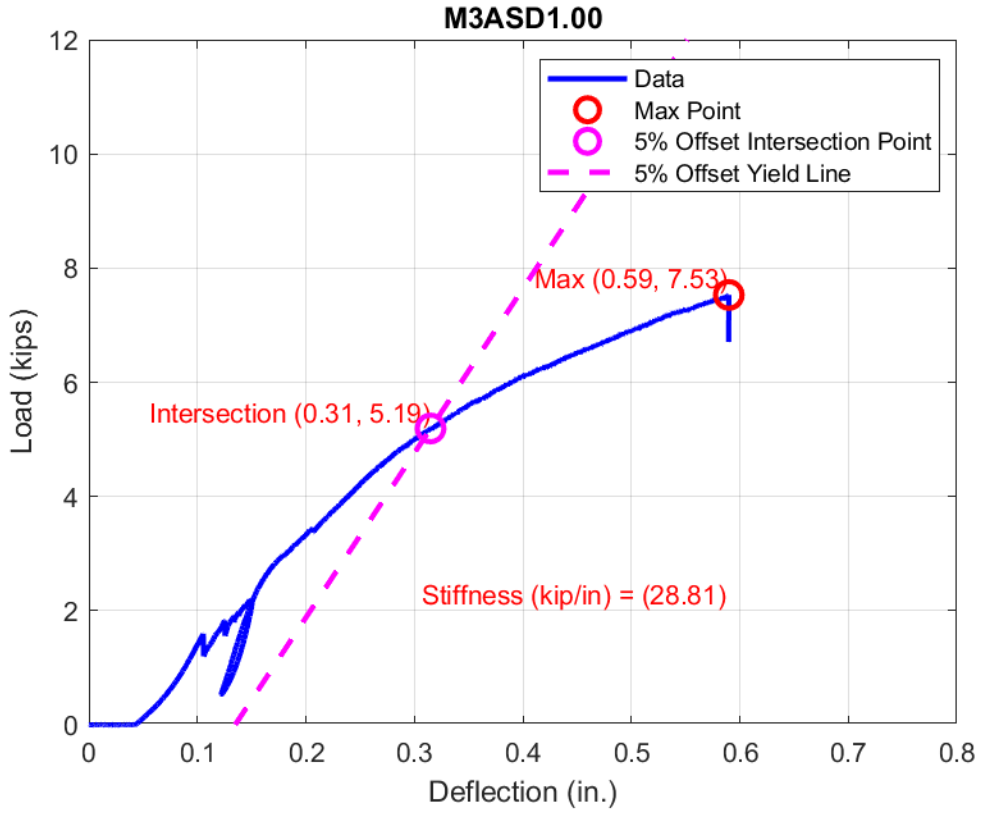
M3ASD1.00
Data
Max Point
5% Offset Intersection Point
5% Offset Yield Line
Max (0.59, 7.53)
Intersection (0.31, 5.19)
Stiffness (kip/in) = (28.81)
Load (kips)
Deflection (in.)
0
2
4
6
8
10
12
0
0.1
0.2
0.3
0.4
0.5
0.6
0.7
0.8

7.2 APPENDIX B – MONOTONIC YELLOW-POPLAR 1 INCH DIAMETER 5% OFFSET YIELD PLOTS

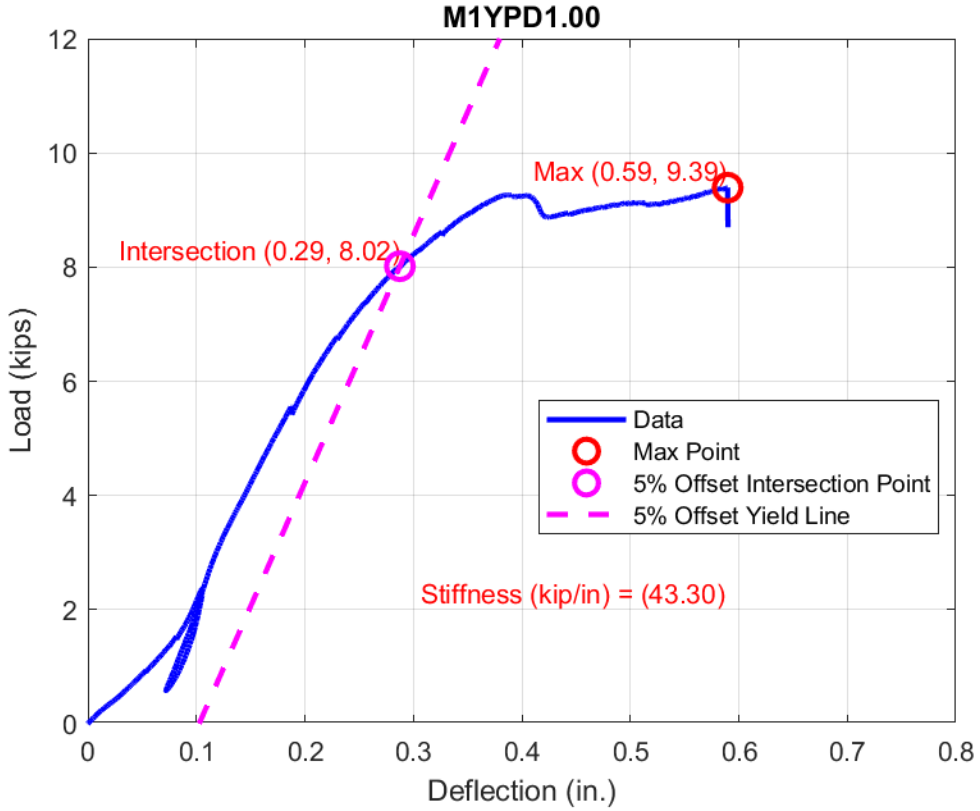

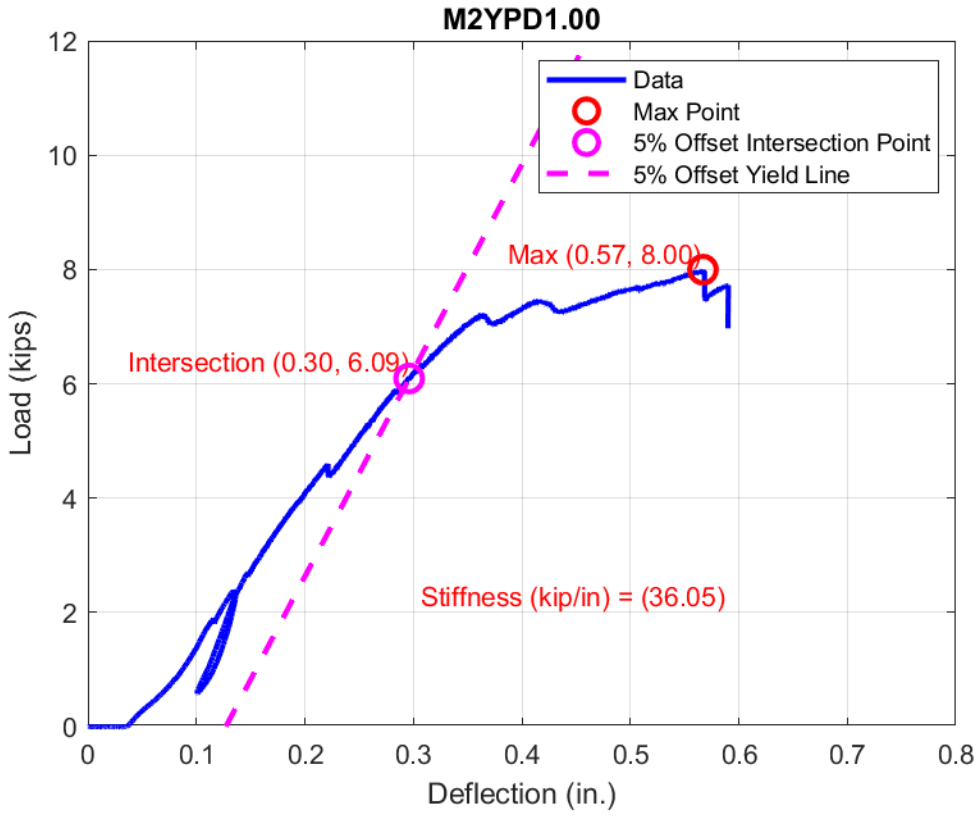
M2YPD1.00
Data
Max Point
5% Offset Intersection Point
5% Offset Yield Line
Max (0.57, 8.00)
Intersection (0.30, 6.09)
Stiffness (kip/in) = (36.05)
Load (kips)
Deflection (in.)
0
2
4
6
8
10
12
0
0.1
0.2
0.3
0.4
0.5
0.6
0.7
0.8

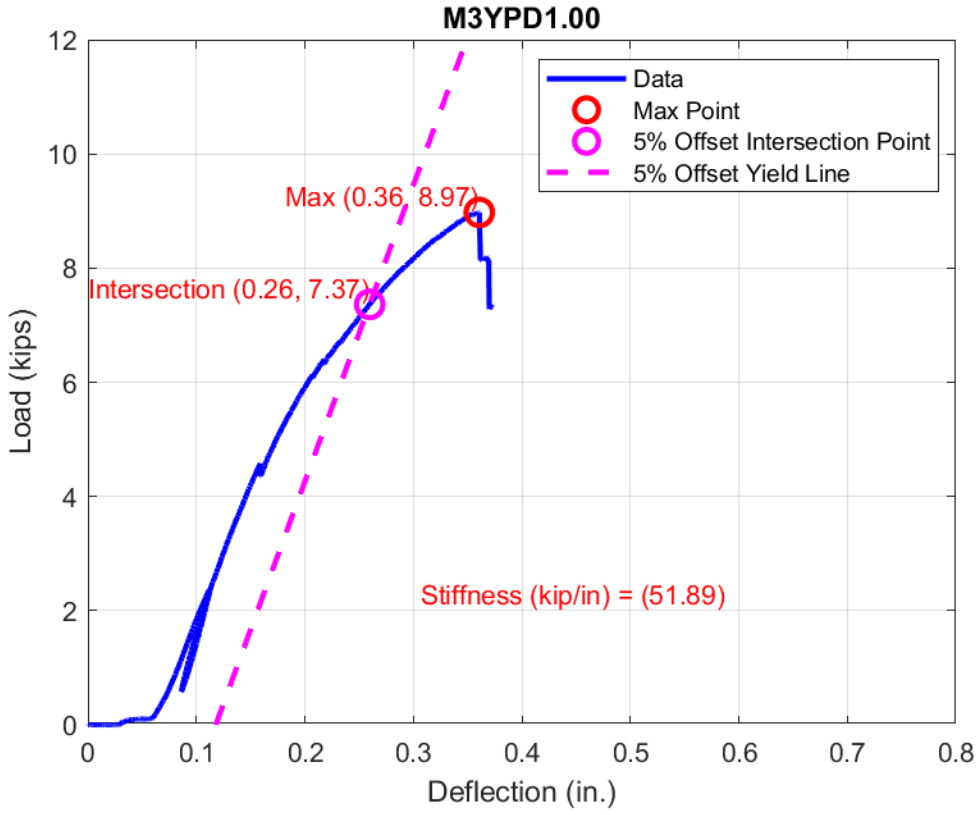
M3YPD1.00
Data
Max Point
5% Offset Intersection Point
5% Offset Yield Line
Max (0.36, 8.97)
Intersection (0.26, 7.37)
Stiffness (kip/in) = (51.89)
Load (kips)
Deflection (in.)
0
2
4
6
8
10
12
0
0.1
0.2
0.3
0.4
0.5
0.6
0.7
0.8

7.3 APPENDIX C – MONOTONIC AUSTRIAN SPRUCE 1.25 INCH DIAMETER 5% OFFSET YIELD PLOTS

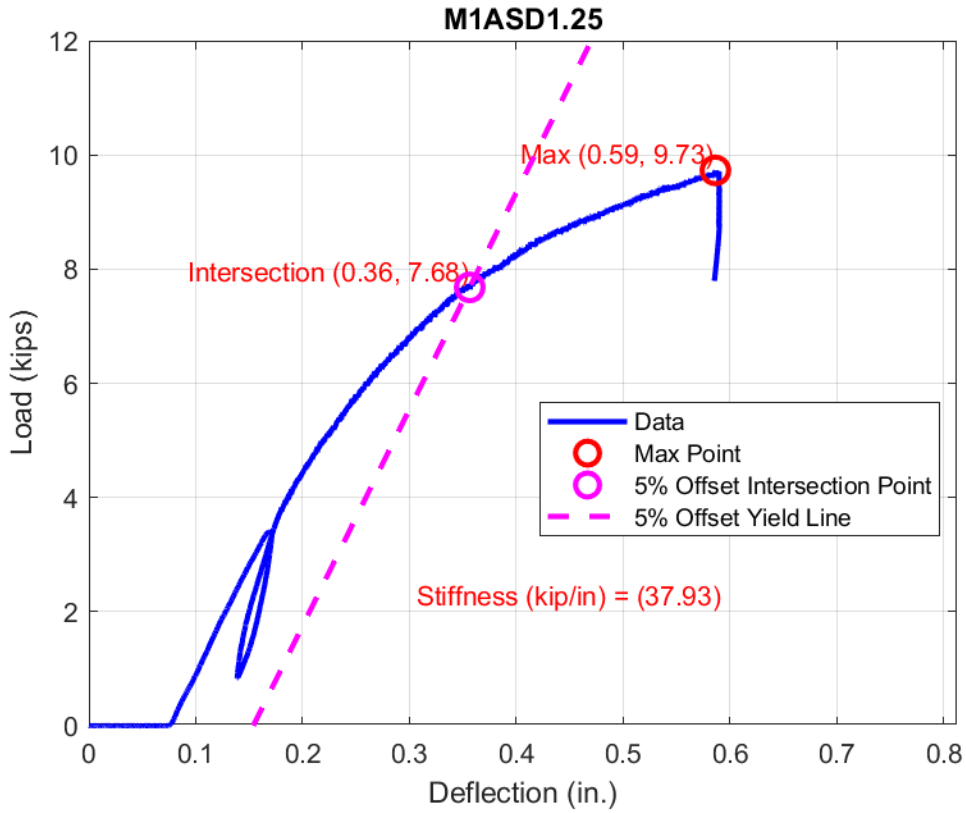

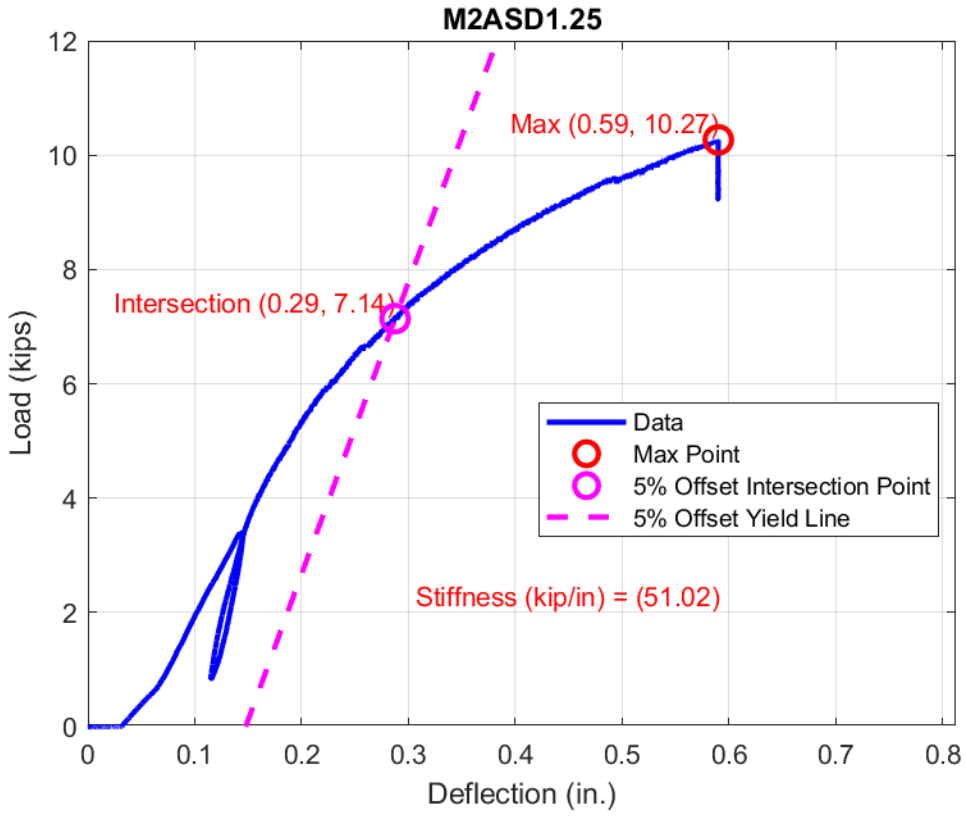
M2ASD1.25
Max (0.59, 10.27)
Intersection (0.29, 7.14)
Stiffness (kip/in) = (51.02)
Data
Max Point
5% Offset Intersection Point
5% Offset Yield Line
Load (kips)
Deflection (in.)
0
2
4
6
8
10
12
0
0.1
0.2
0.3
0.4
0.5
0.6
0.7
0.8

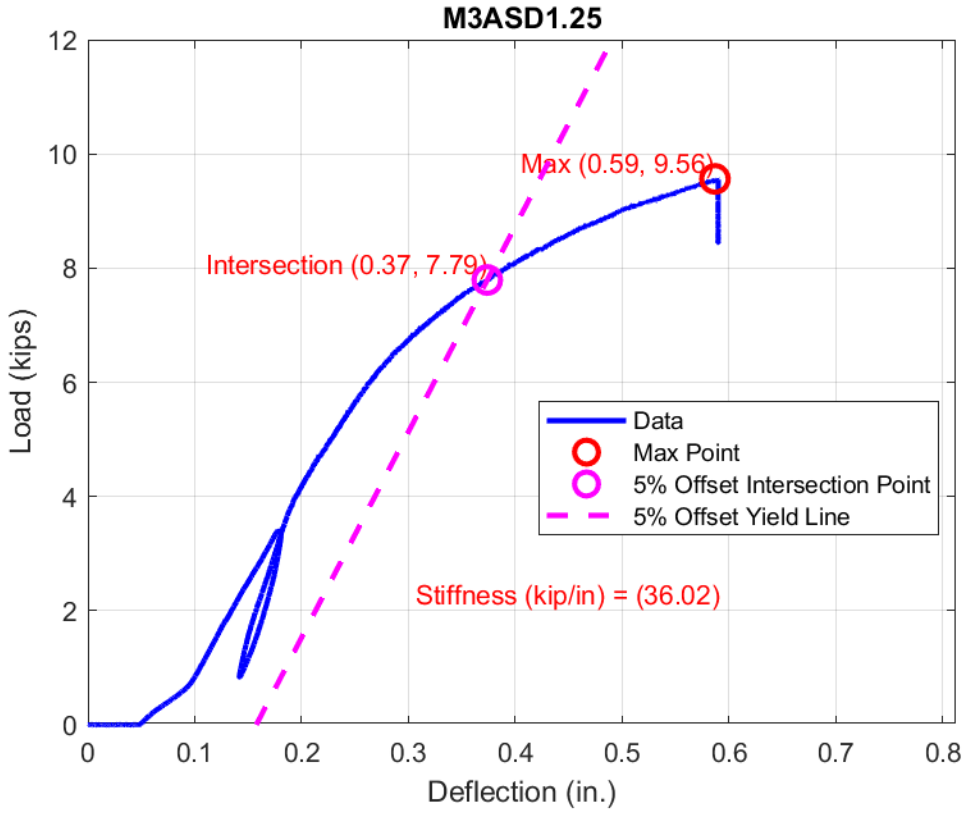
M3ASD1.25
Max (0.59, 9.56)
Intersection (0.37, 7.79)
Stiffness (kip/in) = (36.02)
Data
Max Point
5% Offset Intersection Point
5% Offset Yield Line
Load (kips)
Deflection (in.)
0
2
4
6
8
10
12
0
0.1
0.2
0.3
0.4
0.5
0.6
0.7
0.8

7.4 APPENDIX D – MONOTONIC YELLOW-POPLAR 1.25 INCH DIAMETER 5% OFFSET YIELD PLOTS

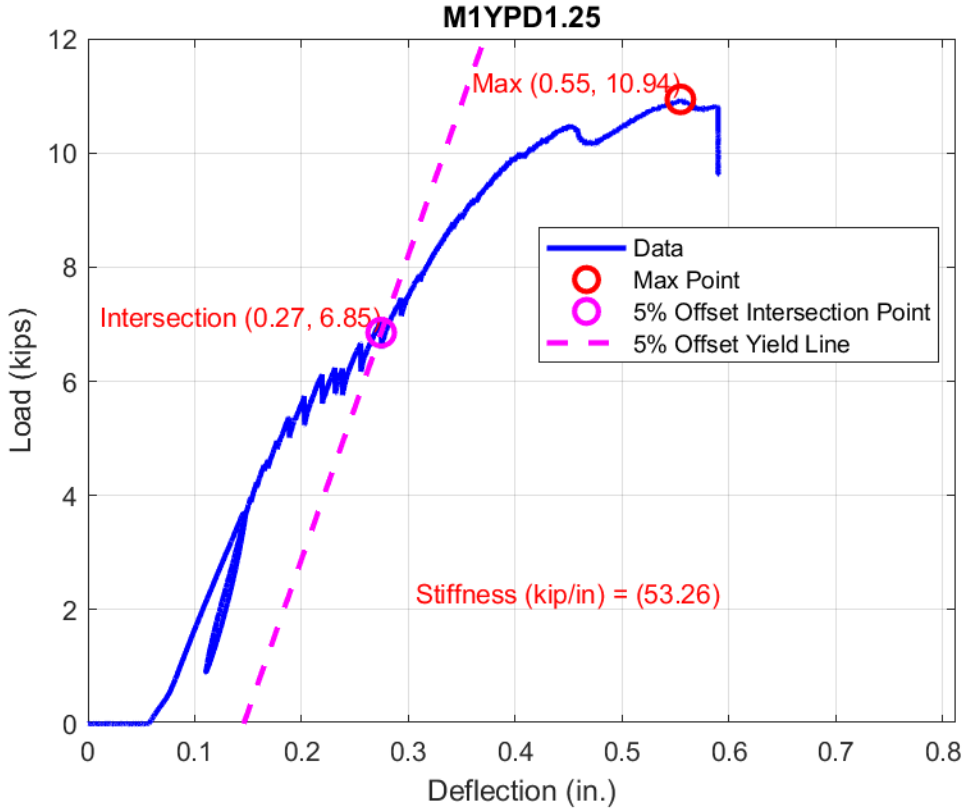

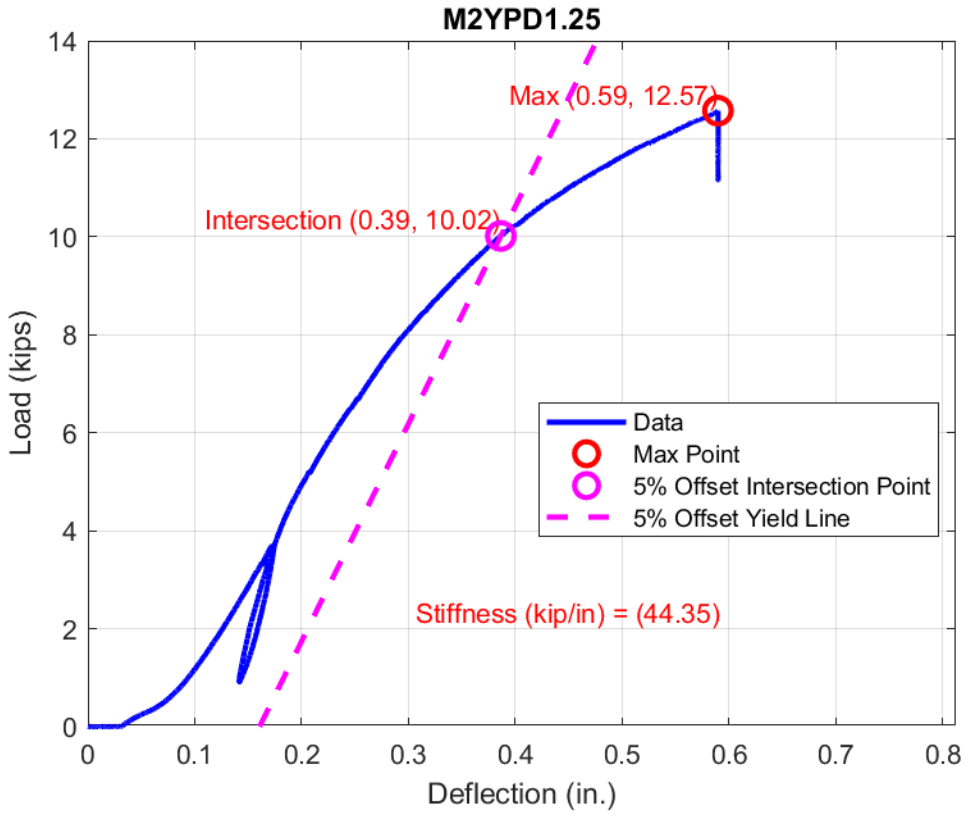
M2YPD1.25
Max (0.59, 12.57)
Intersection (0.39, 10.02)
Stiffness (kip/in) = (44.35)
Data
Max Point
5% Offset Intersection Point
5% Offset Yield Line
Load (kips)
Deflection (in.)
0
2
4
6
8
10
12
14
0
0.1
0.2
0.3
0.4
0.5
0.6
0.7
0.8

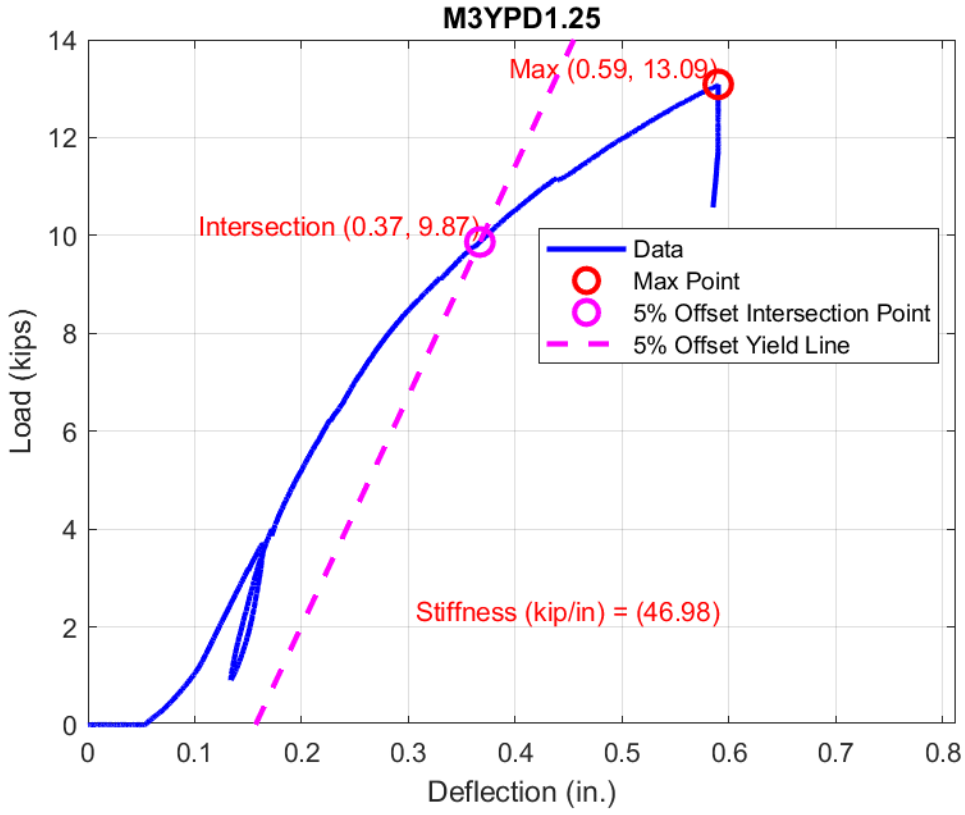
M3YPD1.25
Max (0.59, 13.09)
Intersection (0.37, 9.87)
Stiffness (kip/in) = (46.98)
Data
Max Point
5% Offset Intersection Point
5% Offset Yield Line
Load (kips)
Deflection (in.)
0
2
4
6
8
10
12
14
0
0.1
0.2
0.3
0.4
0.5
0.6
0.7
0.8

7.5 APPENDIX E – CYCLIC AUSTRIAN SPRUCE 1 INCH DIAMETER 5% OFFSET YIELD PLOTS

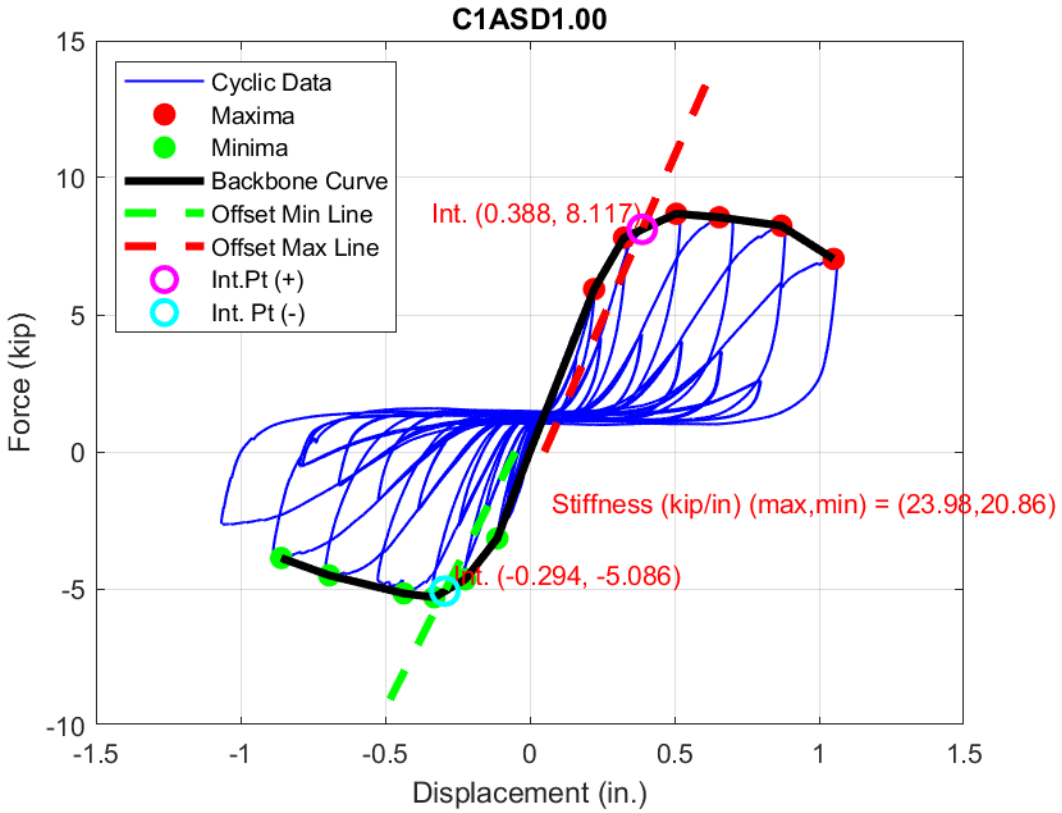

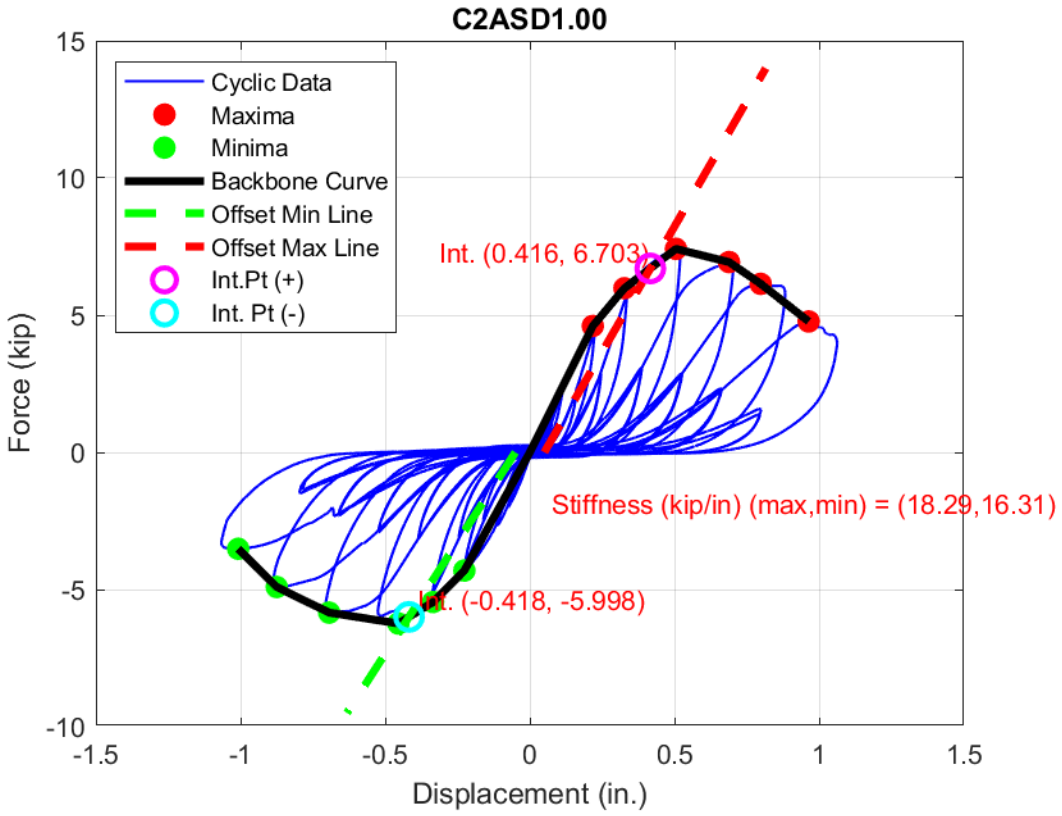
C2ASD1.00
Cyclic Data
Maxima
Minima
Backbone Curve
Offset Min Line
Offset Max Line
Int.Pt (+)
Int. Pt (-)
Int. (0.416, 6.703)
Stiffness (kip/in) (max,min) = (18.29,16.31)
Int. (-0.418, -5.998)
Force (kip)
Displacement (in.)
15
10
5
0
-5
-10
-1.5
-1
-0.5
0
0.5
1
1.5

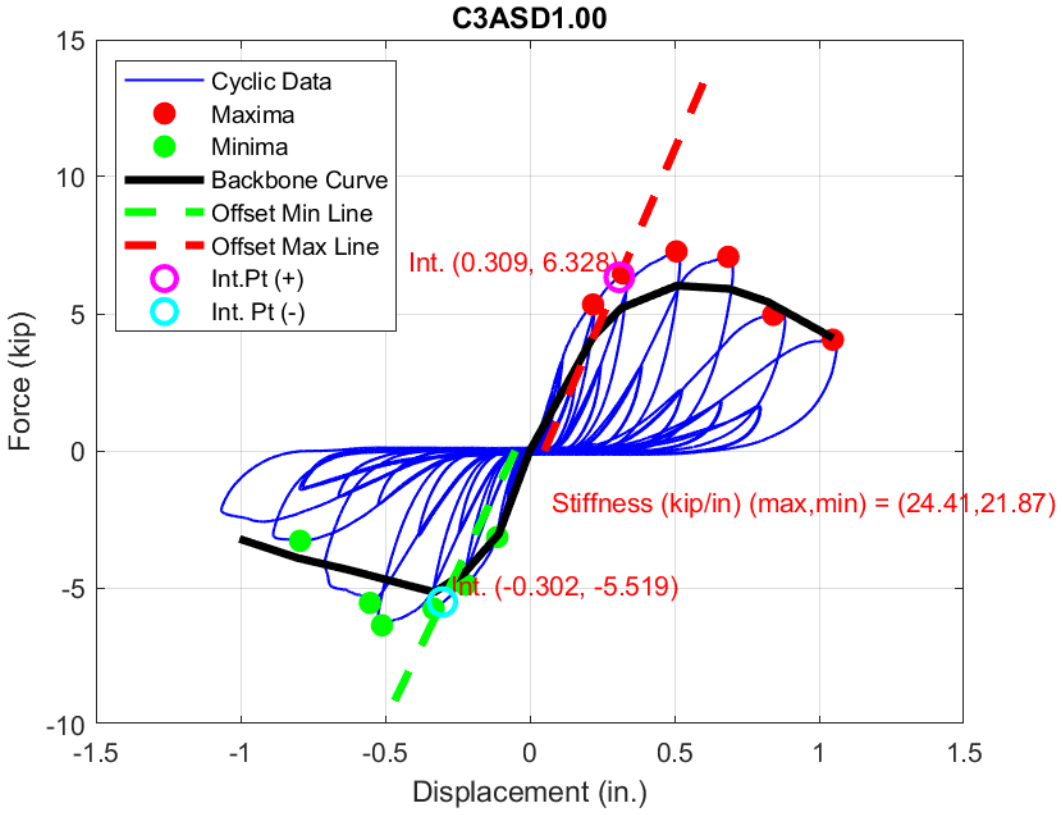
C3ASD1.00
Cyclic Data
Maxima
Minima
Backbone Curve
Offset Min Line
Offset Max Line
Int.Pt (+)
Int. Pt (-)
Int. (0.309, 6.328)
Stiffness (kip/in) (max,min) = (24.41,21.87)
Int. (-0.302, -5.519)
Force (kip)
Displacement (in.)
15
10
5
0
-5
-10
-1.5
-1
-0.5
0
0.5
1
1.5

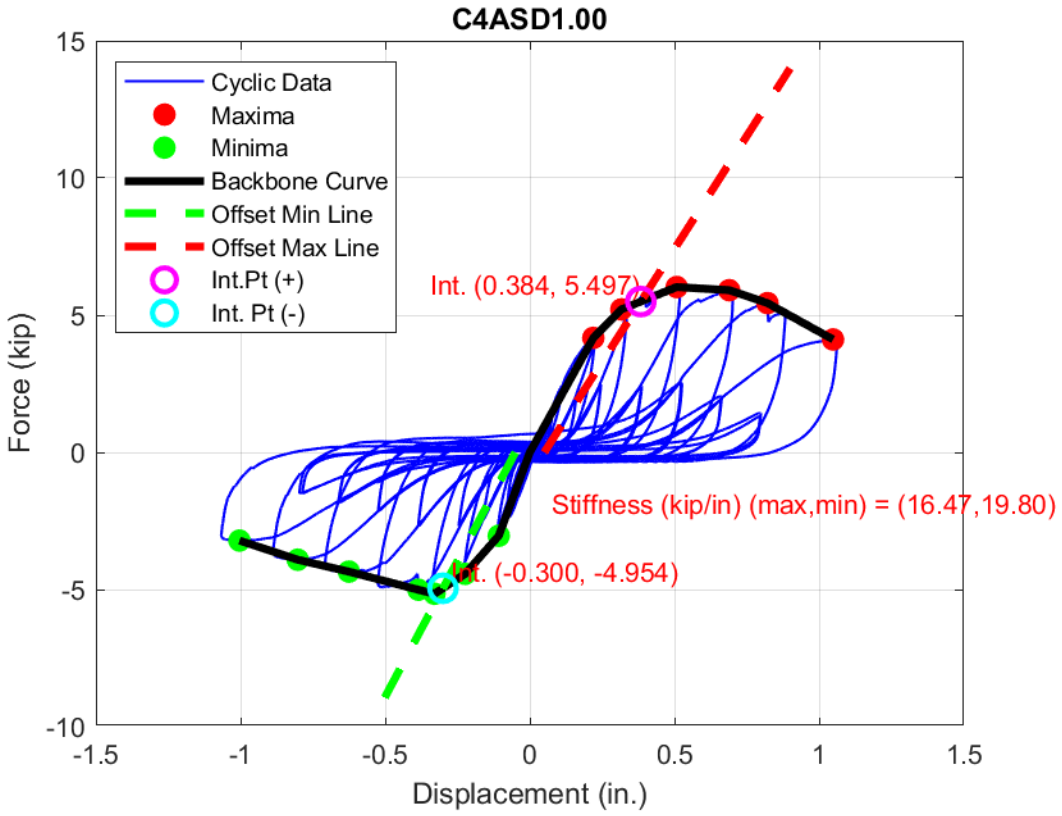
C4ASD1.00
Cyclic Data
Maxima
Minima
Backbone Curve
Offset Min Line
Offset Max Line
Int.Pt (+)
Int. Pt (-)
Int. (0.384, 5.497)
Stiffness (kip/in) (max,min) = (16.47,19.80)
Int. (-0.300, -4.954)
Force (kip)
Displacement (in.)
15
10
5
0
-5
-10
-1.5
-1
-0.5
0
0.5
1
1.5

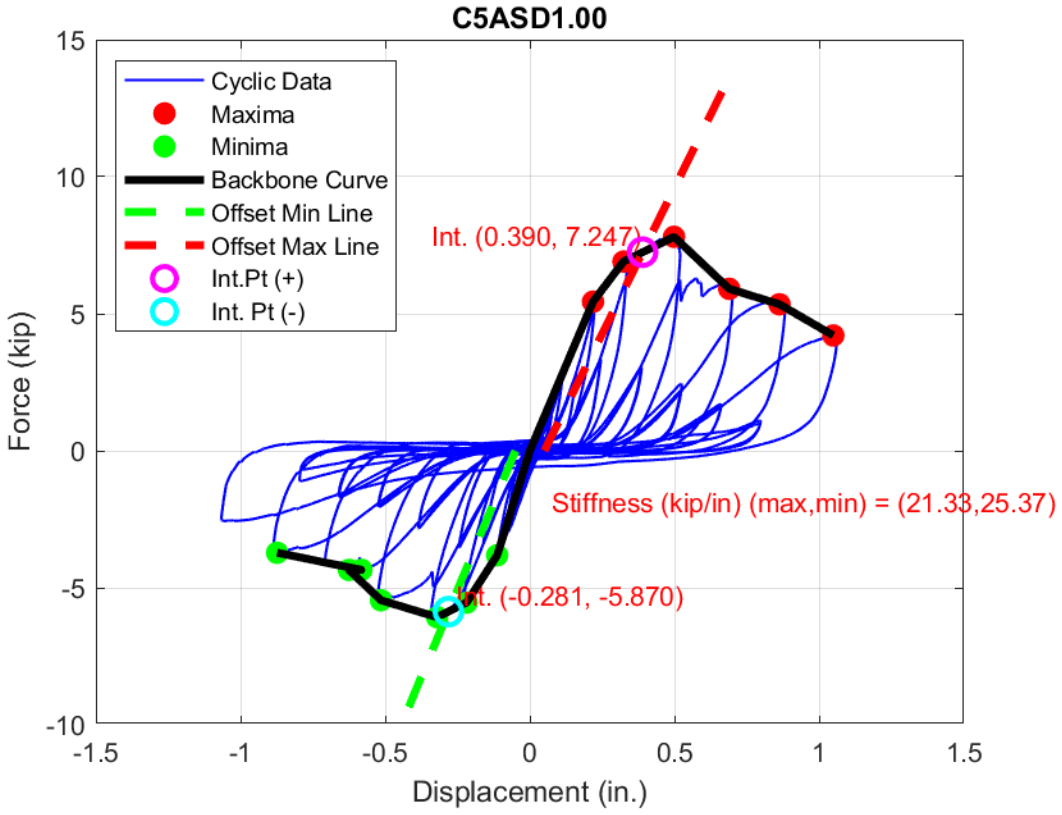
C5ASD1.00
Cyclic Data
Maxima
Minima
Backbone Curve
Offset Min Line
Offset Max Line
Int.Pt (+)
Int. Pt (-)
Int. (0.390, 7.247)
Stiffness (kip/in) (max,min) = (21.33,25.37)
Int. (-0.281, -5.870)
Force (kip)
Displacement (in.)
15
10
5
0
-5
-10
-1.5
-1
-0.5
0
0.5
1
1.5

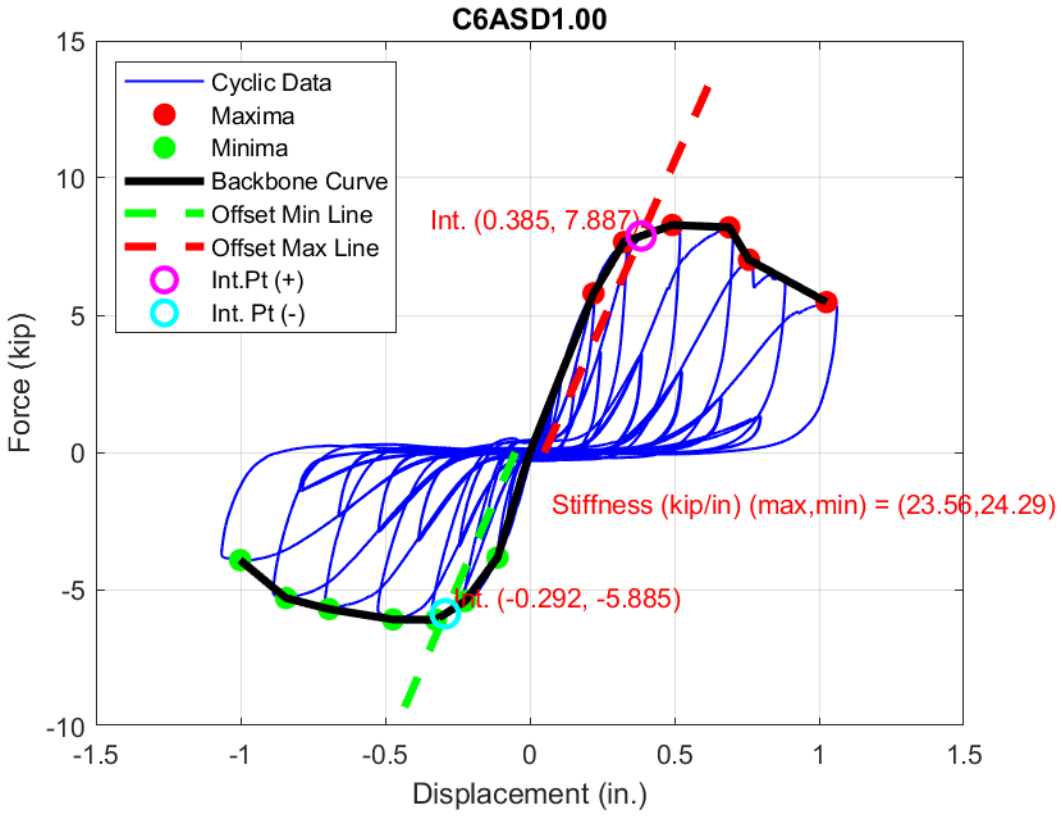
C6ASD1.00
Cyclic Data
Maxima
Minima
Backbone Curve
Offset Min Line
Offset Max Line
Int.Pt (+)
Int. Pt (-)
Int. (0.385, 7.887)
Stiffness (kip/in) (max,min) = (23.56,24.29)
Int. (-0.292, -5.885)
Force (kip)
Displacement (in.)
15
10
5
0
-5
-10
-1.5
-1
-0.5
0
0.5
1
1.5

7.6 APPENDIX F – CYCLIC YELLOW-POPLAR 1 INCH DIAMETER 5% OFFSET YIELD PLOTS

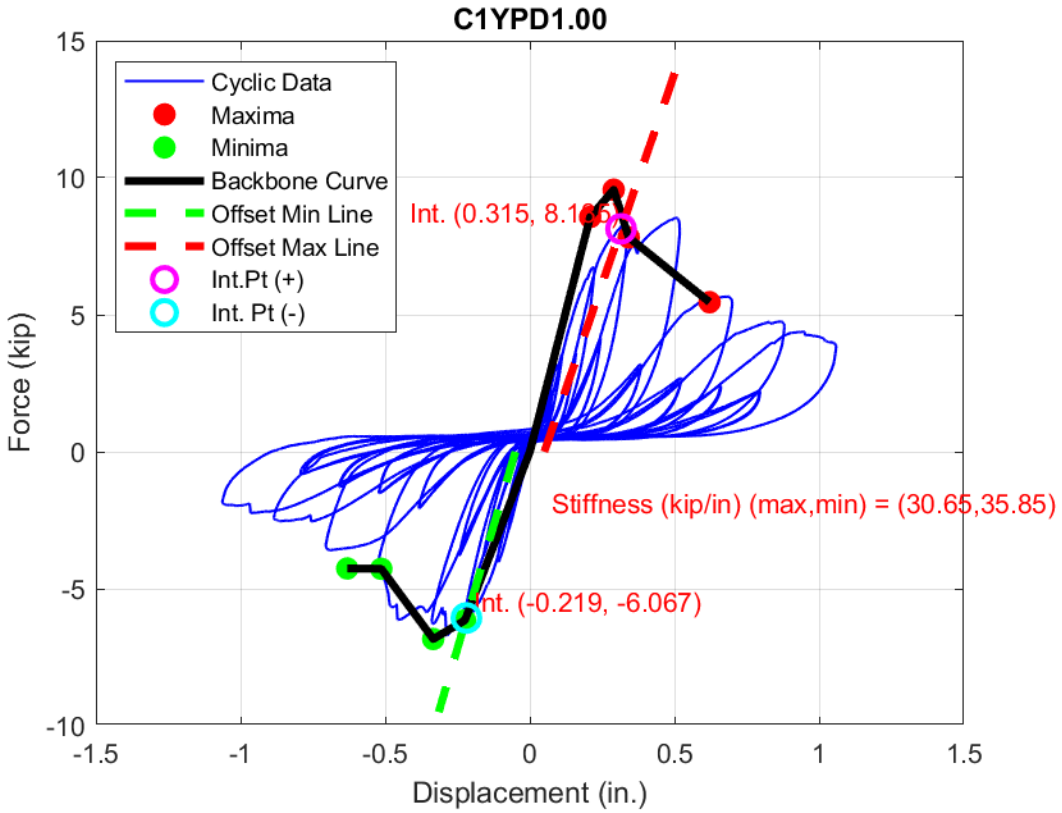

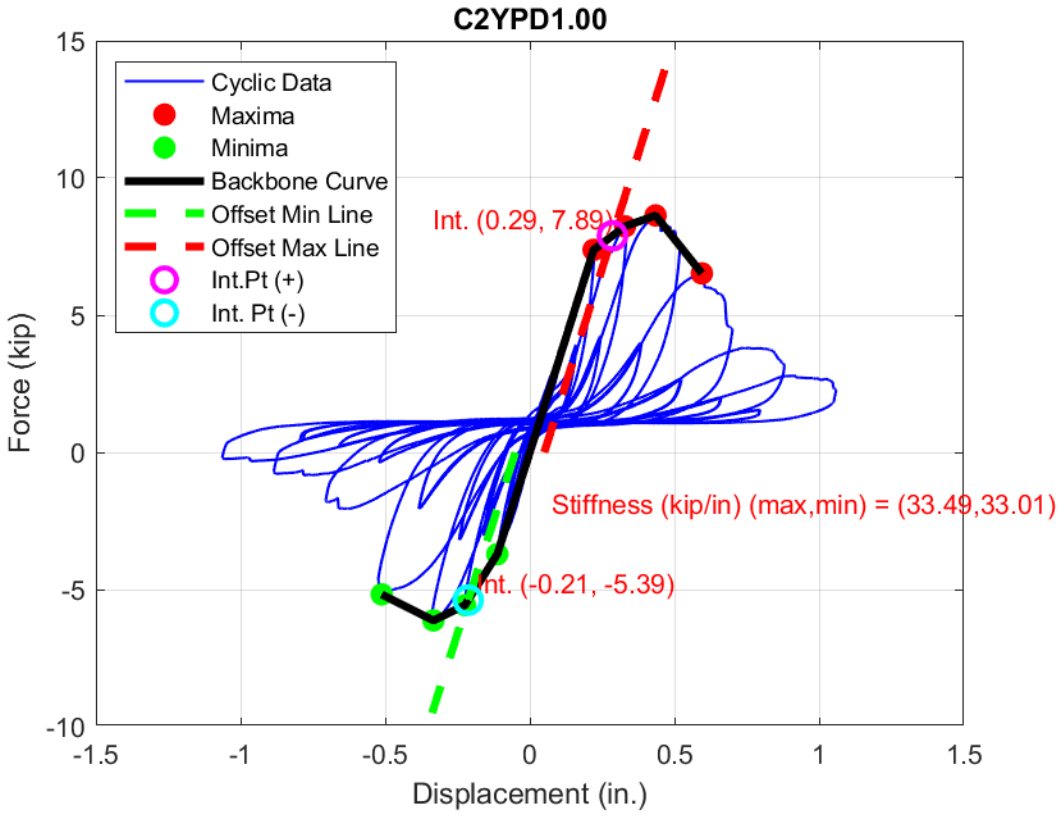
C2YPD1.00
Cyclic Data
Maxima
Minima
Backbone Curve
Offset Min Line
Offset Max Line
Int.Pt (+)
Int. Pt (-)
Int. (0.29, 7.89)
Stiffness (kip/in) (max,min) = (33.49,33.01)
Int. (-0.21, -5.39)
Force (kip)
Displacement (in.)
15
10
5
0
-5
-10
-1.5
-1
-0.5
0
0.5
1
1.5

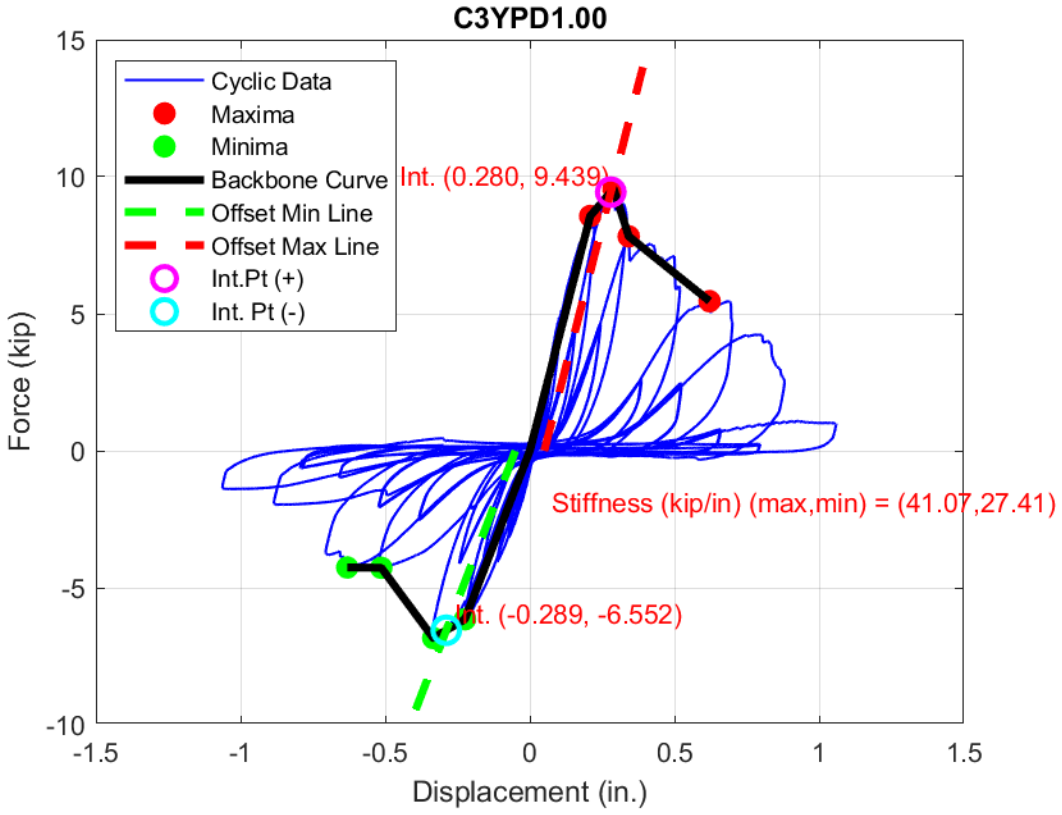
C3YPD1.00
Cyclic Data
Maxima
Minima
Backbone Curve
Offset Min Line
Offset Max Line
Int.Pt (+)
Int. Pt (-)
Int. (0.280, 9.439)
Stiffness (kip/in) (max,min) = (41.07,27.41)
Int. (-0.289, -6.552)
Force (kip)
Displacement (in.)
15
10
5
0
-5
-10
-1.5
-1
-0.5
0
0.5
1
1.5

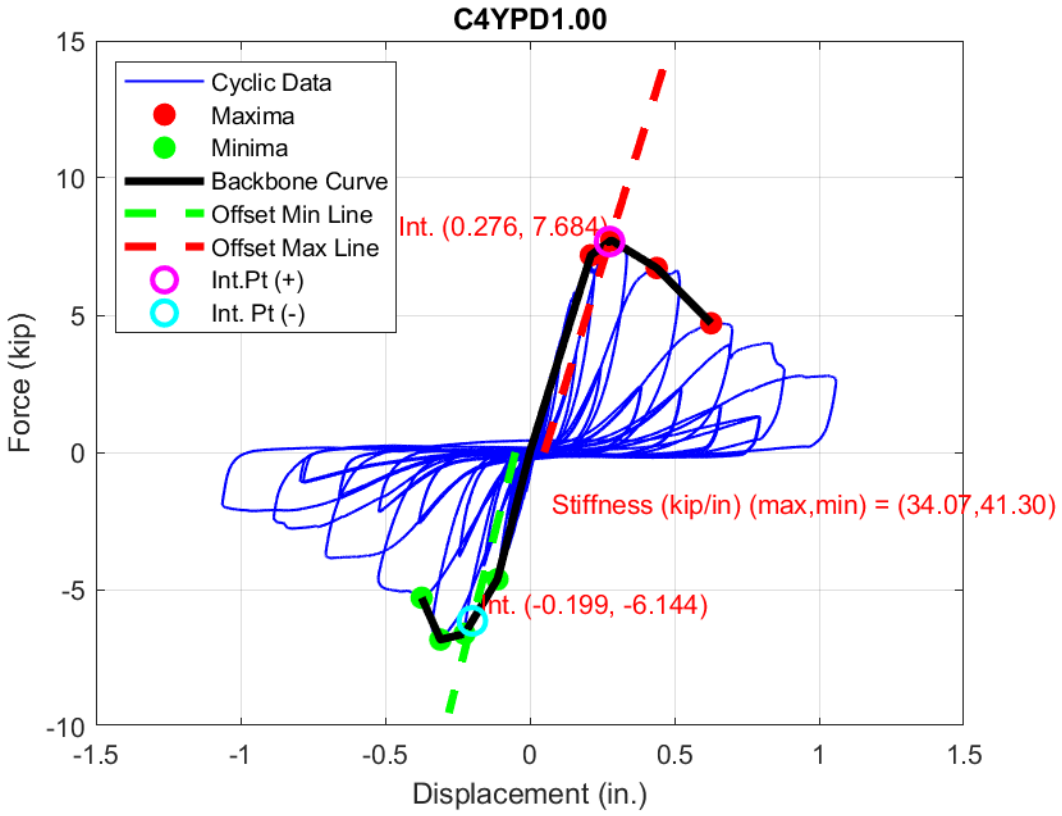
C4YPD1.00
Cyclic Data
Maxima
Minima
Backbone Curve
Offset Min Line
Offset Max Line
Int.Pt (+)
Int. Pt (-)
Int. (0.276, 7.684)
Stiffness (kip/in) (max,min) = (34.07,41.30)
Int. (-0.199, -6.144)
Force (kip)
Displacement (in.)
15
10
5
0
-5
-10
-1.5
-1
-0.5
0
0.5
1
1.5

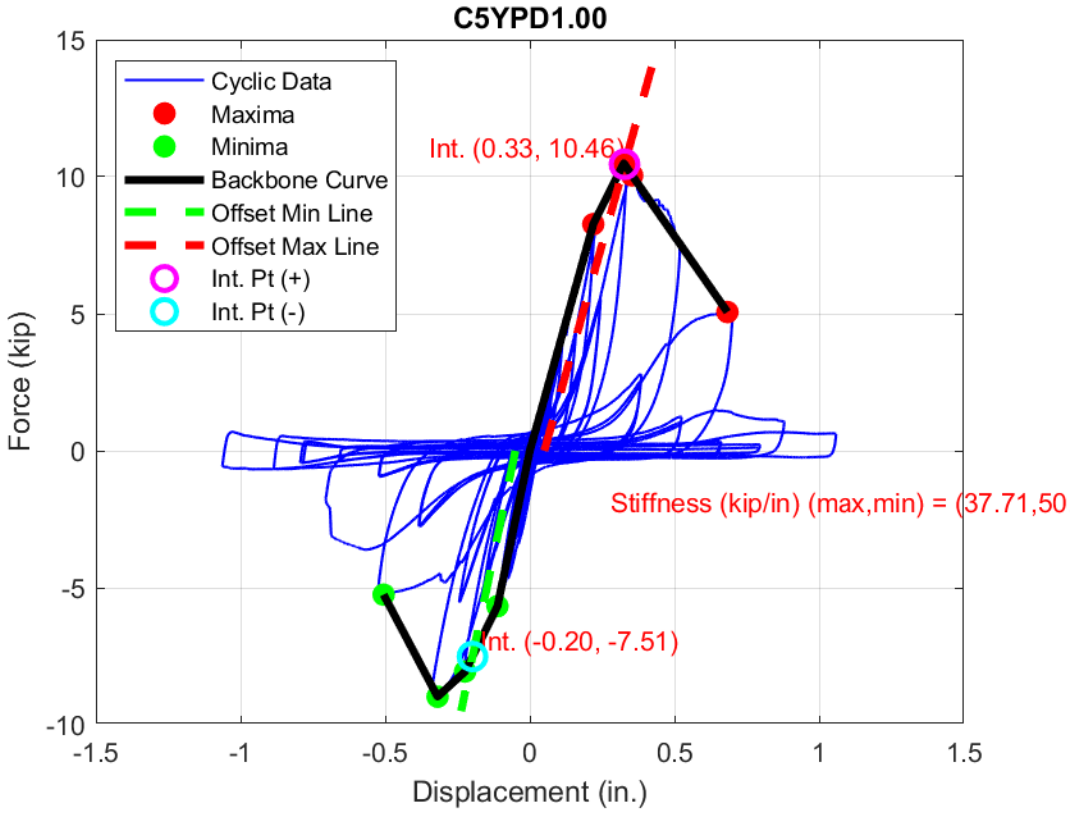
C5YPD1.00
Cyclic Data
Maxima
Minima
Backbone Curve
Offset Min Line
Offset Max Line
Int. Pt (+)
Int. Pt (-)
Int. (0.33, 10.46)
Stiffness (kip/in) (max,min) = (37.71,50
Int. (-0.20, -7.51)
Force (kip)
Displacement (in.)
15
10
5
0
-5
-10
-1.5
-1
-0.5
0
0.5
1
1.5

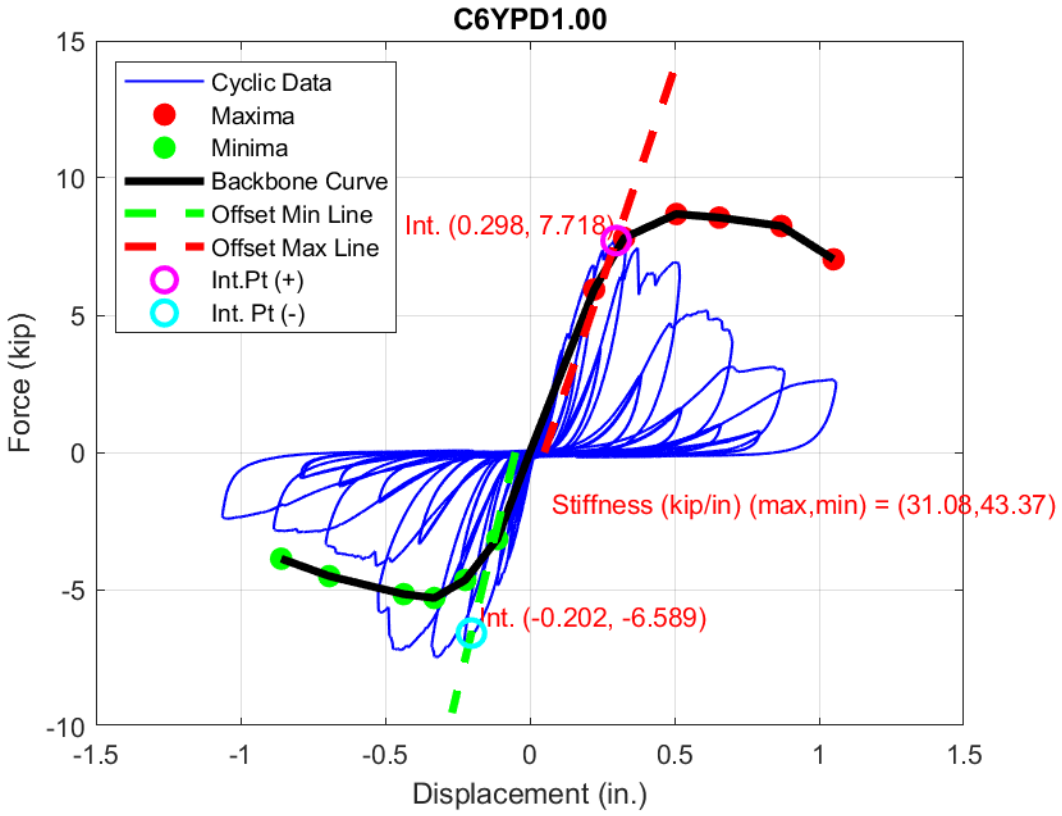
C6YPD1.00
Cyclic Data
Maxima
Minima
Backbone Curve
Offset Min Line
Offset Max Line
Int.Pt (+)
Int. Pt (-)
Int. (0.298, 7.718)
Stiffness (kip/in) (max,min) = (31.08,43.37)
Int. (-0.202, -6.589)
Force (kip)
Displacement (in.)
15
10
5
0
-5
-10
-1.5
-1
-0.5
0
0.5
1
1.5

7.7 APPENDIX G – CYCLIC AUSTRIAN SPRUCE 1.25 INCH DIAMETER 5% OFFSET YIELD PLOTS

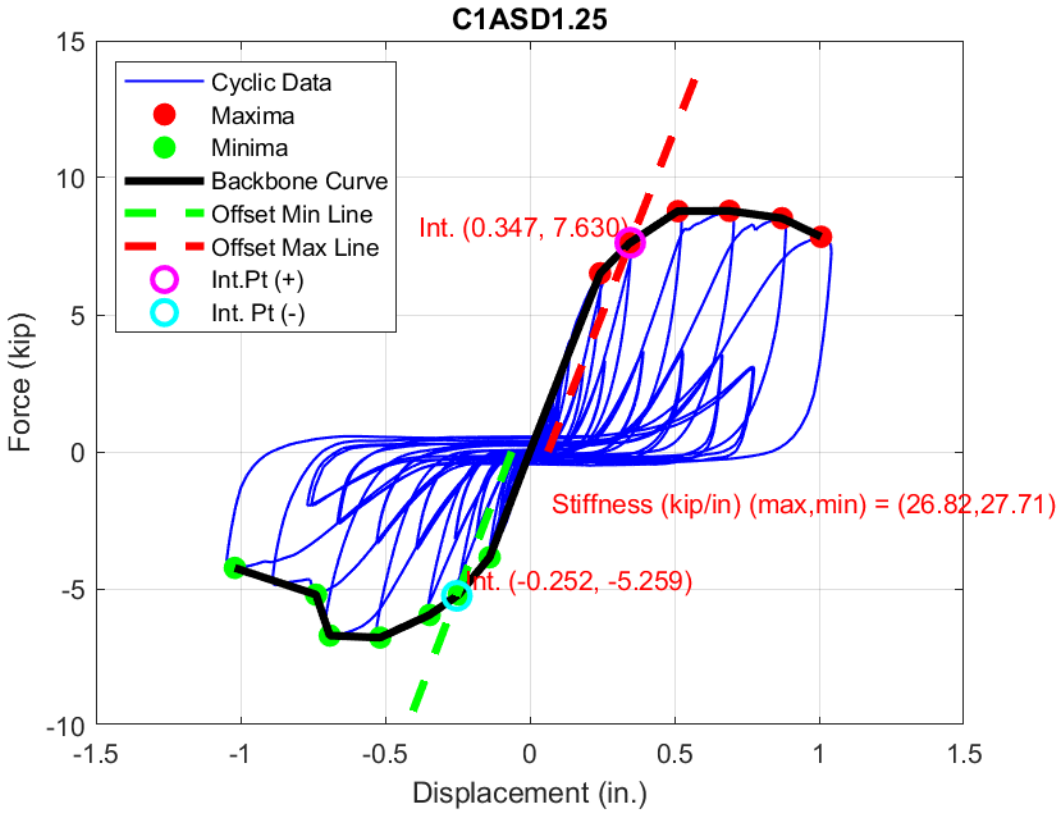

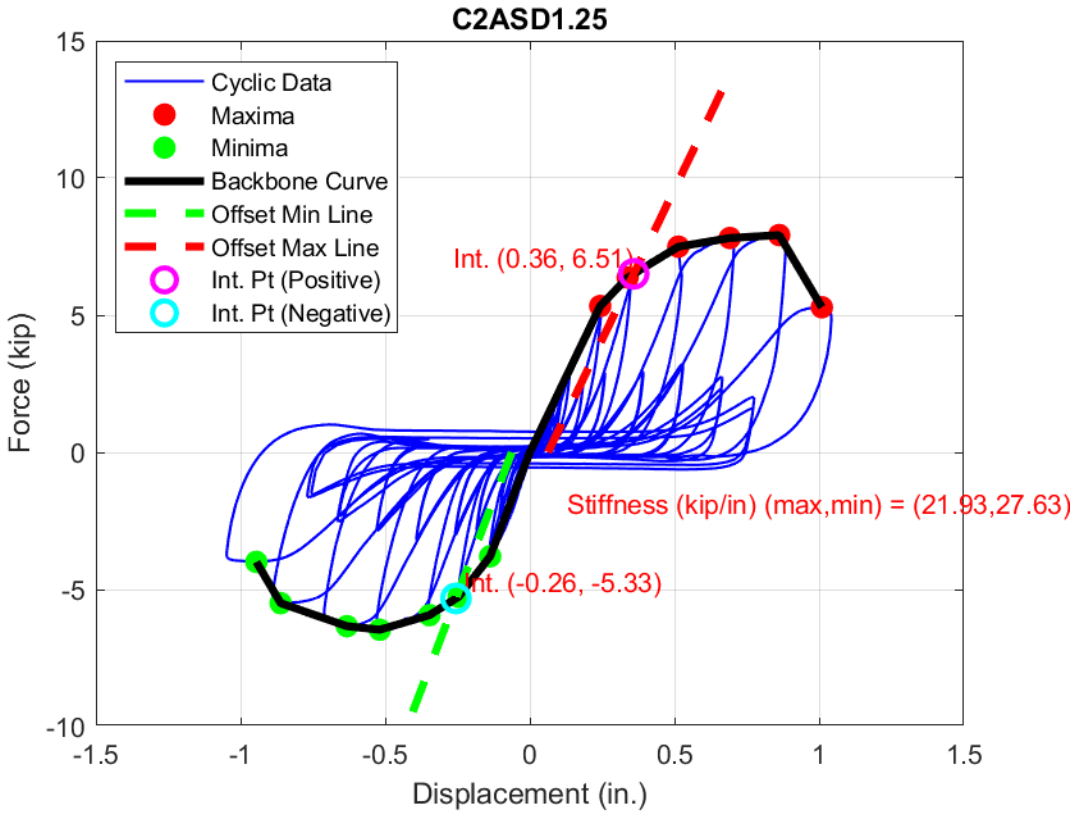
C2ASD1.25
Cyclic Data
Maxima
Minima
Backbone Curve
Offset Min Line
Offset Max Line
Int. Pt (Positive)
Int. Pt (Negative)
Int. (0.36, 6.51)
Stiffness (kip/in) (max,min) = (21.93,27.63)
Int. (-0.26, -5.33)
Force (kip)
Displacement (in.)
15
10
5
0
-5
-10
-1.5
-1
-0.5
0
0.5
1
1.5

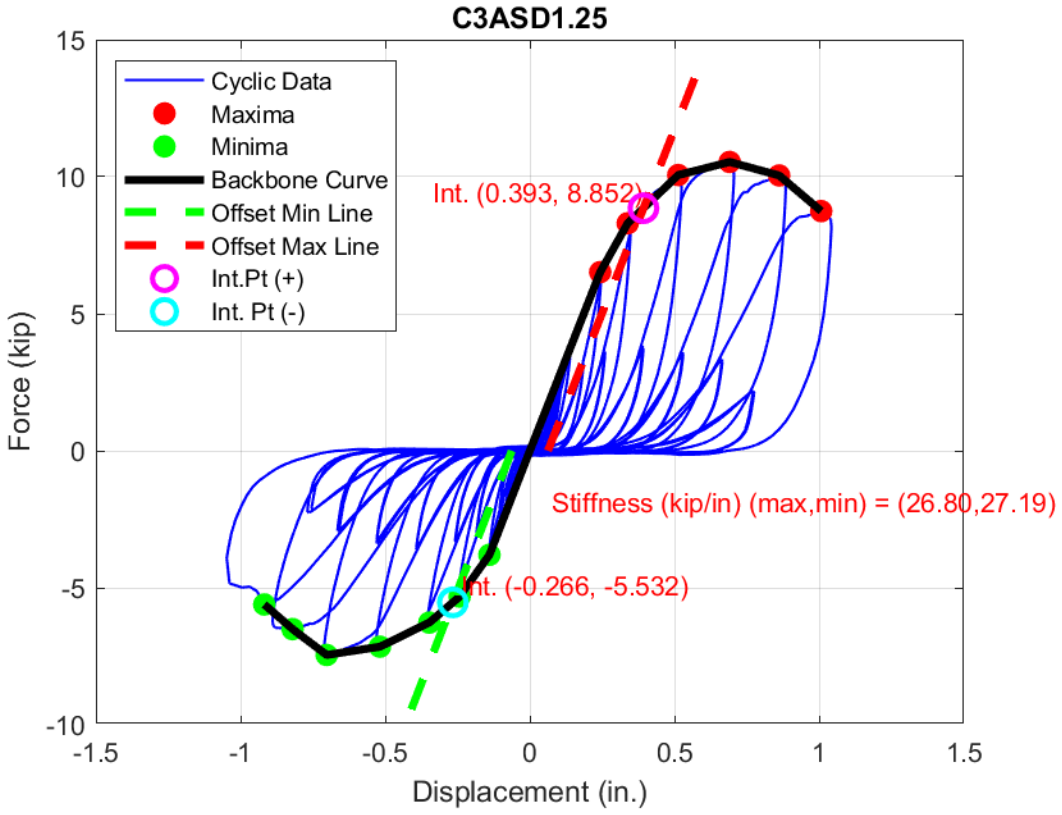
C3ASD1.25
Cyclic Data
Maxima
Minima
Backbone Curve
Offset Min Line
Offset Max Line
Int.Pt (+)
Int. Pt (-)
Int. (0.393, 8.852)
Stiffness (kip/in) (max,min) = (26.80,27.19)
Int. (-0.266, -5.532)
Force (kip)
Displacement (in.)
15
10
5
0
-5
-10
-1.5
-1
-0.5
0
0.5
1
1.5

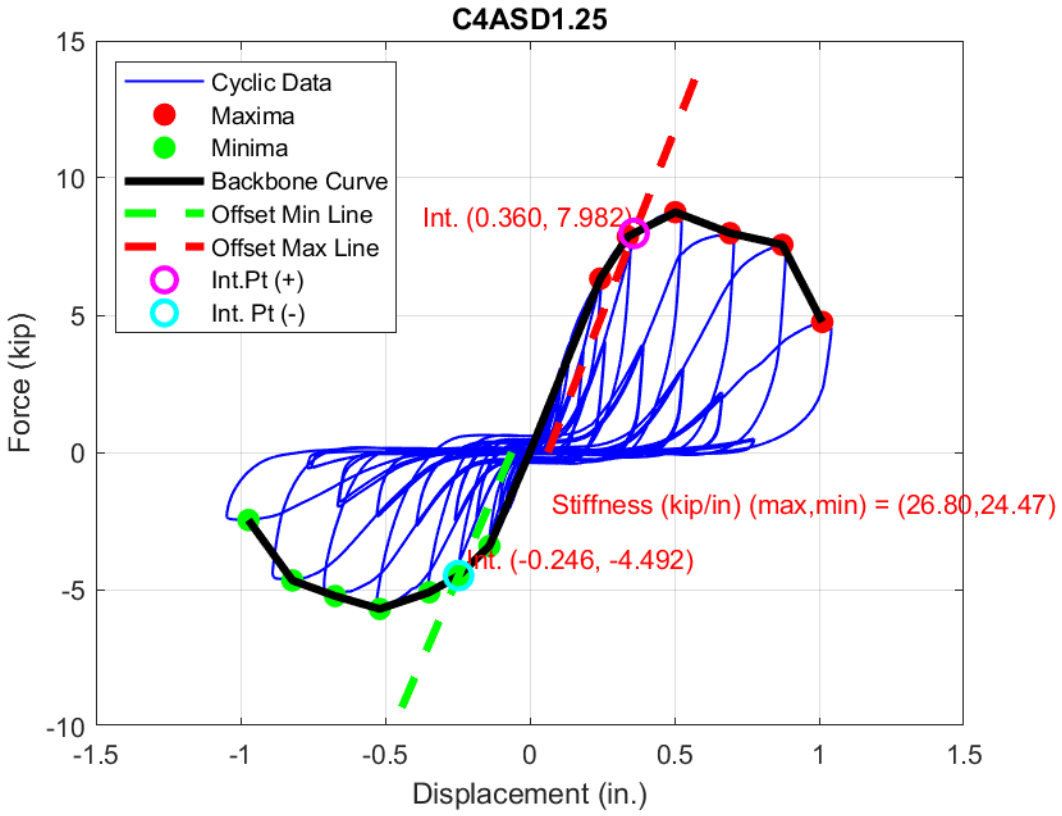
C4ASD1.25
Cyclic Data
Maxima
Minima
Backbone Curve
Offset Min Line
Offset Max Line
Int.Pt (+)
Int. Pt (-)
Int. (0.360, 7.982)
Stiffness (kip/in) (max,min) = (26.80,24.47)
Int. (-0.246, -4.492)
Force (kip)
Displacement (in.)
15
10
5
0
-5
-10
-1.5
-1
-0.5
0
0.5
1
1.5

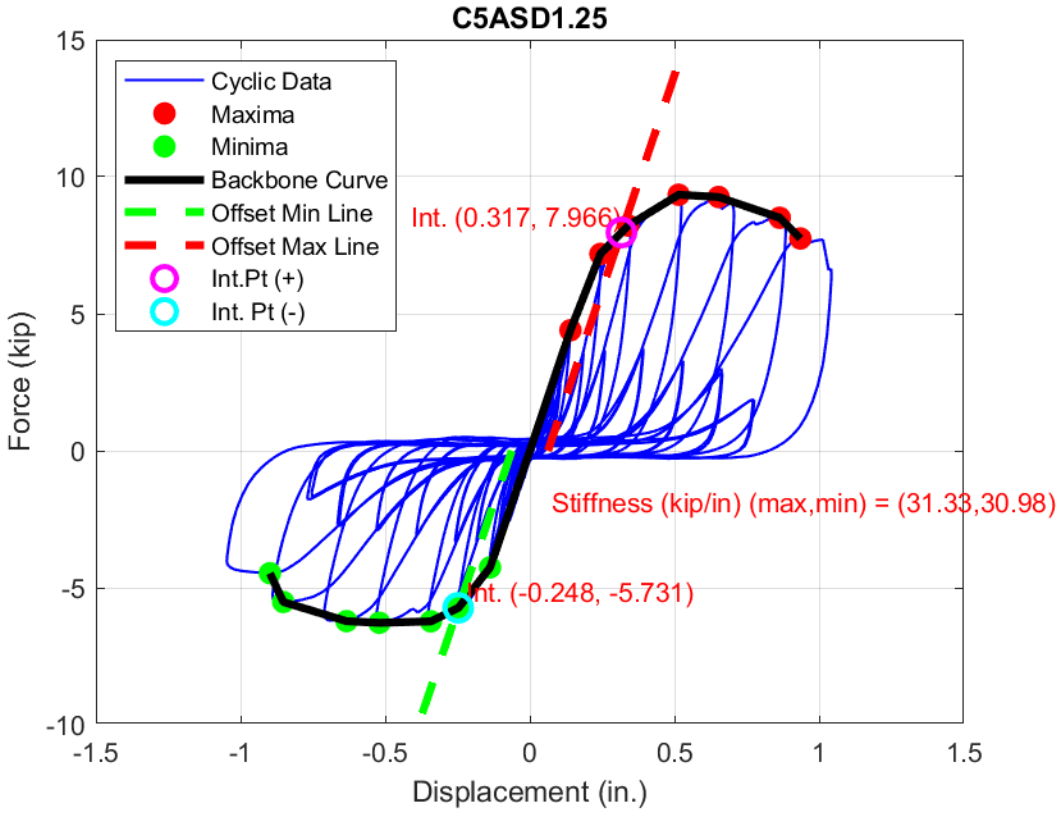
C5ASD1.25
Cyclic Data
Maxima
Minima
Backbone Curve
Offset Min Line
Offset Max Line
Int.Pt (+)
Int. Pt (-)
Int. (0.317, 7.966)
Stiffness (kip/in) (max,min) = (31.33,30.98)
Int. (-0.248, -5.731)
Force (kip)
Displacement (in.)
15
10
5
0
-5
-10
-1.5
-1
-0.5
0
0.5
1
1.5

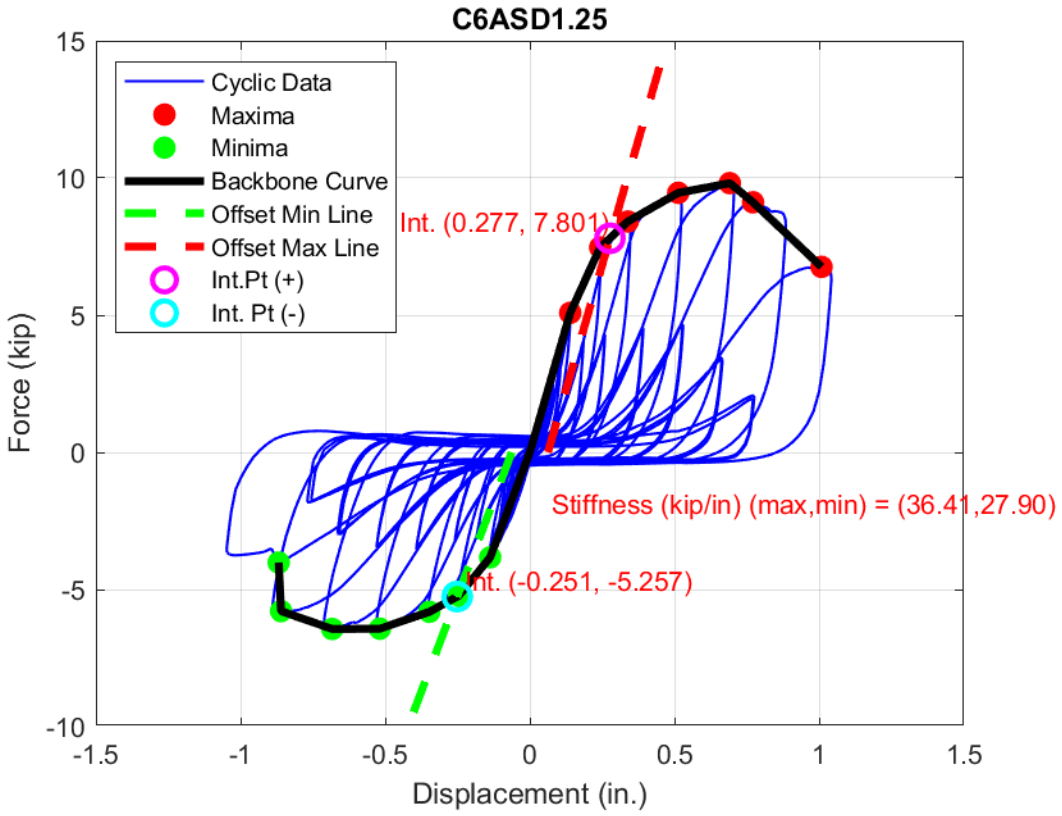
C6ASD1.25
Cyclic Data
Maxima
Minima
Backbone Curve
Offset Min Line
Offset Max Line
Int.Pt (+)
Int. Pt (-)
Int. (0.277, 7.801)
Stiffness (kip/in) (max,min) = (36.41,27.90)
Int. (-0.251, -5.257)
Force (kip)
Displacement (in.)
15
10
5
0
-5
-10
-1.5
-1
-0.5
0
0.5
1
1.5

7.8 APPENDIX H – CYCLIC YELLOW-POPLAR 1.25 INCH DIAMETER 5% OFFSET YIELD PLOTS

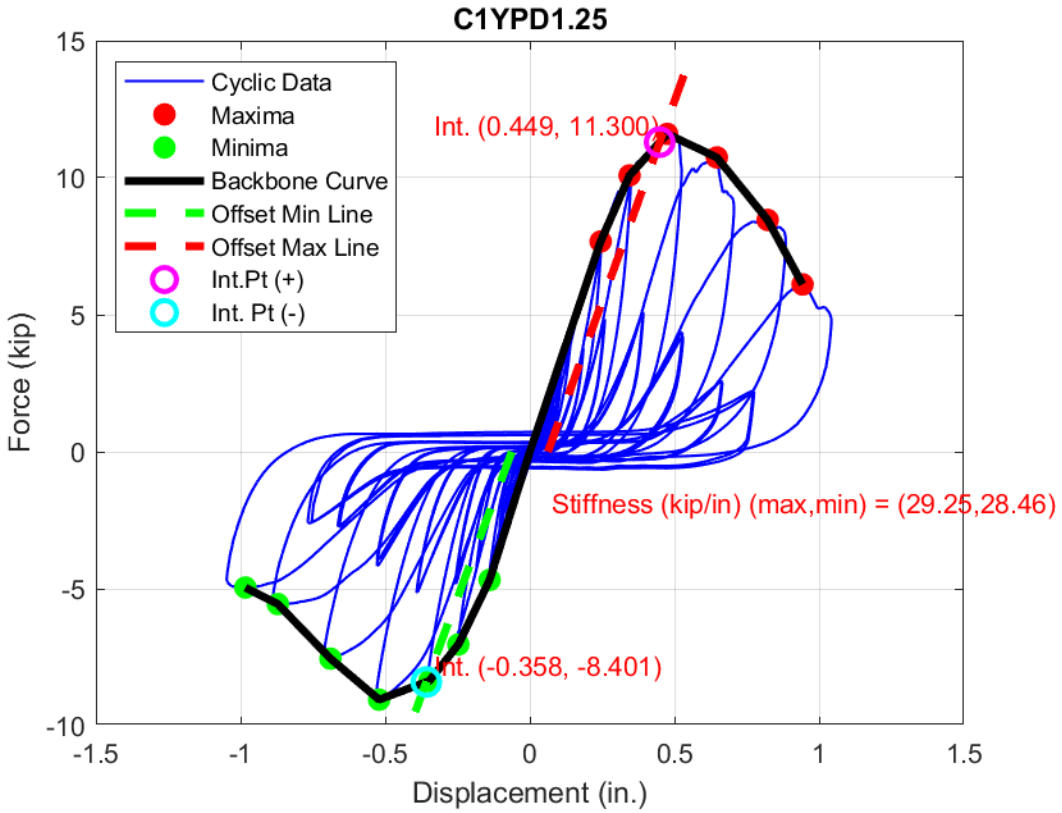

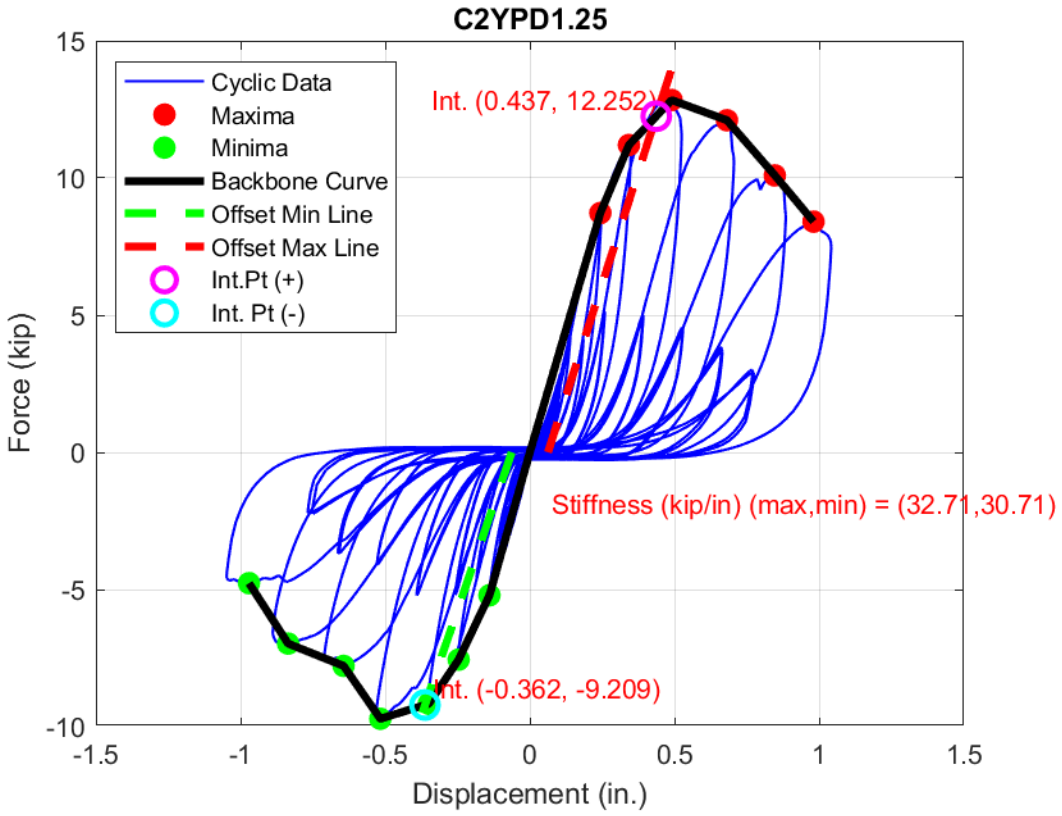
C2YPD1.25
Cyclic Data
Maxima
Minima
Backbone Curve
Offset Min Line
Offset Max Line
Int.Pt (+)
Int. Pt (-)
Int. (0.437, 12.252)
Stiffness (kip/in) (max,min) = (32.71,30.71)
Int. (-0.362, -9.209)
Force (kip)
Displacement (in.)
15
10
5
0
-5
-10
-1.5
-1
-0.5
0
0.5
1
1.5

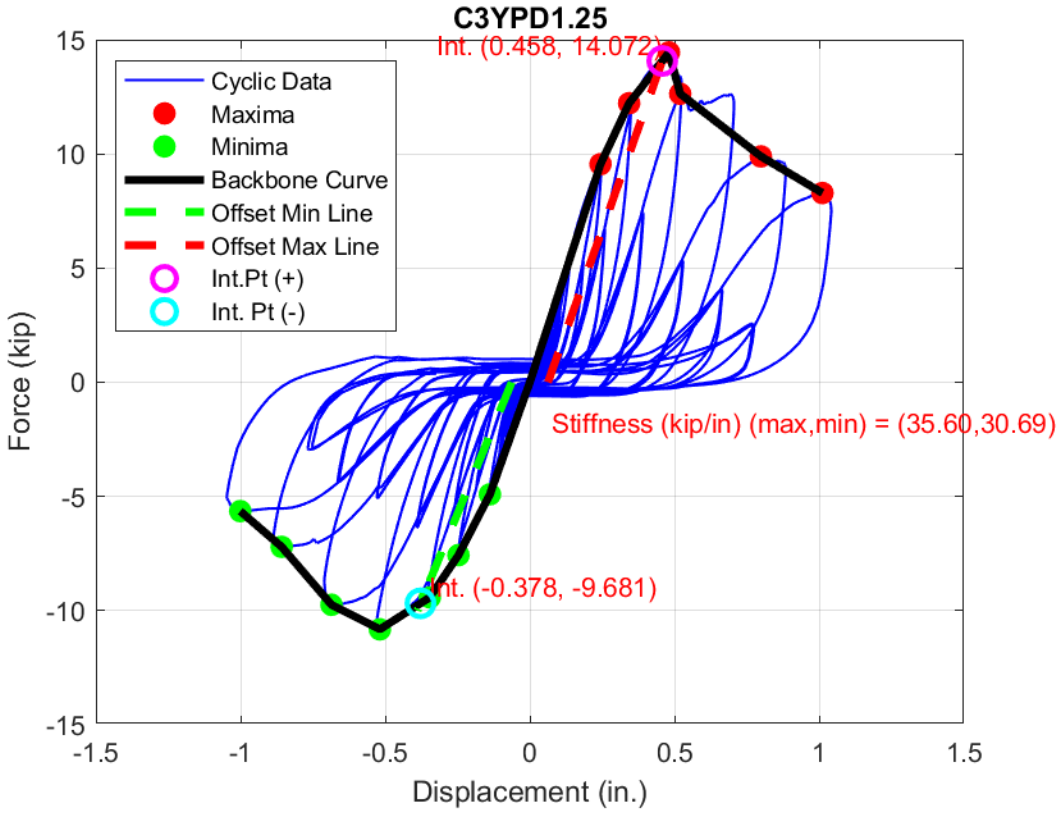
C3YPD1.25
Cyclic Data
Maxima
Minima
Backbone Curve
Offset Min Line
Offset Max Line
Int.Pt (+)
Int. Pt (-)
Int. (0.458, 14.072)
Stiffness (kip/in) (max,min) = (35.60,30.69)
Int. (-0.378, -9.681)
Force (kip)
Displacement (in.)
15
10
5
0
-5
-10
-15
-1.5
-1
-0.5
0
0.5
1
1.5

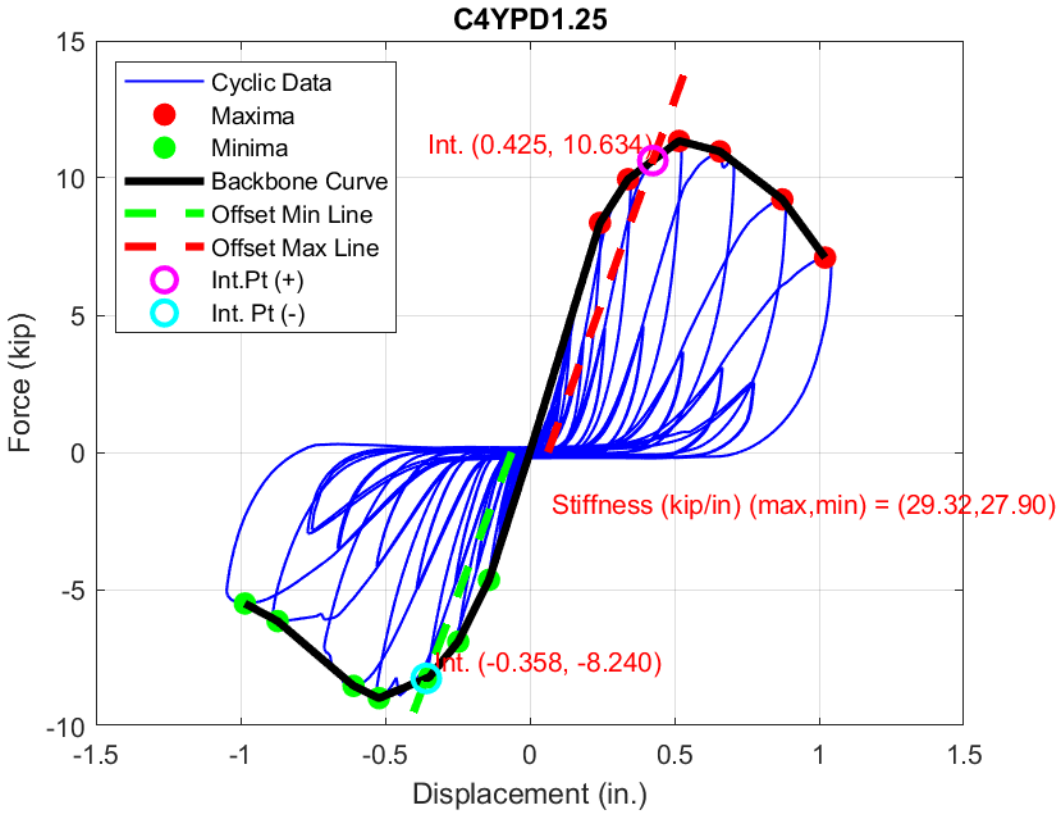
C4YPD1.25
Cyclic Data
Maxima
Minima
Backbone Curve
Offset Min Line
Offset Max Line
Int.Pt (+)
Int. Pt (-)
Int. (0.425, 10.634)
Stiffness (kip/in) (max,min) = (29.32,27.90)
Int. (-0.358, -8.240)
Force (kip)
Displacement (in.)
15
10
5
0
-5
-10
-1.5
-1
-0.5
0
0.5
1
1.5

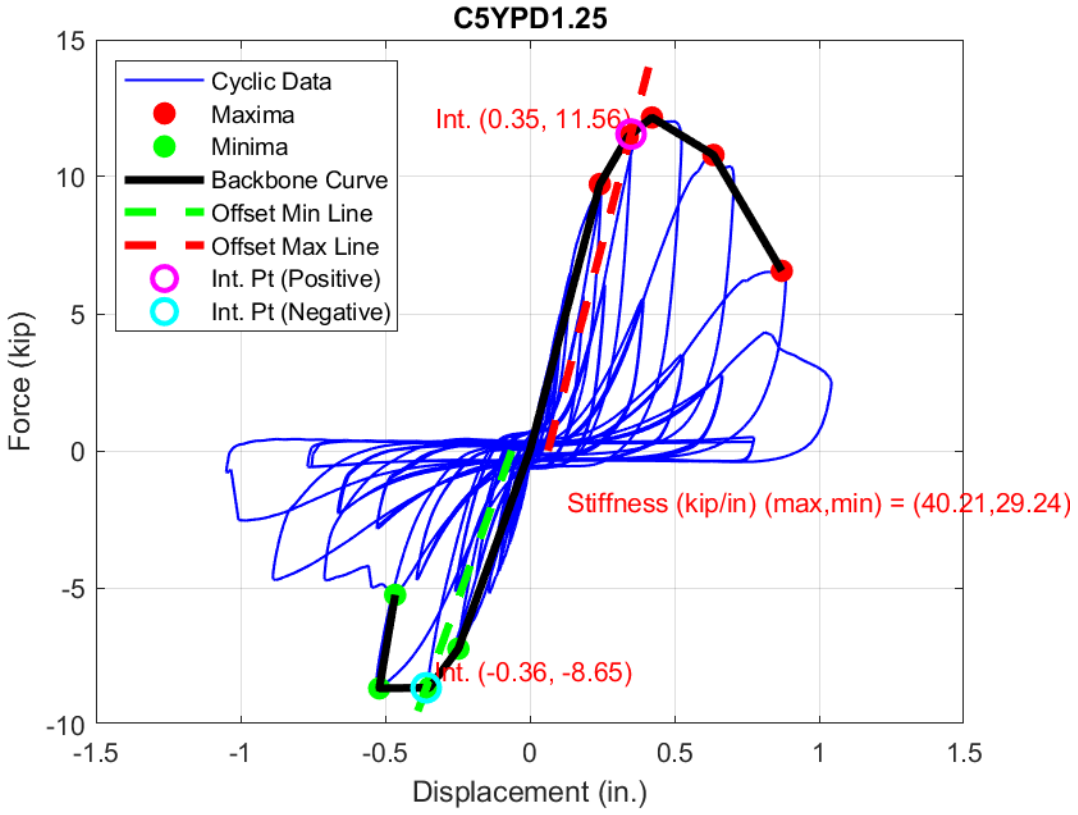
C5YPD1.25
Cyclic Data
Maxima
Minima
Backbone Curve
Offset Min Line
Offset Max Line
Int. Pt (Positive)
Int. Pt (Negative)
Int. (0.35, 11.56)
Stiffness (kip/in) (max,min) = (40.21,29.24)
Int. (-0.36, -8.65)
Force (kip)
Displacement (in.)
15
10
5
0
-5
-10
-1.5
-1
-0.5
0
0.5
1
1.5

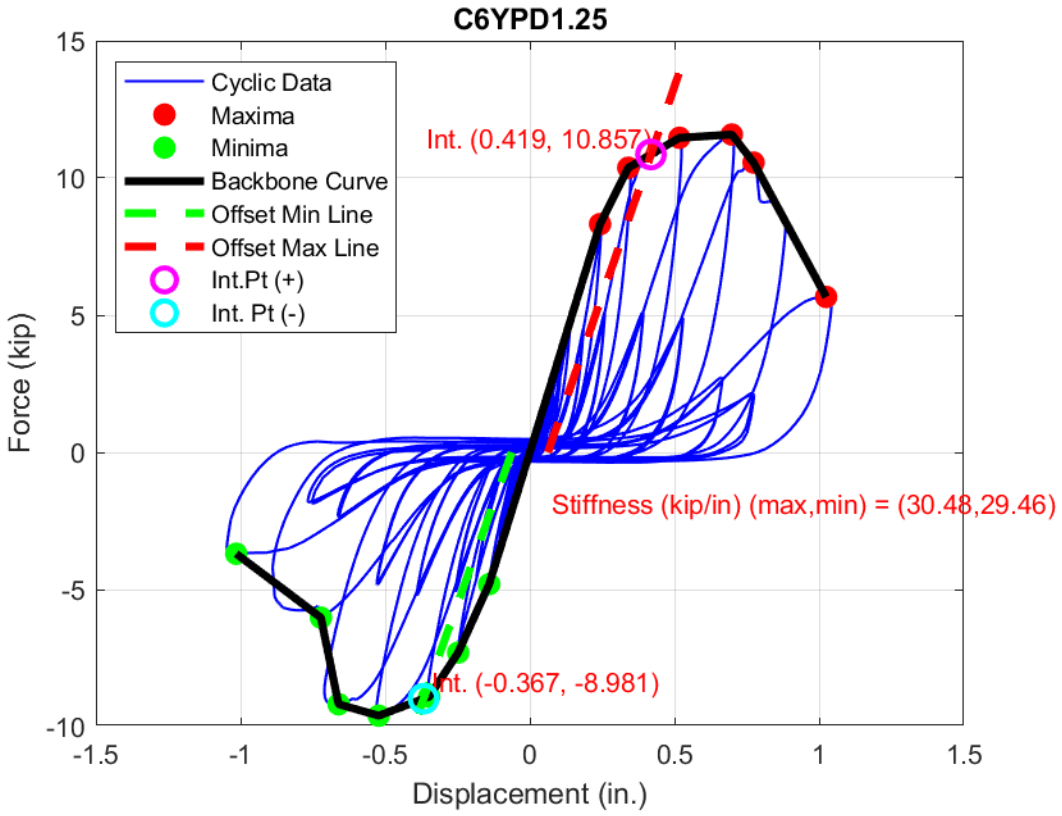
C6YPD1.25
Cyclic Data
Maxima
Minima
Backbone Curve
Offset Min Line
Offset Max Line
Int.Pt (+)
Int. Pt (-)
Int. (0.419, 10.857)
Stiffness (kip/in) (max,min) = (30.48,29.46)
Int. (-0.367, -8.981)
Force (kip)
Displacement (in.)
15
10
5
0
-5
-10
-1.5
-1
-0.5
0
0.5
1
1.5